A History of Tectono-Magmatism along the Parga Chasma Rift System on Venus

by

Jamie Graff

A thesis submitted to the Faculty of Graduate and Postdoctoral Affairs in partial fulfillment of the requirements for the degree of

Master of Science

in

Earth Sciences

Carleton University
Ottawa, Ontario

Abstract

Parga Chasma is a discontinuous rift system marking the southern boundary of the BAT region on Venus. Along a 1,500 km section of Parga Chasma, detailed mapping has revealed 5 coronae, 11 local rift segments distinct from a regional extension pattern, and 47 graben-fissure systems. These systems are often centred within coronae or large volcanoes, but many are isolated and indicate cryptic centres. Some of these magmatic centres are further observed as the loci of triple-junction rifting, collectively comprising the 11 local rift segments. Cross-cutting relationships between the corresponding graben-fissures and rift faults reveal synchronous formation, implying a genetic association. Additionally, cross-cutting relationships reveal these local events to postdate the regional extension, further indicating multiple stages of rifting. This provides an explanation for the discontinuous morphology of Parga Chasma, and its result has implications to explain the morphologies of other rift systems, both on Venus and Earth.

Acknowledgements

To begin I especially thank my supervisors, Dr. Richard Ernst and Dr. Claire Samson, for offering me the M.Sc. opportunity to further my Venus research. Their careful guidance throughout the years helped keep me well on track with steadily producing new ideas, insights, and results from my work. I thank them for providing edits and suggestions when producing a number of abstracts, posters, and oral presentations for various conferences over the last two years, and especially for providing financial support to allow me to attend and present my research at the Lunar and Planetary Science Conference in Houston, Texas. I am also incredibly appreciative for their suggestions, comments, and careful edits during the process of developing the ideas for and writing this thesis.

I thank everyone involved in our Venus Working Group, featuring representative attendance from the GSC and a variety of universities, including: Carleton, Ottawa, Mount Royal, Wesleyan, Brown, and Rey Juan Carlos. Discussions with students, professors, and research scientists from these institutions provided valuable feedback on multiple research directions, ideas, and insights involved when developing this thesis.

I thank Dr. Ellen Stofan and Dr. David Miller for meeting with our Venus research group at the CASI ASTRO 2016 conference in Ottawa. Dr. Stofan's expertise on Venusian geology provided wonderful insights regarding my research topics.

Thank you to Erin Bethell for the informative discussions regarding Venusian geology, research methods and ideas, and for her assistance when exploring some unfamiliar territory in ArcMap. Thank you to Kim Klausen for her assistance as I was learning to use CorelDraw to produce great quality figures for this thesis. Additionally, I offer tremendous thanks to Sarah Davey for her expertise and assistance regarding each these topics, from geological concepts and research methods to her assistance with both ArcMap and CorelDraw on countless occasions. I also thank Sarah for providing me with well modified figures and diagrams that have found a place in this thesis (with acknowledgement).

I thank the entire faculty and staff of the Earth Sciences Department and of course my fellow graduate students who have and continue to make my experience here at Carleton truly enjoyable and memorable.

Lastly, my deepest thanks goes to my Mom, Dad, and my brother, Kevin for providing me with continuous and unwavering encouragement and support throughout my academic career. I also thank my whole extended family – my grandparents, aunts, uncles, and cousins – in British Columbia, Washington, and Nevada, for their interest in my work and their similar support throughout the years. I also thank Bruce Foreman for his interest and curiosity regarding my research, and Rick Nelson – who will always be a part of the family and like an uncle to me.

Table of Contents

List of Tables

List of Figures

1 Chapter: Introduction

1.1 Our Sister Planet, Venus

The celestial object which would later become known as the planet Venus was first observed with the naked eye by Babylonian astronomers as early as 3000 BCE. This planet, or "wandering star", would be visible either prior to sunrise or just after sunset, depending on the season and geographic location of the observer – leading ancient civilizations to name it as the "morning" and "evening" stars. Venus was known as the morning star *Phosphoros* (the "Bringer of Light") and the evening star *Hesperos* (the "star of the evening") to the ancient Greeks; and likewise known as *Lucifer* and *Vesper* to the ancient Romans. It was not until the sixth century BCE that the ancient Greeks identified it as a single planet and named it after their goddess of love and beauty, Aphrodite. The name it is known as today comes from the Roman goddess of love and beauty, Venus. Confirmation of Venus' planetary status, however, was not obtained until the year 1610 when Galileo Galilei observed the celestial object and detected that it had phases similar to those of the Moon. These observations also helped to support the emerging Copernican model of the Solar System (Waerden, 1974; Phillips and Hansen, 1994; Chaisson and McMillan, 2010; Taylor, 2014).

Venus is known as Earth's sister planet because they both have similar size, mass, and density (*Figure 1.1*). It is the second planet from the Sun, and third brightest celestial object in the sky, preceded only by the Moon and Sun. Venus' brightness is due to the high reflectivity of its thick atmosphere (Donahue and Russell, 1997; ESA, 2007a,b; Chaisson and McMillan, 2010). Similar to all other planets in our Solar System, Venus

orbits the Sun in a counter clockwise, prograde motion. It is the only planet, however, which rotates in a clockwise fashion with respect to its axis of rotation. A well-accepted theory to explain this unusual retrograde rotation invokes a large impact during the early years of the Solar System. The impact would have hit the young planet with enough force to stop its original prograde rotation and initiate a slow retrograde rotation. Because of its slow rotation, an average Venus day (approximately 243 Earth days) is longer than an average Venus year (approximately 225 Earth days) (Chaisson and McMillan, 2010). A combination of slow rotational velocity and the lack of a convecting core is likely preventing the formation of a dynamo force within its core, thereby hindering the generation of a sustainable intrinsic magnetic field. A weak extrinsic magnetic field is present due to interactions between charged particles within its upper atmosphere and the incoming solar wind (ESA, 2007b; Chaisson and McMillan, 2010).

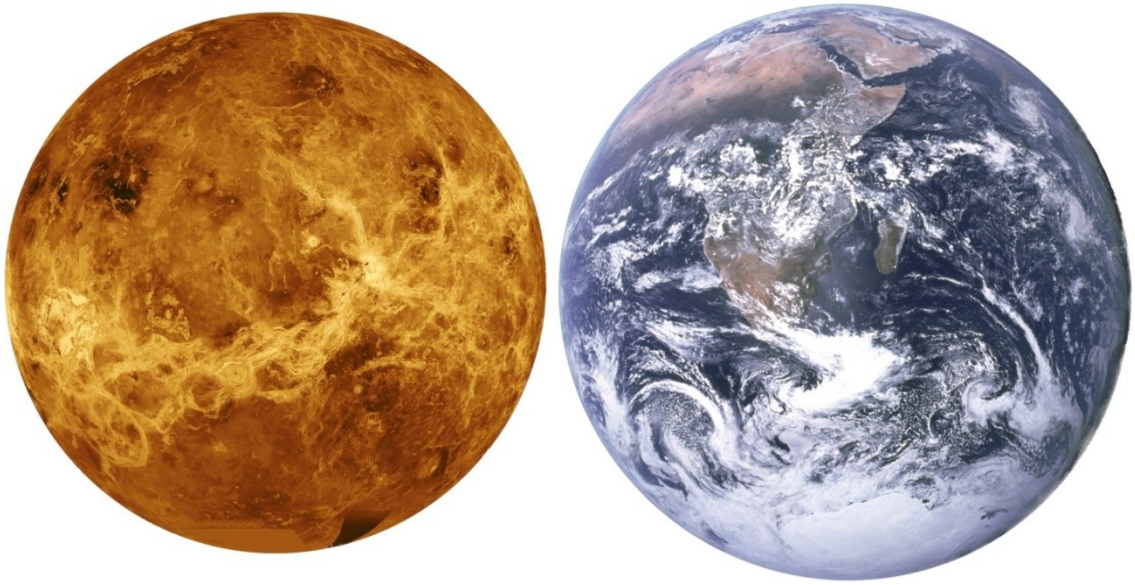

Figure 1.1. Size comparison of Venus and Earth. Venus (6051 km mean radius) shown on the left, imaged using the microwave spectrum; Earth (6371 km mean radius) on the right, imaged at the visible spectrum.

Before the Soviet Union began the Venera project in the early 1960's, existing knowledge of Venus' surface conditions and topography remained purely speculative. Because of Venus' similarities to Earth with respect to bulk properties, scientists initially believed that their internal dynamic processes and geologic evolution would also be similar. Following early investigations by the space organizations of both the Soviet Union and the United States, significant differences between Venus and the Earth became clear. Venus exhibits average surface temperatures of 460^{o}C and average near-surface atmospheric pressures of 9000 kPa. These values, much higher than the corresponding values for Earth, are largely due to Venus' thick atmosphere which is composed of large amounts of carbon dioxide (CO_2), with lesser quantities of nitrogen gas (N_2), hydrogen sulphide (H_2S), and low-lying cloud layers of sulphuric acid (H_2SO_4) droplets. The abundance of these gases creates a runaway greenhouse effect by trapping nearly all of the Sun`s incoming radiation, in addition to any internal heat dissipated from the planetary interior (Donahue and Russell, 1997; Chaisson and McMillan, 2010; Taylor, 2014).

In 1989, NASA launched the Magellan spacecraft to map the surface of Venus (*Figure 1.2*) at a resolution of 75-100 m/pixel using Synthetic Aperture Radar (SAR) imaging (Young, 1990; Saunders et al., 1990, 1992; Saunders and Pettengill, 1991). All basemap SAR and topography images presented herein were obtained by NASA's Magellan mission and were compiled by the US Geological Survey (USGS) Astrogeology Science Center (http://astrogeology.usgs.gov/), unless otherwise noted.

Magellan SAR images have provided scientists with detailed information regarding Venus` surface geology and have primarily been used to identify and map tectono-

magmatic structures and volcanic units (Phillips and Hansen, 1994; Ivanov and Head, 2013). From these radar images, it was also noted that plate tectonics is not currently active on Venus due to the lack of any observable plate boundaries (Phillips and Hansen, 1994). Contrary to Earth, Venus is understood to be operating predominantly in a single plate, stagnant lid regime, with all magmatism occurring in intra-plate settings (Solomatov and Moresi, 1996; Nimmo and McKenzie, 1998; Ernst and Desnoyers, 2004). However, it has been proposed that Venus may have at one time operated in a mobile lid regime due to the fact that many highland mountainous areas would have required significant crustal convergence to be formed (Kiefer, 2013). SAR images are the primary source of data used herein to identify and map the tectono-magmatic structures of Venus, most importantly the radar-bright extensional lineaments associated with graben-fissure systems and rift zones.

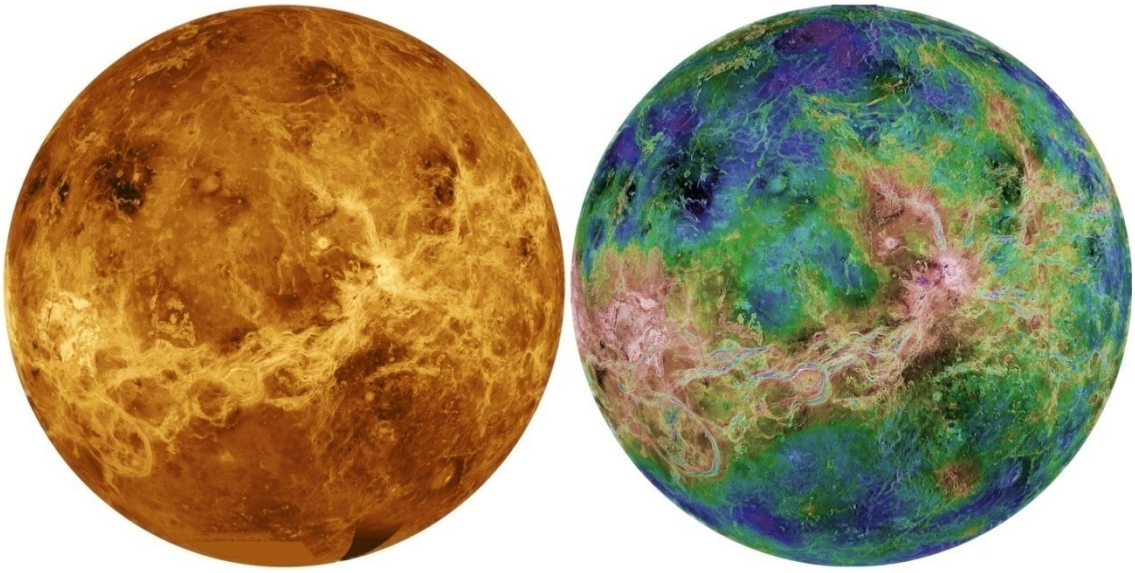

Figure 1.2. Radar images of Venus in true colour (left) and false colour (right). Both images display the same view of Venus for comparison with north at the top. False colour image uses varying shades of dark and light blue to indicate lower elevations, greens show middle elevations and reds to white display higher elevations. Source NASA/JPL.

1.2 Research Objectives

On Venus, there exists a geologically complex area known as the Beta-Atla-Themis (BAT) region, located within the coordinates of 180^{o} – 300^{o}E and 50^{o}S – 50^{o}N (*Figure 1.3*), where a diversity of tectono-magmatic structures have been preserved (Head et al., 1992; Squyres et al., 1992; Crumpler et al., 1993; Hamilton and Stofan, 1996). These structures include, but are not limited to, large volcanic rises (Stofan et al., 1995; Smrekar et al., 1997; Ivanov and Head, 2011, 2013), rift zones (often referred to as *chasmata*) (Hamilton and Stofan, 1996; Stofan et al., 2000; Martin and Stofan, 2004; Martin et al., 2007; Ivanov and Head, 2011, 2013; Graff et al., 2015), graben-fissure systems, believed to be underlain by mafic dyke swarms (Grosfils and Head, 1994; Ernst et al., 1995, 2001, 2003; Studd et al., 2010; Davey et al., 2013; Graff et al., 2015), pit crater chains (Davey et al., 2013; Sawford et al., 2015), and coronae (Stofan et al., 1991, 2000; Martin and Stofan, 2004; Martin et al., 2007).

The overarching goal of this study is to identify and map the extensional lineaments associated with major graben-fissure systems and rift zones, produced by internal tectonic and magmatic processes in the BAT region. The primary objectives are as follows: (1) resolving the relative chronology of tectono-magmatic events within a detailed study area along a section of the Parga Chasma rift system, a major component of the BAT region (Chapter 4); and (2) analyzing the genetic association between local rift segments and isolated magmatic centres (Chapter 5).

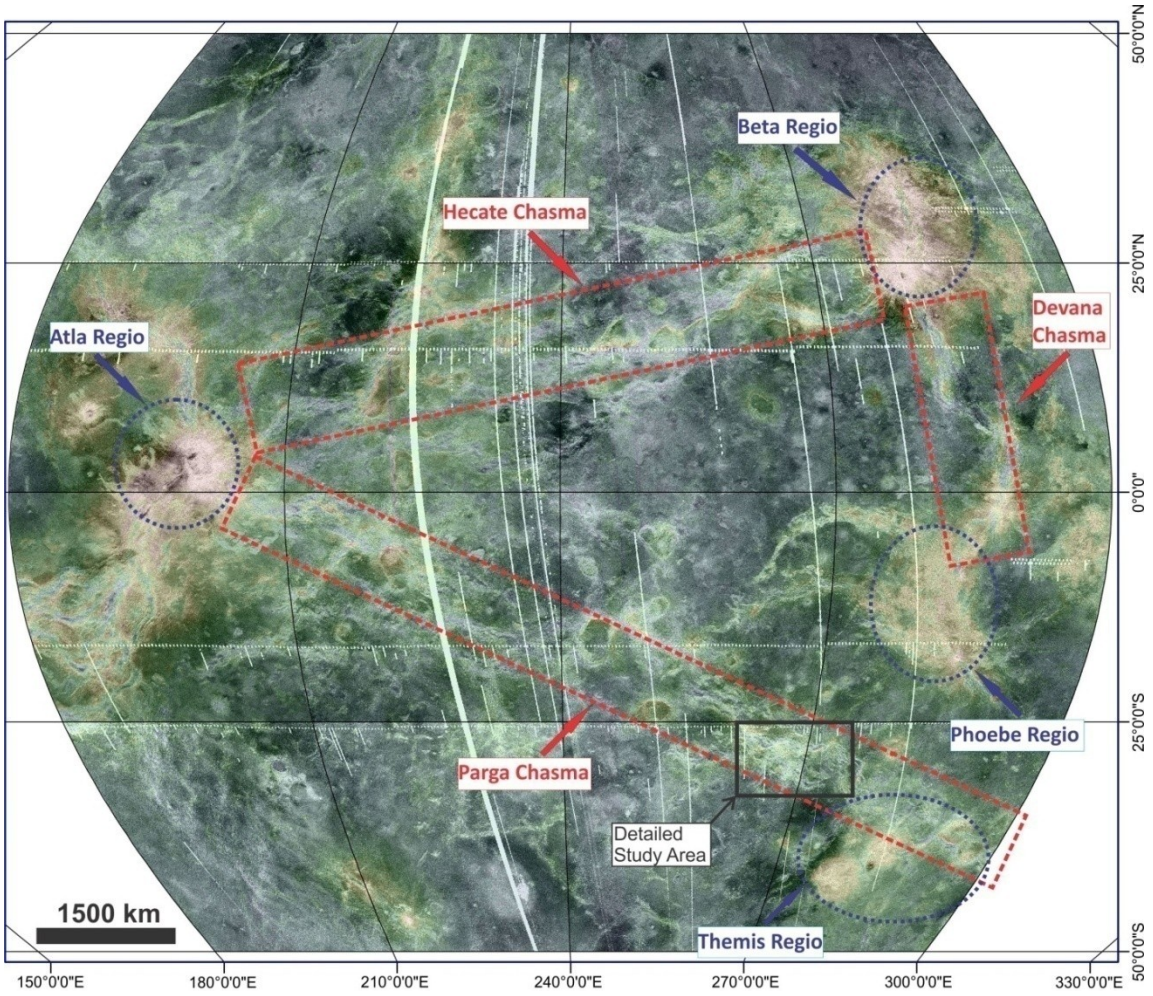

Figure 1.3. Magellan synthetic aperture radar (SAR) image of the BAT region, overlain by topography at 75% transparency. Lower elevations are displayed with faded shades of blue and green; higher elevations are displayed with faded shades of yellow and red. Identified are the prominent volcanic structures of Atla, Beta, Phoebe, and Themis Regiones, which are bounded by the three major rift systems Hecate, Devana, and Parga Chasmata. The location of the detailed study area is indicated by the black square. Basemap source: USGS.

To achieve the first objective (Chapter 4), a detailed study area has been selected in the southeast of the BAT region. Within both of the Helen Planitia and Themis Regio quadrangles, lies a complex section of the Parga Chasma rift system, located approximately within the coordinates of 260^{o} – 275^{o}E, 25^{o} – 33^{o}S (*Figure 1.3*). This location is host to a variety of tectono-magmatic structures, including many graben-fissure systems and rift segments; multiple coronae structures and large volcanoes; as well as young lava flows scattered against a radar-dark background of volcanic plains

material. Of particular interest to this research are the following activities: detailed linework mapping of the radar-bright lineaments representing individual graben-fissures; grouping graben-fissures into separate systems of different geometries; performing cross-cutting analyses to generate a relative chronology; and reconstructing the tectono-magmatic history of the study area. Radar-bright lineaments interpreted to represent local and regional rift faults associated with the regional extension of Parga Chasma were also mapped. From cross-cutting relationships, a relative chronological timeline for the formation of separate graben-fissure systems relative to the regional rifting along Parga Chasma has been created. The final detailed map of the study area will become part of the Venus Global Dyke Swarm Map project (Ernst et al., 2009; Studd et al., 2010a,b,c; Studd et al., 2011), with the ultimate goal of providing a comprehensive and detailed global map of all graben-fissure systems and dyke swarms on Venus.

The second objective (Chapter 5) concerns the differing morphology of the three major rift systems of the BAT region: Hecate, Devana, and Parga Chasmata. These rift systems form a regional enclosure between the prominent volcanic structures of the BAT region, terminating at the topographically high volcanic rises of Beta, Atla, and Phoebe Regiones, and the corona-dominated volcanic plateau of Themis Regio (Head et al., 1992; Crumpler et al., 1993; Martin et al., 2007). A quick observation of the regional morphologies of these three rift systems reveals that each exhibits different levels of continuity between their respective loci of formation (i.e. large volcanic rises, such as Beta or Atla Regio). In particular, Parga Chasma is significantly more discontinuous than Hecate and Devana Chasmata, and contains an abundance of coronae within close proximity to several individual rift segments. To explain these observations I introduce

the hypothesis that Parga Chasma is predominantly developed as a series of local events of triple-junction style rifting from isolated magmatic centres (i.e. coronae, large volcanoes, and sources of radiating and/or circumferential graben-fissure systems). In addition to the detailed mapping in the study area (Section 4.2), I also examine Parga and Hecate Chasmata at a regional scale to further observe the relationship between isolated magmatic centres and local rift segments (Section 5.2). This rifting model is also applied to the Atlantic Rift System to serve as a terrestrial analogue to the rift system morphology observed on Venus (Section 5.3).

2 Chapter: Background Information

2.1 Venus' Geological History

Venus, like other terrestrial planets and planetary bodies, experiences some form of mantle circulation from internal heat dissipation, resulting in large-scale magmatism, volcanism, and tectonic deformation (Turcotte, 1995; Ivanov and Head, 2013). Before the Magellan mission, preconceptions about Venus' internal processes were split between an Earth-like plate tectonics model resulting from whole mantle convection, versus global heat loss dominated by a combination of lithospheric conduction, recycling, thermal thinning, and volcanism (Kaula and Phillips, 1981; Solomon and Head, 1982; Grimm and Solomon, 1987, 1989; Head and Crumpler, 1990). Following the Magellan mission, Venus was understood to have the appropriate size, and compositional and gravitational potentials that would support long-lasting volcanism from both convection and advection (Ivanov and Head, 2013). However, with high mantle viscosity and the lack of observable plate tectonics on Venus, the currently most accepted model involves a global regime of stagnant lid convection, which inhibits transient motion of the thick lithosphere (Solomatov and Moresi, 1996; Nimmo and McKenzie, 1998). Venus may have also once operated in a mobile lid regime akin to Earth-like plate tectonics due to the fact that many highland and mountainous areas would have required significant crustal convergence from whole mantle convection to form. This model also supports the possibility that liquid water may have once flowed on the planetary surface as liquid water is a common agent that promotes the development of large-scale fault zones by lowering pore pressures and the coefficient of friction of rock materials (Kiefer, 2013).

From crater counting, the age of Venus' surface is interpreted to be only 500 – 700 Ma, supporting the well-accepted idea that Venus experiences global resurfacing events as a primary method of global heat loss (McKinnon et al., 1997; Ernst and Desnoyers, 2003; Ivanov and Head, 2013; Head, 2014). The exact style of global resurfacing is still under debate as to whether it occurs via catastrophic or steady-state processes. Catastrophic processes would involve a near-instantaneous episodic global overturn of the planetary crust, followed by short-lived global resurfacing from extreme volcanism and extensive lava flows (Turcotte, 1995; Herrick, 1999; Ivanov and Head, 2011, 2013). Steady-state resurfacing would involve Earth-like magmatic processes for which volcanic and tectonic events are randomly distributed in time and space (Phillips and Hansen, 1994; Hansen and Young, 2007). Regardless of how exactly Venus experienced resurfacing, scientists generally agree that fresh surface material is covering the majority of the planetary surface and destroyed all observable traces of older tectonic and volcanic structures, in addition to any impact craters that were emplaced earlier than 1 Ga (Strom et al., 1992, 1994; Bindschadler, 1995; Ernst and Desnoyers, 2003; Studd et al, 2011).

2.2 Venus' Tectono-Magmatic Structures

Following the Magellan mission, many tectono-magmatic structures on Venus have been readily observed and studied from the analysis of SAR images (Young, 1990; Head et al., 1992; Phillips and Hansen, 1994). These structures include, but are not limited to: large volcanoes and volcanic rises; graben-fissure systems and rift zones created as a result of local and regional extensional deformation; lava flooded plains material featuring clusters of shield volcanoes; densely packed extensional lineations, and contractional groove belt structures; coronae; pit crater chains; and major highland

mountain belts and heavily deformed tessera terrain – interpreted as the oldest units on Venus' surface (Head et al., 1992; Grosfils and Head, 1994a; Phillips and Hansen, 1994; Ernst et al., 2001, 2003; Martin et al., 2007; Ivanov and Head, 2011, 2013). Understanding the possible genetic associations between major volcanic edifices, graben-fissure systems, coronae, and rift zones are most relevant to this research and are discussed in detail below.

2.2.1 Volcanic Edifices

On Venus, mantle upwellings result in clusters of volcanic edifices ranging from small volcanoes (<30 km in diameter) and shield plains, large volcanoes and coronae (>100 km diameters), to major volcanic rises (>1000 km diameters) (Masursky et al., 1980; M^{c}Gill et al., 1981; Stofan and Head, 1990; Head et al., 1992; Stofan et al., 1992, 1995; Smrekar et al., 1997). Many volcanic edifices are associated with weakly to mildly tectonized terrains and are built up from extrusive volcanic material. Clusters of shield volcanoes are commonplace on Venus and characterize the presence of shield plains and shield cluster units (Bindschadler, 1995; Ivanov and Head, 2011, 2013). Flow units from these volcanoes produce numerous lava channels and extensive flow fields (often referred to as *flucti*) (McGill et al., 1981; Guest et al., 1992). Rising mantle plumes and superplumes form both individual volcanoes with diameters larger than 100 km (*Figure 2.1*) and major topographic rises dominated by one or more volcanic vents, such as the volcanic rises of Beta and Atla Regiones (Stofan et al., 1995; Smrekar et al., 1997; Ernst, 2014). These large volcanic edifices (as well as coronae) are also commonly the focal points of major radiating and circumferential graben-fissure systems, in addition to

smaller local segments of rift zones (Head et al., 1992; Ernst et al., 1995; Martin et al., 2007).

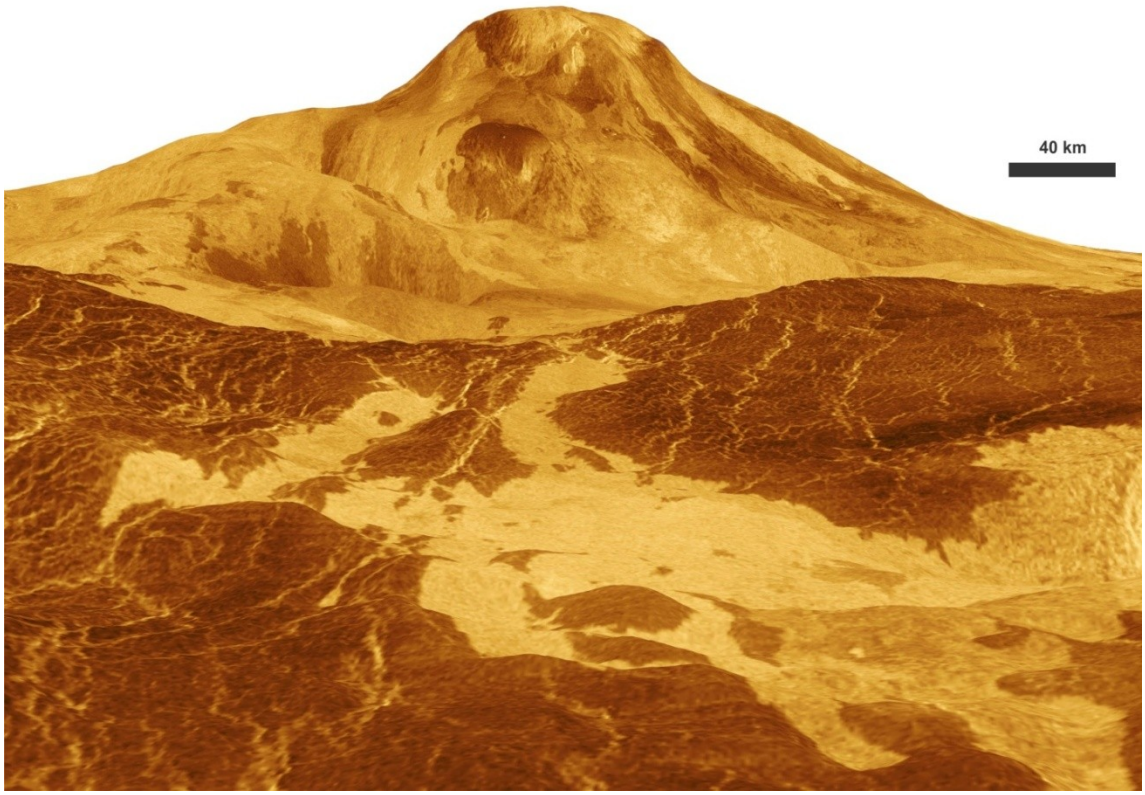

Figure 2.1. Three-dimensional perspective view of Ma'at Mons on Venus created by NASA Jet Propulsion Laboratory based on Magellan radar images. Ma'at Mons rises 5 km above the surrounding plains with a total elevation of 8 km above MPR. Vertical scale in image is exaggerated by a scale of 22.5; no exaggeration on the horizontal scale, shown to the right of the image. Source: NASA/JPL.

2.2.2 Graben-Fissure Systems

Dyke swarms are interpreted to represent part of the plumbing system of flood basalts, allowing for the vertical and lateral motion of magma derived from partial melting of mantle plumes or diapirs that have ascended to the base of thinned lithosphere (*Figure 2.2*) (Ernst and Buchan, 1997a,b, 2001). Similarly on Venus, dyke swarms are described as laterally propagating subsurface mafic magma (Grosfils and Head, 1994a; Ernst et al., 1995b, 2001, 2003), while graben-fissures are interpreted to be the surficial expression of these underlying dykes (*Figure 2.3*). They are expressed as radar-bright lineaments on SAR images (Ernst et al., 2003; Studd et al., 2011; Graff et al., 2015) and commonly exhibit radiating, linear, and circumferential geometries (*Figure 2.4*), all of which can be readily observed on Venus (Ernst et al., 1995a,b, 2001, 2003; Ernst and Buchan, 2001; Studd et al., 2011; Grosfils et al., 2014). Multiple styles of graben-fissure systems are often found in spatial (and probable genetic) association with large volcanoes, coronae, and rift zones (Baer et al., 1994; Grosfils and Head, 1994a; Studd et al., 2011; Graff et al., 2015).

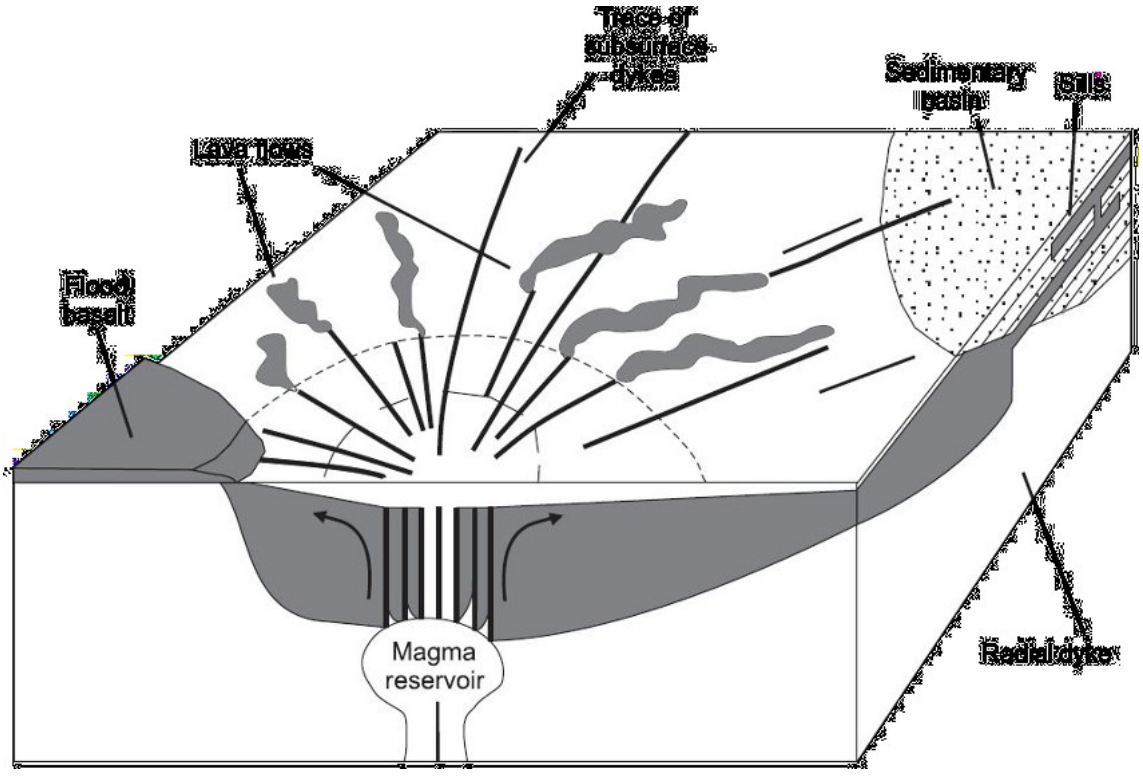

Figure 2.2. Lateral emplacement of dykes from a central magmatic upwelling. Radial subsurface dykes represent feeder systems to distal sills within sedimentary basins, and to surface lava flows and flood basalts. Source: Ernst, 2014.

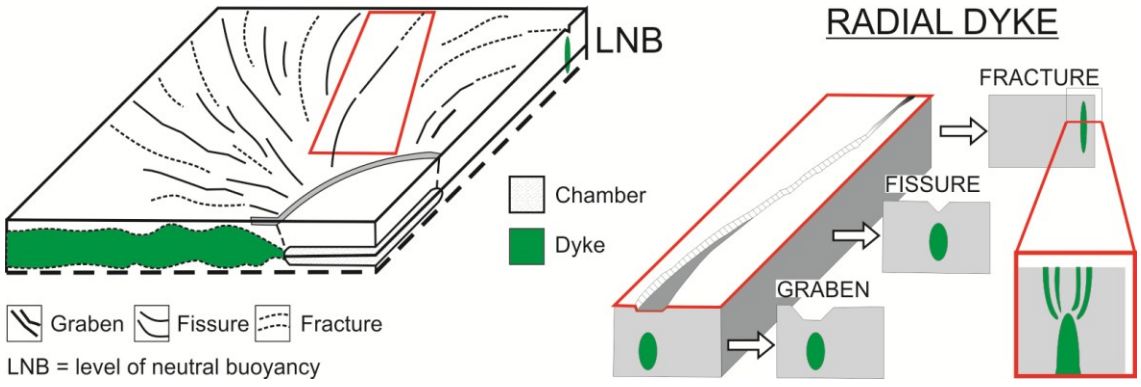

Figure 2.3. Cross-sectional view indicating how laterally propagating subsurface dykes influence surface deformation. Depending on both the proximity to the source and the volume of magma, surface deformation will respond by producing either full graben, fissures, or fractures. Source: Grosfils and Head, 1994b with colours added (courtesy of S. Davey).

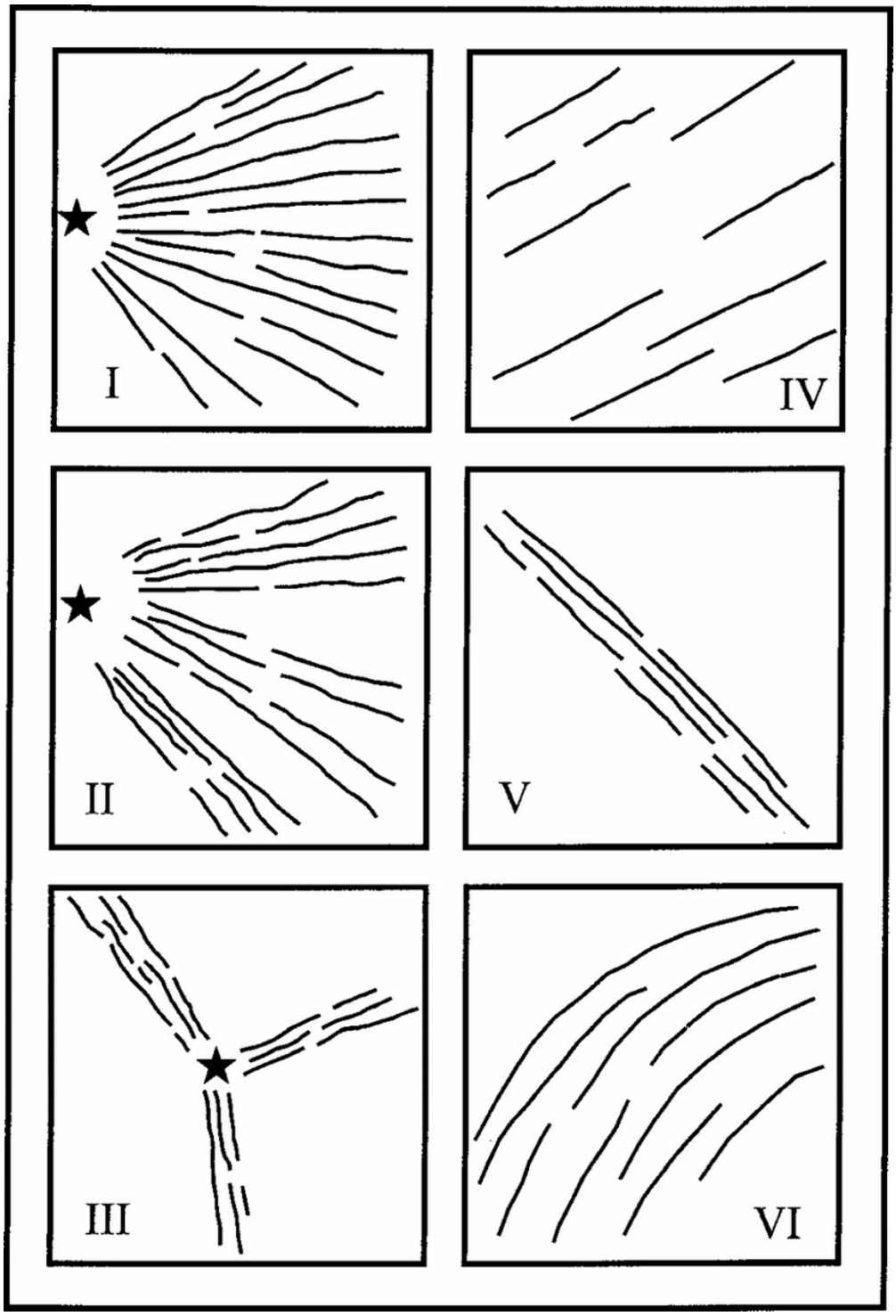

Figure 2.4. Characteristic geometries of dyke swarms or graben-fissure systems. I – continuous fanning pattern; II – fanning pattern divided into separate subswarms; III – subswarms of subparallel dykes radiating from a common point; IV – subparallel dykes over a broad area; V – subparallel dykes in a narrow zone; VI – arcuate pattern, often representing a section of a circumferential swarm. Stars indicate source centres defined by the convergence of the radial dyke pattern. Source: Ernst and Buchan, 2001.

2.2.3 Coronae

Coronae are enigmatic volcanic formations initially believed to be unique to Venus but possible analogue structures (giant circumferential dyke swarms) have recently been discovered on Earth (Bethell et al., 2016; Buchan and Ernst, 2016). Coronae are quasi-circular volcanic structures, often featuring a depressed centre and a raised exterior annulus of circumscribing fractures (Stofan et al., 1991; Stofan et al., 2000; Martin and Stofan, 2004; Dombard et al., 2007; Martin et al., 2007). Coronae are most commonly 200-500 km in diameter, although some can reach diameters larger than 1000 km. The largest is Artemis Corona, with an outer rim diameter of 2400 km (Stofan et al., 1991; Hansen and Olive, 2010). Coronae are interpreted to result from mantle upwellings, such as plumes or diapirs, and frequently occur in zones of regional extensional deformation resulting in areas of thinned lithosphere (Stofan et al., 1991; Herrick, 1999). The radiating extensional fractures and those circumscribing corona annuli are interpreted to result from local lithospheric stresses generated either by the rising/collapsing mantle upwelling (Stofan et al., 1991; Grosfils and Head, 1994b), or from the intrusion of radiating and/or circumferential dyke swarms from the central magmatic source (Ernst et al., 2003, 2007; Bethell et al., 2016; Buchan and Ernst, 2016).

Figure 2.5. Magellan SAR image of Gashan-Ki Corona, centred at 243.5°E, 12°N. The SAR image shows the extensional fractures circumscribing the corona rim, in addition to a major radiating dyke swarm originating from its centre. Source: USGS.

2.2.4 Rift Zones (Chasmata)

Rift zones on Venus generally display geomorphologies similar to those of rifts on other terrestrial planetary bodies in the Solar System. Based on the observations from Magellan SAR and altimetry data, *chasmata* (as catalogued by the International Astronomical Union – IAU) are large fracture zones characterized by a central valley bounded by elevated walls created as a result of normal faulting (Stofan et al., 2000; Martin and Stofan, 2004; Martin et al., 2007; Graff et al., 2015). Rift zones are also thought to be one of the youngest tectonic units in Venus' history, accounting for only 5-6% of surface area. They are composed of many broad and densely-packed extensional structures and commonly overprint underlying material unit morphologies (Ivanov and Head, 2011, 2013). On SAR images, individual rift faults appear as clusters of densely-

packed, thicker, and more sinuous radar-bright lineaments than graben-fissures (Section 3.4) (Graff et al., 2014, 2015).

Figure 2.6. Magellan SAR image of the northern Devana Chasma rift system, centred at 282^{o}E, 19^{o}N. Observable on the SAR image are the dense clustering of thick and sinuous radar-bright lineaments, interpreted as rift faults. Source: USGS.

2.2.4.1 Chasmata of the BAT Region

The BAT region is defined by the prominent volcanic structures of the Beta, Atla, and Themis Regiones, which are enclosed by the major rift systems of Hecate, Devana, and Parga Chasmata. Each of these rift systems extend between two of these major structures, however, Devana Chasma terminates within the volcanic rise of Phoebe Regio to the north of Themis Regio. Atla, Beta, and Phoebe Regiones (*Figure 2.7a-f*) each host multiple local rift segments extending from their respective volcanic rises in triple-junction style rifting. Themis Regio (*Figure 2.7g-h*) however, is heavily dominated by an abundance of coronae and other smaller volcanic structures, with no primary magmatic centre at the southeast end of the Parga Chasma rift system.

2.2.4.1.1 Hecate Chasma

Hecate Chasma (205 – 278^{o}E, 3 – 29^{o}N) is an 8,000 km long rift system that extends ENE-WSW between Atla and Beta Regiones (*Figure 2.8*). It is characterized as a discontinuous fracture and trough zone (Hamilton and Stofan, 1996), more so than Devana but significantly less compared to Parga. Similarly to Devana, Hecate Chasma contains prominent segments extending directly from the large volcanic rises of Atla and Beta Regiones, while the central portion of Hecate Chasma, distal from the ends of this rift system, are characterized by shorter rift segments that typically converge on local magmatic centres (often coronae). This style is similar to that observed along Parga Chasma (Section 2.2.4.1.3).

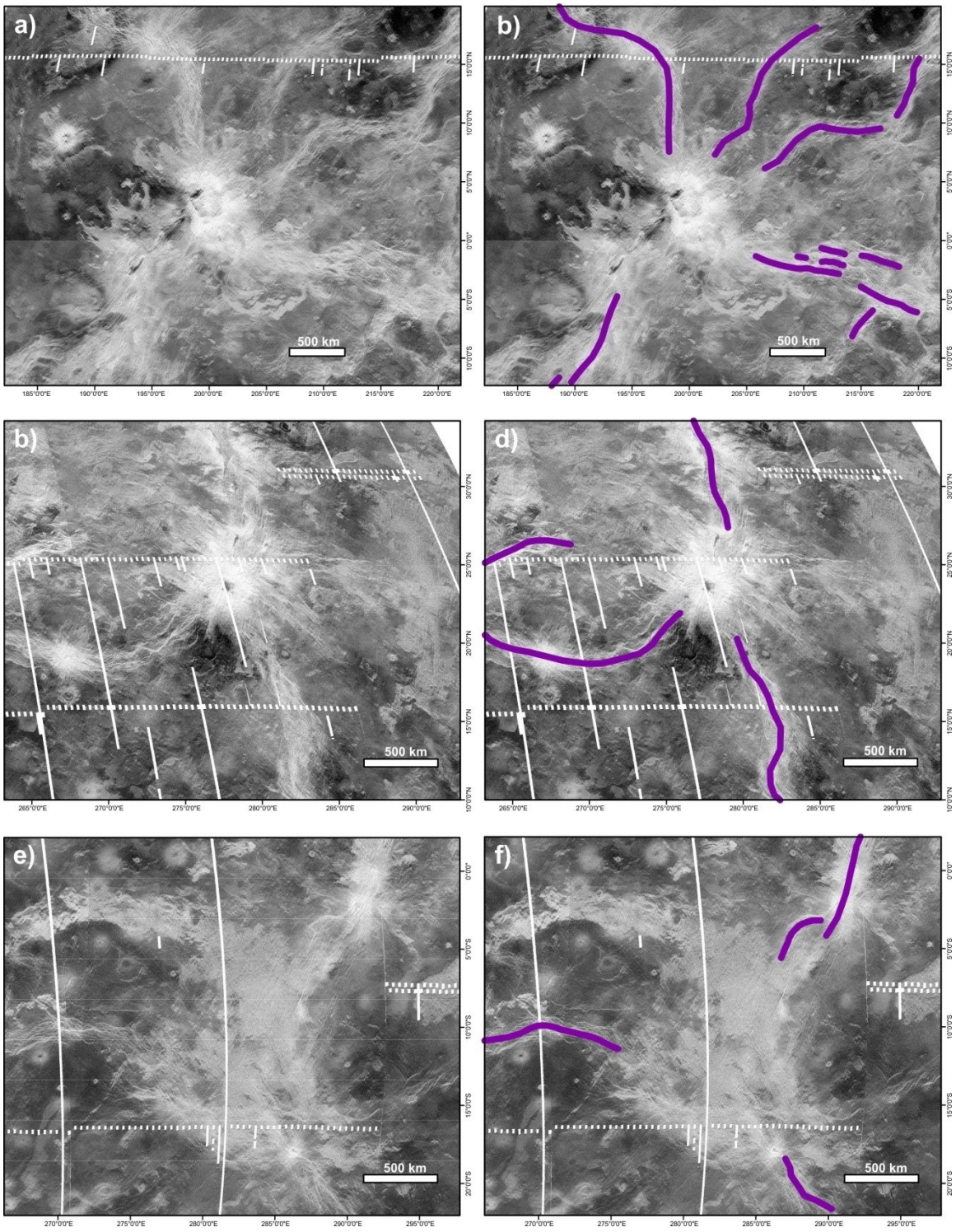
a)
b)
b)
d)
e)
f)
500 km

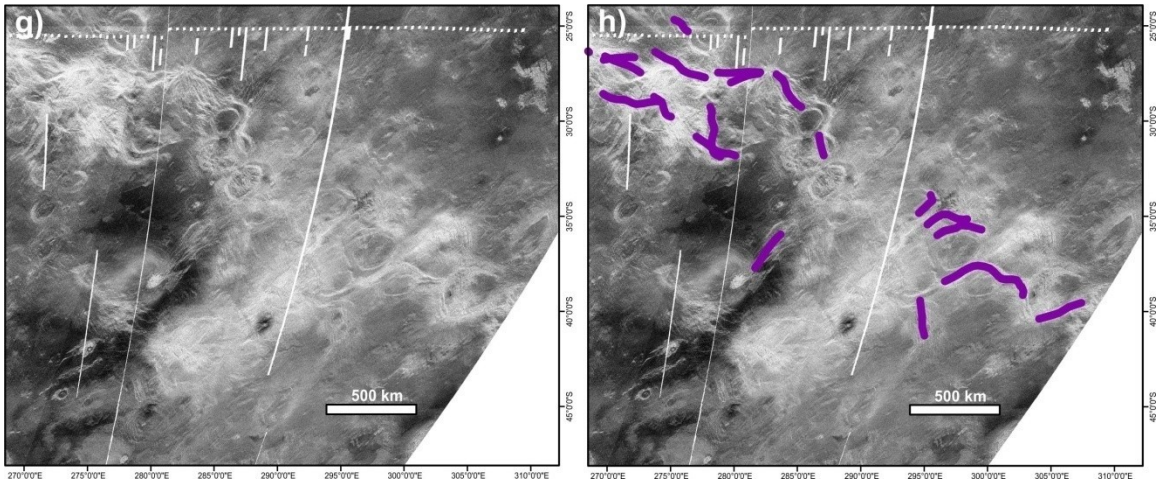

Figure 2.7. Magellan SAR images of (a, b) Atla Regio volcanic rise (204°E / 2°N centre); (c, d) Beta Regio volcanic rise (280°E / 22°N centre); (e, f) Phoebe Regio volcanic rise (280°E / 9°S centre); and (g, h) Themis Regio volcanic plateau (281°E / 35°S centre). Purple lines (b), (d), (f), and (h) denote the interpreted trend of individual rift segments focussed on their respective magmatic centres. Basemap source: USGS.

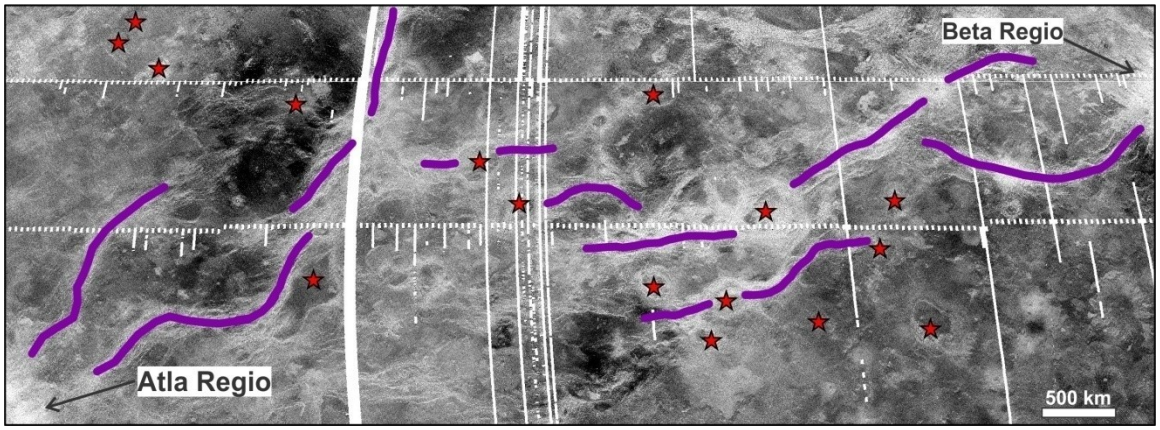

Figure 2.8. Magellan SAR image of Hecate Chasma, centred at 240°E, 16°N. Purple lines denote interpreted individual rift segments. Red stars denote centres of IAU catalogued coronae. Basemap source: USGS.

2.2.4.1.2 Devana Chasma

Devana Chasma (280 – 290°E, -4 – 21°N) is a 3,000 km long rift system that connects the large volcanic rises of Beta and Phoebe Regiones (*Figure 2.9*). This rift system exhibits a nearly continuous collection of densely clustered and near parallel rift faults, but with a clear left-lateral offset (~75 km) at 7.5°N. Because of this, Devana Chasma has been suggested to be composed of two separate rift segments, one segment extending southward from Beta Regio and the other extending northward from Phoebe Regio, and which meet up in the middle with a ~75 km offset (Kiefer and Peterson, 2003; Kiefer and Swafford, 2004, 2006).

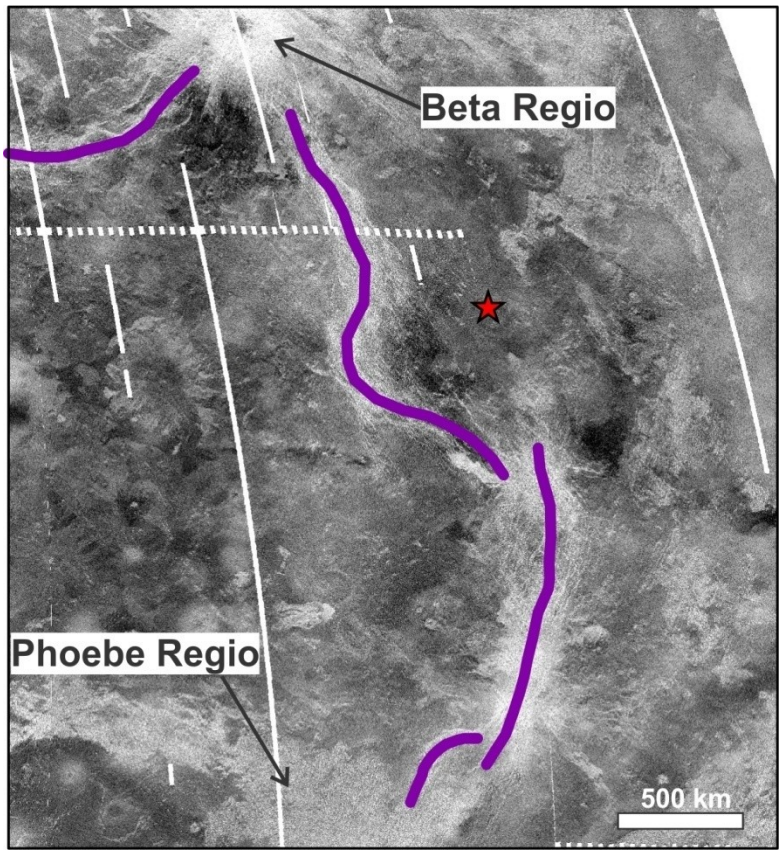

Figure 2.9. Magellan SAR image of Devana Chasma, centred at 282°E, 9°N. Major volcanic structures are identified. Purple lines denote interpreted individual rift segments. Red stars denote centres of IAU catalogued coronae. Basemap source: USGS.

2.2.4.1.3 Parga Chasma

Parga Chasma (207^{o} – 300^{o}E, 0^{o} – 40^{o}S) is a 10,000 km long, NW-SE trending rift system extending between the volcanic rise of Atla Regio and the corona-dominated volcanic plateau of Themis Regio (*Figure 2.10*). It is characterized by discontinuous fracture and trough zones, containing up to fourteen branching segments between Atla and Themis Regiones (Stofan et al., 2000; Martin and Stofan, 2004; Martin et al., 2007). Within the Parga Chasma region, regional NE-SW extension has occurred (Section 4.2.2; *Figure 4.3*), interpreted to have resulted from the formation of the volcanic rise and plateau of Atla Regio and Themis Regio, respectively (Martin et al., 2007; Lopez and Hansen, 2008; Stofan and Brian, 2012). This extension caused regional rifting, resulting in crustal thinning that further allowed for subsequent mantle upwellings to occur throughout the weakened crust (Herrick, 1999) and form the many coronae, volcanoes, and graben-fissure systems observed throughout this region (Grosfils and Head, 1994a,b; Ernst et al., 2001; Martin et al., 2007).

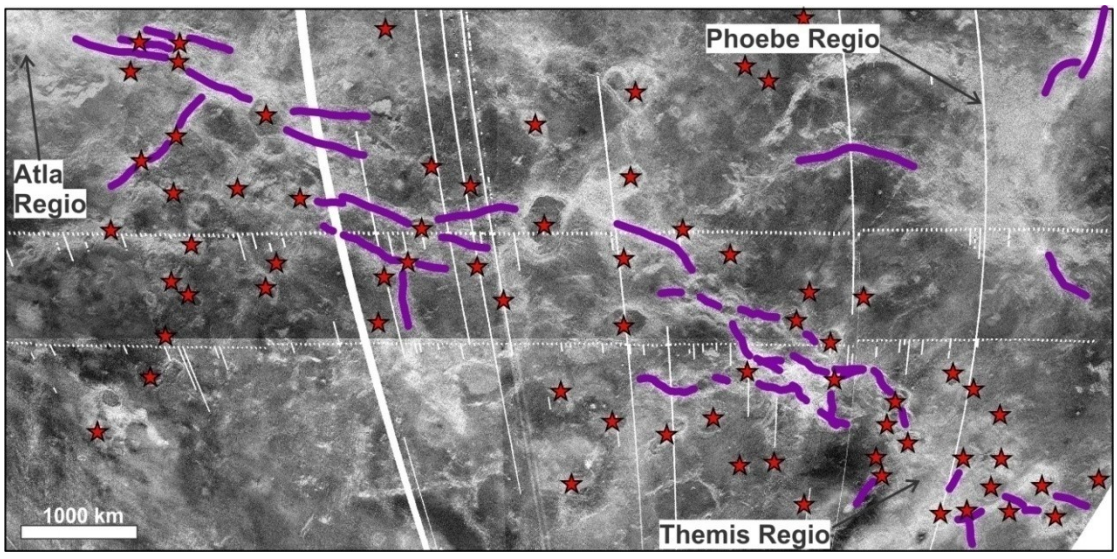

Figure 2.10. Magellan SAR image of Parga Chasma, centred at 245^{o}E, 20^{o}S. Major volcanic structures are identified. Purple lines denote interpreted individual rift segments. Red stars denote centres of IAU catalogued coronae. Basemap source: USGS.

3 Chapter: Methodology

3.1 Magellan Images Used

This research utilizes Magellan SAR, topography, and meter scale slope images to identify and map the tectono-magmatic structures of the study area in detail. Used at the highest resolution available (75 – 100 m/pixel), the SAR images are the most useful dataset. SAR images are greyscale images that utilize pixel brightness to indicate the intensity of radar signal return, due to either surface roughness or the orientation of a structure relative to the incident radar pulse (*Figure 3.1*).

During the later stages of the Magellan mission, measurements were taken of Venus' surface elevation using radar altimetry. This information was then compiled into both topography and meter scale slope images (*Figure 3.2*) at a lower resolution of 3 – 5 km/pixel. When analyzing large-scale areas, this altimetry data is particularly useful to identify vast zones of topographic lows – indicative of rift valleys – and to locate highland mountainous regions and elevated volcanic structures, such as large volcanoes and coronae.

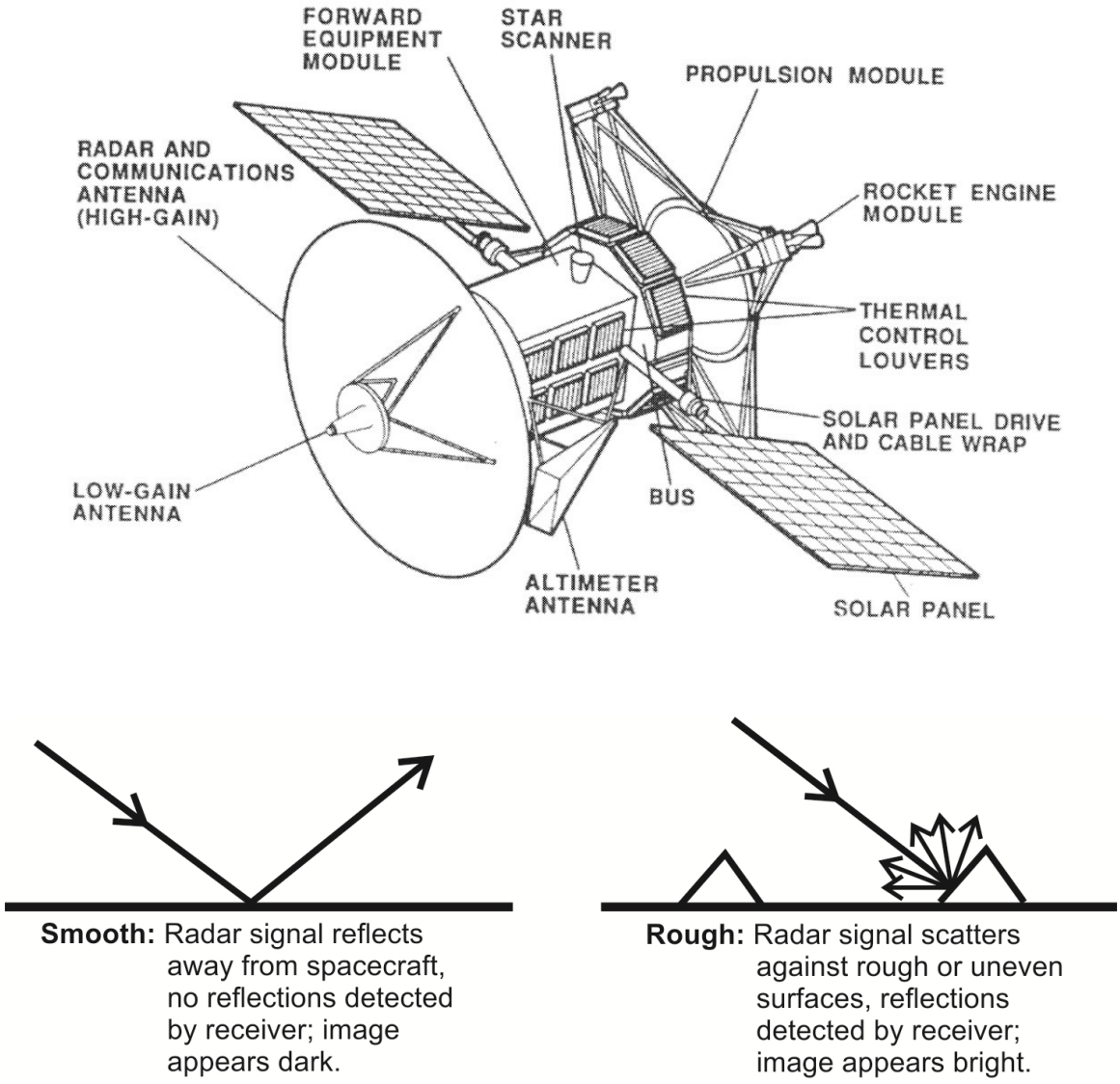

Figure 3.1. (Top) Schematic of the Magellan spacecraft. Source: NASA/JPL. (Bottom) Schematic diagram representing how the emitted microwave radar pulses from Magellan were reflected on various surfaces. Modified from Figure 2 in Leung (2013).

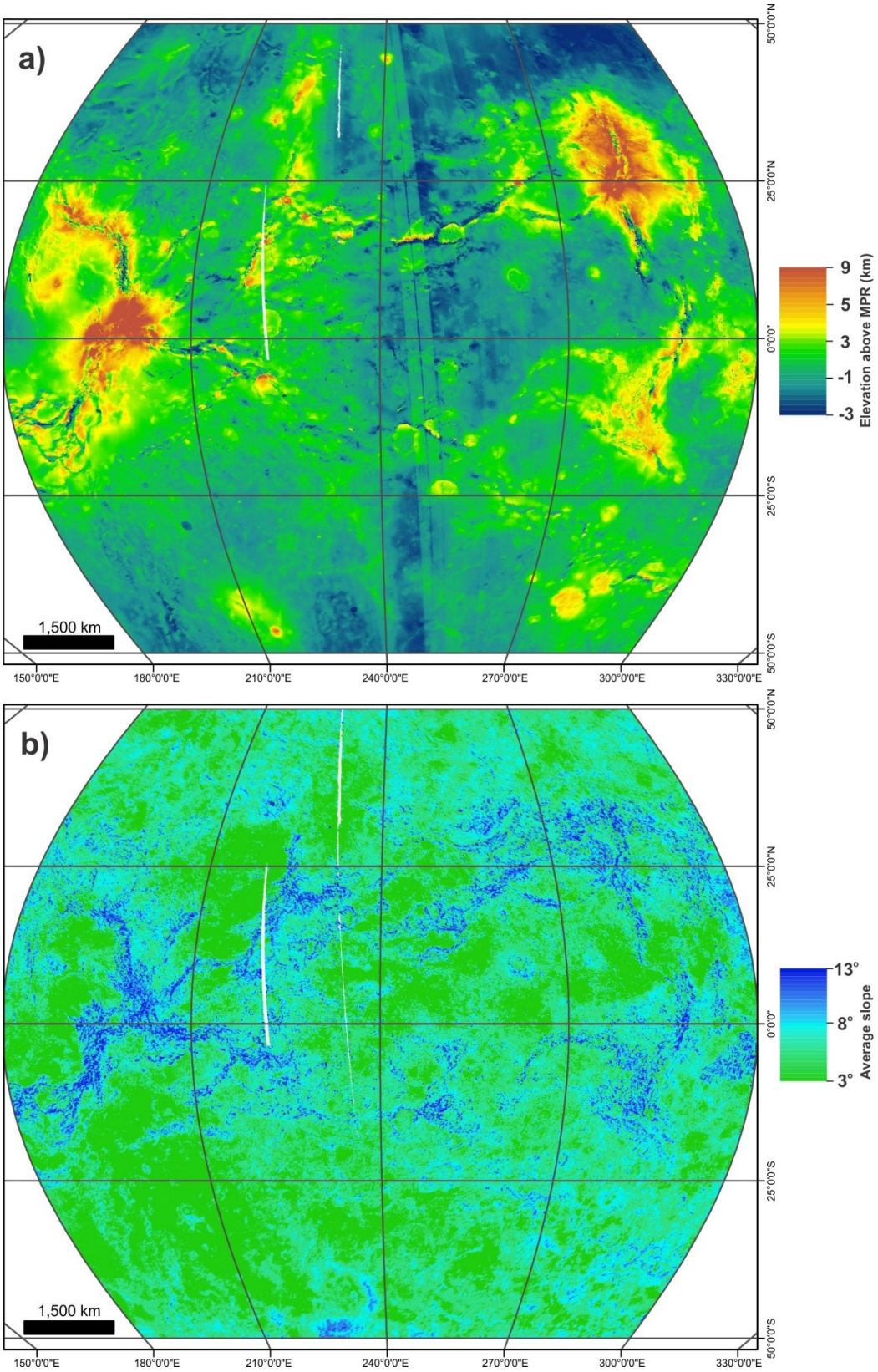

Figure 3.2. Magellan (a) topography and (b) meter scale slope images. Mean Planetary Radius (MPR) = 6051 km. Source: USGS.

3.2 Mapping and Imaging Software

This research was conducted primarily by using ArcGIS software, in particular the ArcMap and ArcCatalog programs (https://www.arcgis.com). All basemap images were imported and displayed in ArcMap 10.3, providing the framework for preliminary observations of large-scale structures and early reconnaissance mapping of a variety of tectono-magmatic structures throughout the southeastern BAT region. The ArcCatalog function allows for the creation of editable layers known as shapefiles, useful for tracing out the detailed radar-bright linework corresponding to tectono-magmatic structures, including graben-fissure systems, rift zones, coronae, and large volcanoes. Within ArcCatalog also lies the function to adjust the geographic coordinate systems of projected data, thereby ensuring all images were projected using the GCS (Global Coordinate System) Venus, as established following the Magellan mission (Davies et al., 1992).

Another function within ArcMap is the ArcToolbox, which is used for applying various edits and manipulations to the basemap images in order to satisfy the appropriate needs of the user during specific tasks. By using some of these specific functions, it was possible to automatically generate a resultant map layer that highlighted all candidate areas for hosting possible rift zones within the BAT region (*Figure 3.3*). This was done by manipulating and combining attributes from topography and slope datasets to highlight the locations of topographic lows and steep slopes, often indicative of zones of rifting (Graff et al., 2015).

Lastly, nearly all images and figures used for this research have been created and often modified using CorelDraw and Corel Photo-Paint software. These manipulations allow for the best possible presentation of figures for this research.

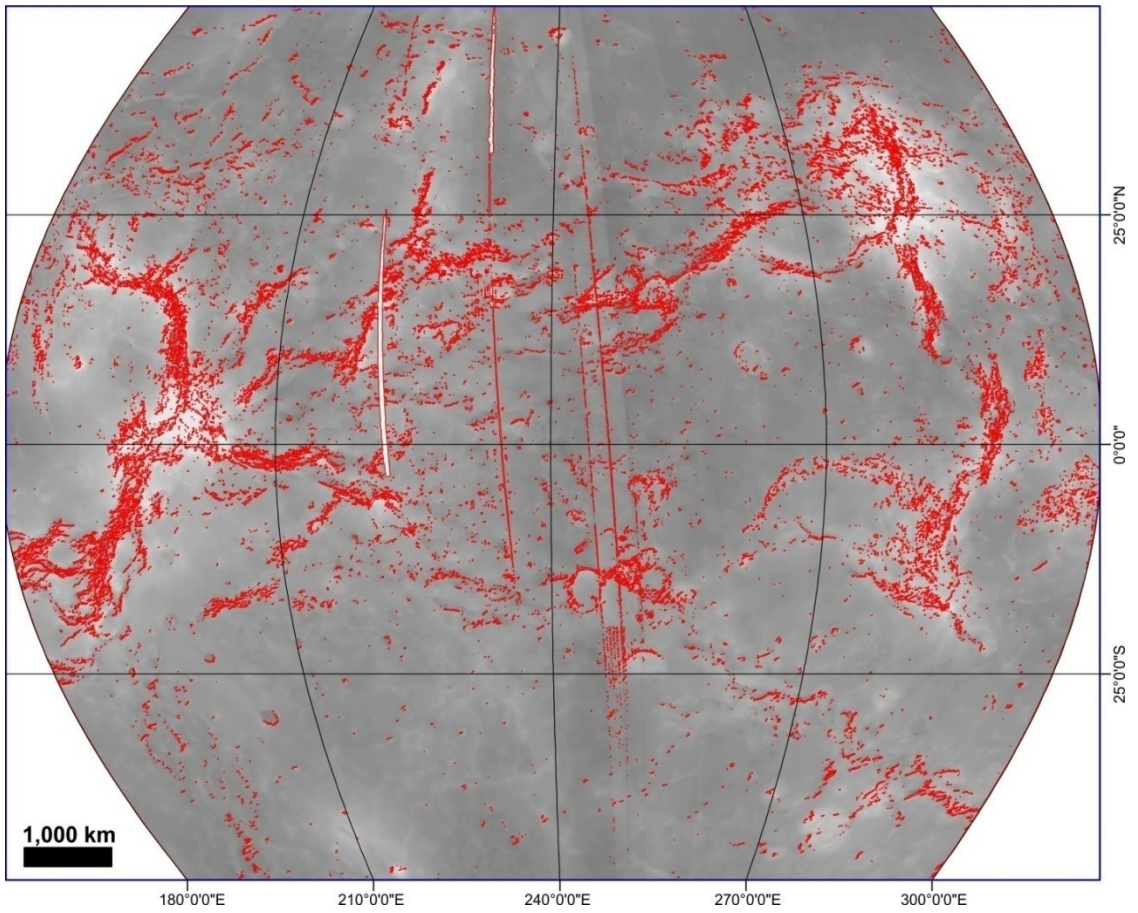

Figure 3.3. Topography map of the BAT region at 30% transparency (source: USGS). Areas in red show the locations of major rift systems as automatically calculated using the ArcMap program. Modified from Figure 1 in Graff et al. (2015).

3.3 Study Area

The overarching goal of this research (Section 1.2) is to identify, map, and analyze the spatial and temporal relationships between rift faults, large volcanoes and coronae, and graben-fissure systems within the BAT region (*Figure 1.3*). Specifically, detailed linework mapping of the extensional lineaments associated with tectono-magmatic structures has been completed within a smaller study area located across both of the Helen Planitia and Themis Regio quadrangles (*Figures 1.3 and 3.4*). Mapping within this smaller area is particularly informative with regards to the first research objective (Section 1.2) as detailed linework and classification of individual graben-fissures into

specific systems are necessary to interpret the relative chronology of magmatic events via analysis of cross-cutting relationships. This allows for temporal comparisons to be drawn between the emplacement of magmatic dyke swarms and the large-scale rifting of Parga Chasma. Parga Chasma (*Figure 2.10*) is a unique structure due to its discontinuous character between Atla and Themis Regiones, in addition to it containing an abundance of coronae, large volcanoes, and graben-fissure systems within close proximity – and of uncertain relationship – to the local and regional rifting.

The detailed study area, located approximately at 260^{o} – 275^{o}E, 25^{o} – 33^{o}S (*Figures 1.3 and 3.4*), contains five coronae as catalogued by the International Astronomical Union (IAU), numerous isolated segments of the Parga Chasma rift zone, and over forty graben-fissure systems (mapped herein), exhibiting radiating, linear, and circumferential geometries. This study area is also situated on the southwestern edge of the regional Parga Chasma rift system, and topography data clearly reveal an elevated plateau bounded on the southern side by a sudden down-dropped fault-like escarpment feature. The orientation of the NW-SE rift fault pattern in this area correlates with the NE-SW regional extension of the large-scale Parga Chasma rifting (Lopez and Hansen, 2008). Regional and local rift faults are grouped under separate layers but both are interpreted to be linked with the formation of Parga Chasma. Local rift faults are linked to separate smaller rift segments interpreted to be focussed on isolated magmatic centres within the study area (Section 5.1).

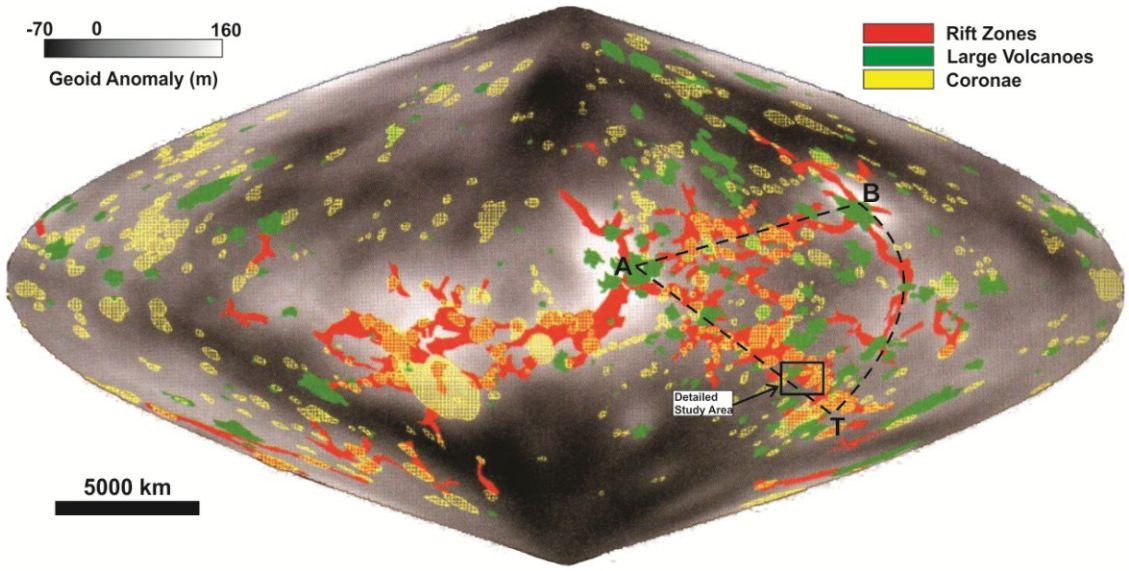

Figure 3.4. Sinusoidal projection of the entirety of Venus' surface (central meridian at 180°E). Major structures, including rift zones, large volcanoes, and coronae are identified. The area confined by the Beta-Atla-Themis (BAT) Region is outlined by dashed lines; the location of the study area is indicated by the open black square. Modified from Figure 2 in Herrick (1999).

3.4 Detailed Linework Mapping

In SAR images, graben are described as having observable floors, fissures are typically narrower than graben lineaments and appear V-shaped, while fractures display unresolved relief. Graben-fissures are formed by extensional stresses during the subsurface propagation of underlying dyke swarms, and they appear as thin sets of radar-bright lineaments, displaying specific illumination dependent on their orientation relative to the radar-looking direction of the orbiting satellite (Grosfils and Head, 1994a,b; Ernst et al., 1995; Ernst et al., 2003; Studd et al., 2011; Graff et al., 2015). When observing graben-fissure lineaments perpendicular to the imaging direction only the far wall of the graben trough will be illuminated, while lineaments parallel to the imaging direction will be illuminated on both walls, often displaying the radar-dark graben floor (*Figure 3.5*).

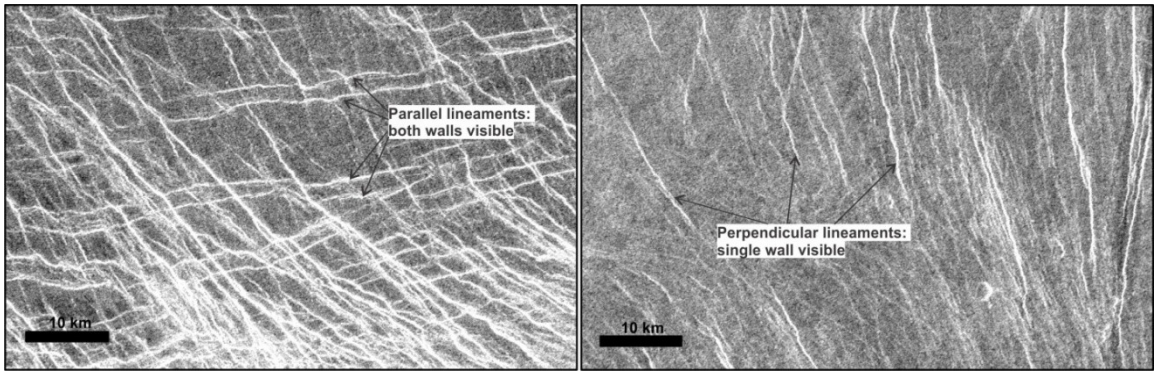

Figure 3.5. Graben-fissure lineament orientations, parallel (left image, centred on 266°E, 27°S) and perpendicular (right image, centred on 273°E, 27°S) to the radar looking direction. Parallel (E-W) lineaments exhibit illumination on both graben-fissure walls and the darkened trough can be observed. Perpendicular (N-S) lineaments have only a single wall illuminated.

This research also involves making a distinction between the radar-bright lineaments associated with rifting from those linked to dyke swarm emplacement (i.e. graben-fissures). This process follows the same approach as outlined in Graff et al. (2014, 2015), who developed criteria for accurate distinction of these morphologically similar features via a combination of qualitative and quantitative attributes.

Firstly, qualitative attributes from topography and slope data can be used to provisionally identify large-scale rift zones by a characteristic signature of topographically low valleys and steeply bounded walls – both of which can be observed on these images (*Figure 3.2*). Secondly, the quantitative characteristics of lineament thickness and sinuosity can also help to distinguish graben-fissures from rift faults. Lineament thickness represents the magnitude of exposed fault offset of either a rift fault or graben-fissure wall. Sinuosity captures the departure from a linear trend and is calculated by taking the ratio of total length measured along the lineament compared to its end-to-end length (*Figure 3.6*). These properties were utilized in the study by Graff et al. (2015), who drew comparisons between Venusian graben-fissures and rift faults with

terrestrial mafic dykes and rift faults from the East African Rift System (e.g. Table 1 and Figure 3 in Graff et al., 2015).

Results show, that in general, rift faults exhibit both larger lineament thicknesses and sinuosity than graben-fissures (Graff et al., 2014, 2015). Using this approach, separate rift segments were provisionally identified based on topographic signature (*Figures 3.2 and 3.3*). Further analysis on SAR images then revealed the presence of densely clustered, thicker, and very sinuous radar-bright lineaments commonly observed in rift zones. Furthermore, the regional rift fault pattern of Parga Chasma extension has also been mapped out – interpreted based on a NW-SE orientation of the corresponding rift faults – following similar procedures used for mapping the local rift faults on SAR images.

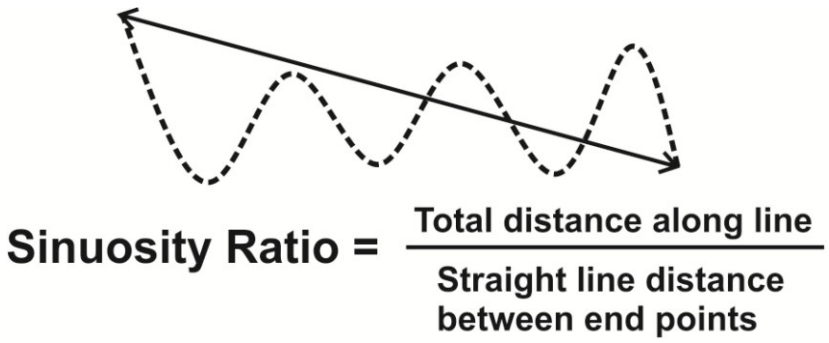

Figure 3.6. (Top) Schematic diagram for obtaining the sinuosity of a lineament by measuring both the total distance along the line and the straight line distance between the end points. (Bottom) Ratio equation for calculating the sinuosity of a lineament.

Lastly, detailed summary maps of the study area (*Figures 4.1 – 4.3*) have been completed that display the following: (1) all graben-fissure systems (radiating, linear, and circumferential); (2) the regional rift fault pattern produced from the regional NE-SW extension of Parga Chasma; and (3) the local rift segments (and associated rift faults) observed to be extending from isolated magmatic centres via triple-junction rifting.

4 Chapter: Tectono-Magmatic History of the Study Area

4.1 Approach

A relative chronology of the events located along a 1500 km section of Parga Chasma was determined predominantly by examining the following: (1) cross-cutting relationships between the lineaments of separate graben-fissure systems; (2) cross-cutting relationships between graben-fissures interacting with local and regional rifting of Parga Chasma; and (3) the effect of young lava flows obscuring the trace of both graben-fissures and/or rift faults (Section 4.2). Cross-cutting between interacting graben-fissures and rift faults is observed in both *direct* and *indirect* ways. Direct interactions result when the lineaments from graben-fissure systems or rift faults are observed to be physically cross-cutting the lineaments belonging to other structures/events (i.e. younger lineaments directly overprinting older lineaments). Indirect interactions result when the lineaments from separate graben-fissure systems are observed to interact with a mutual geologic feature (e.g. a lava flow), but not directly with each other. For example, the graben-fissures from system 'A' are observed extending towards and across a lava flow, while the graben-fissures from system 'B' are observed extending towards the same flow but are abruptly cut and overprinted by it. Despite a lack of direct cross-cutting between the lineaments belonging to the two systems, it can be inferred that system 'A' is younger than system 'B' based on each system's relation to the lava flow.

The relative chronology of graben-fissure system formation was determined for radiating and linear systems; circumferential systems are temporally linked to the formation of an associated centrally located radiating system or geologic structure (i.e. coronae or large volcanoes). Cross-cutting relationships are the primary method of

determining said chronology by analyzing the tectonic deformation caused to older systems via the formation of younger systems. Key characteristics that were observed included the effect of younger system lineaments creating disturbances or discontinuities in the trend of older lineaments. Contrasts in radar backscatter intensity were also observed, often when younger systems overprint older systems.

The distribution of graben-fissure system size (Section 4.2.4) and topographic variation (Section 4.2.5) within the study area was examined by generating histogram and scatter plot diagrams. Lastly, age relationships were assessed via cross-cutting relationships and used to produce a relative chronology (Section 4.3) and summary map (Section 4.4) of system formation relative to the regional rifting of Parga Chasma.

4.2 Overview of Tectono-Magmatic Structures in the Study Area

4.2.1 Extensional Lineaments Interpreted as Graben-Fissures

All extensional lineaments interpreted to represent graben-fissures have been systematically mapped within the designated study area (260 – 275^{o}E and 25 – 33^{o}S). These lineaments were then grouped into 47 separate graben-fissure systems – 28 radiating, 12 linear, and 7 circumferential systems (*Figure 4.1; Tables 4.1 – 4.3*). Within and closely surrounding the study area, more than 11,000 individual graben-fissure lineaments were identified and mapped, with over 10,000 assigned to the 47 grouped systems. The remaining mapped lineaments consist of isolated and/or unassigned sets of graben, fissures, or fractures. These may belong to unidentified radiating, linear, or circumferential systems, or unrecognized distal portions to already grouped systems (cf. Ernst et al., 2003).

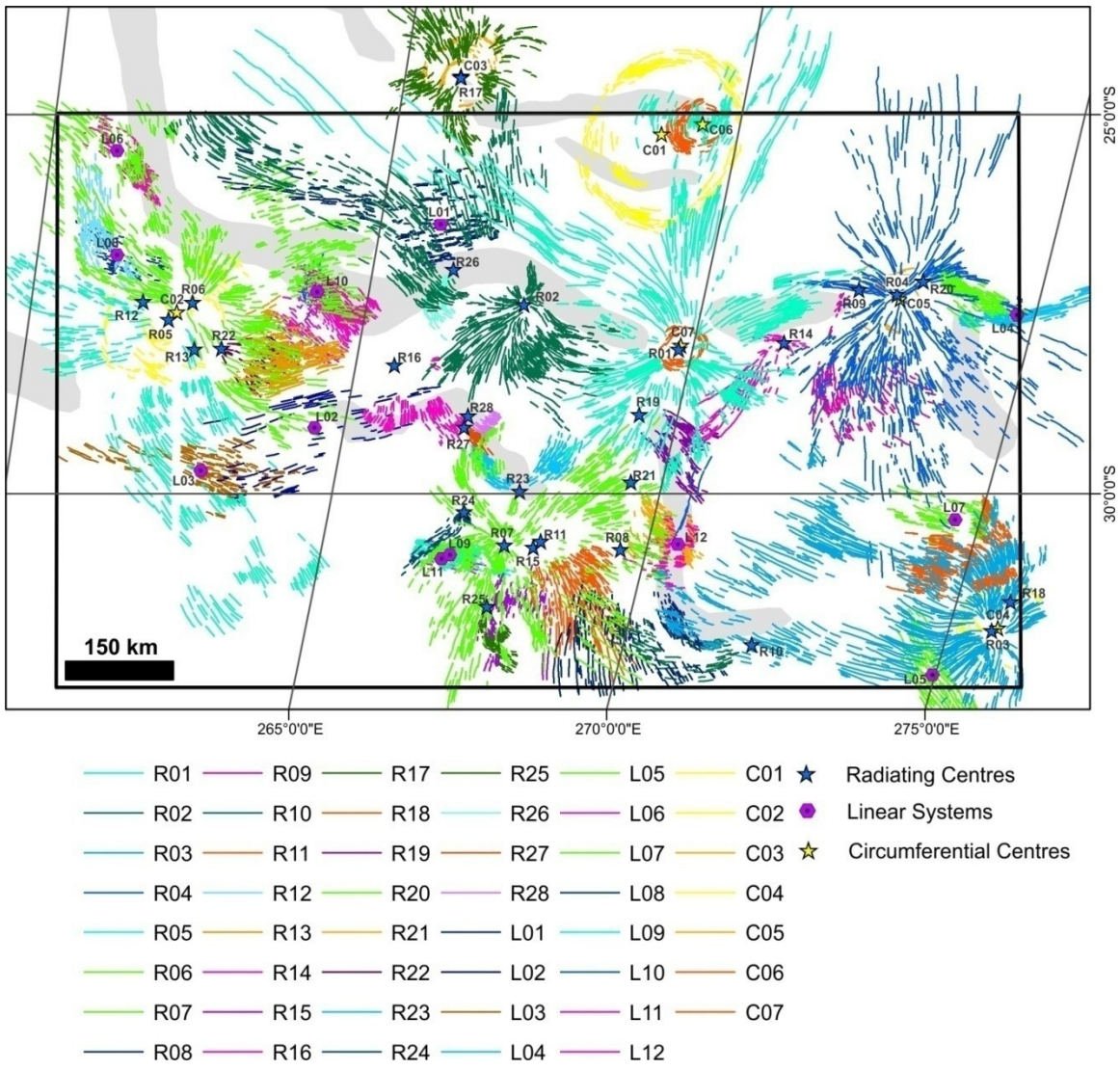

Figure 4.1. Distribution of mapped radiating (R#), linear (L#), and circumferential (C#) graben-fissure systems within the study area. Blue and yellow stars denote centres of radiating and circumferential systems, respectively; purple hexagons indicate central positions of linear systems. Number coding corresponds to the mapped systems that are catalogued in *Tables 4.1 – 4.3*. The location of topographic troughs, coinciding with Parga Chasma, is indicated in grey.

Table 4.1. Properties of the radiating graben-fissure systems mapped in the study area. See text for details on column headings.

System	Longitude (°E)	Latitude (°S)	Max radius (km)	Arc (°)	# of mapped lineaments	Central elevation (km)	Elevation above MPR (km)	Within corona?	Associated Structure
R01	269.75	28.00	747	360	733	6052.9	1.9	Y	Xmukane Corona
R02	267.5	27.50	560	210	763	6051.8	0.8	N	
R03	275.75	31.75	475	190	700	6052.5	1.5	Y	Obiemi Corona
R04	273.00	27.25	471	320	634	6053.2	2.2	N	Ts'an Nu Mons
R05	262.00	28.00	448	50/45	344	6052.5	1.5	Y	Kulimina Corona
R06	262.50	27.50	352	250	711	6052.2	1.2	Y	Kulimina Corona
R07	268.00	30.50	280	335	834	6051.7	0.7	N	
R08	269.50	30.75	232	60	218	6052.2	1.2	N	
R09	272.25	27.25	230	75	162	6052.5	1.5	N	
R10	272.00	32.00	226	40	117	6052.1	1.1	N	
R11	268.25	30.75	221	95	237	6052.3	1.3	N	
R12	261.75	27.50	213	50	136	6052.8	1.8	Y	Kulimina Corona
R13	262.50	28.00	203	90	172	6052.5	1.5	Y	Kulimina Corona
R14	271.25	28.00	203	65/10/5	112	6053.6	2.6	N	
R15	268.25	30.50	197	60	106	6052.3	1.3	N	
R16	265.50	28.25	196	85/70/25	309	6052.4	1.4	N	
R17	266.00	24.50	186	330	391	6051.7	0.7	Y	Chuku Corona
R18	275.75	31.50	175	80	302	6052.6	1.6	Y	Obiemi Corona
R19	269.50	29.00	154	55	122	6051.9	0.9	N	
R20	273.25	27.25	152	85	75	6053.2	2.2	N	
R21	269.50	29.75	148	60	132	6052.2	1.2	N	
R22	263.00	28.00	114	65	63	6052.3	1.3	Y	Kulimina Corona
R23	268.00	23.00	111	60/35	110	6051.7	0.7	N	
R24	267.00	30.00	107	90	74	6052.8	1.8	N	
R25	267.75	31.50	99	60	104	6051.7	0.7	N	Otohime Tholus
R26	266.25	27.00	99	35	85	6051.5	0.5	N	
R27	266.75	29.00	57	40	38	6051.9	0.9	N	
R28	267.00	23.00	46	70	38	6051.9	0.9	N	

Table 4.2. Properties of the linear graben-fissure systems mapped in the study area. See text for details on column headings.

System	Longitude (°E)	Latitude (°S)	Length x width (km)	# of mapped lineaments	Central elevation (km)	Elevation above MPR (km)	Within corona?	Associated structure
L01	266.00	26.50	393 x 148	248	6052.7	1.7	N	
L02	264.50	29.00	343 x 134	87	6052.4	1.4	N	
L03	263.00	29.75	341 x 104	133	6052.5	1.5	N	
L04	273.75	27.75	195 x 43	79	6052.3	1.3	N	
L05	274.00	31.50	187 x 73	122	6052.0	1.0	Y	Obiemi Corona
L06	260.25	25.25	164 x 56	119	6052.9	1.9	N	
L07	275.50	30.50	152 x 54	194	6052.2	1.2	Y	Gertjon Corona
L08	262.25	27.00	150 x 54	84	6052.6	1.6	Y	Kulimina Corona
L09	266.25	30.50	143 x 58	236	6051.6	0.6	N	
L10	264.25	26.75	108 x 54	82	6051.8	0.8	N	
L11	266.25	30.75	92 x 40	49	6051.7	0.7	N	
L12	271.25	31.00	88 x 107	157	6052.5	1.5	N	

Table 4.3. Properties of the circumferential graben-fissure systems mapped in the study area. See text for details on column headings.

System	Longitude (°E)	Latitude (°S)	Max radius (km)	Arc (°)	# of mapped lineaments	Central elevation (km)	Elevation above MPR (km)	Within corona?	Associated structure
C01	269.00	25.25	138	360	273	6052.1	1.1	Y	Hervor Corona
C02	262.25	27.50	121	130/90	89	6052.6	1.6	Y	Kulimina Corona
C03	265.75	24.50	75	320	119	6051.7	0.7	Y	Chuku Corona
C04	275.75	31.75	74	280	45	6052.6	1.6	Y	Obiemi Corona
C05	273.00	27.50	70	300	30	6053.3	2.3	N	Ts'an Nu Mons
C06	269.50	25.25	52	330	97	6051.3	0.3	Y	Hervor Corona
C07	269.75	28.00	39	340	34	6052.9	1.9	Y	Xmukane Corona

All grouped graben-fissure systems were catalogued using a code-designated numbering system: R# for radiating systems (*Table 4.1*); L# for linear systems (*Table 4.2*); and C# for circumferential systems (*Table 4.3*). Physical characteristics for all systems were also obtained, including: maximum radius (for radiating and circumferential systems) or length and width (for linear systems); system arc angle (for radiating and circumferential systems); number of mapped lineaments; and the central elevation. Also indicated for each system is whether or not it is located within a corona, or associated with an IAU catalogued geologic structure (i.e. corona, large volcano, etc.). Maximum radius is measured from the centre of a radiating or circumferential system to its farthest identified lineament; while the maximum length and width of a linear system are measured across the entire set of mapped lineaments. The arc of radiating and circumferential systems captures the overall amount of angular spread created by the collection of mapped lineaments (*Figure 4.2*). The central elevation was obtained from the Magellan topography data, which provided the planetary radius at the interpreted system centre. This elevation value was also calculated as an elevation above Mean Planetary Radius (MPR) by subtracting 6051 km (Venus' MPR value – analogous to Earth's sea level).

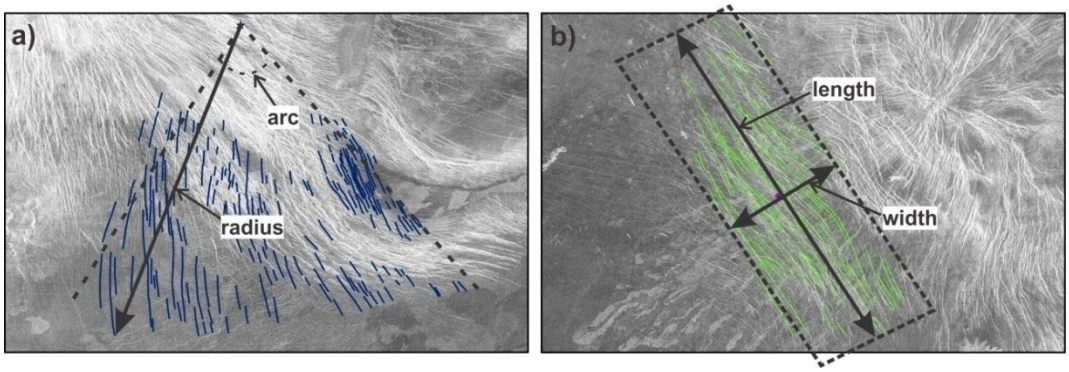

Figure 4.2. Process of measuring (a) the maximum radius and arc of a radiating system, and (b) the length and width of a linear system. Examples shown for systems R08 (*Table 4.1*) and L05 (*Table 4.2*).

4.2.2 Extensional Lineaments Interpreted as Rift Faults

Extensional lineaments associated with rifting along Parga Chasma were also mapped. Regional rift faults are situated in a NW-SE orientation and are associated with the overall regional NE-SW extension of Parga Chasma (catalogued as *RF01*). Local rift faults are distinguished from regional when they are observed as separate rift segments extending from individual magmatic centres. In the study area there are 11 local rift segments (catalogued as *RF02 – RF12*). However, as both of these lineament groups (regional and local) are interpreted to be rift-related, they exhibit similar morphologies on SAR images, including high radar-brightness, thickness, and sinuosity (Section 3.4). Within the study area over 1,500 rift-related lineaments were systematically mapped, corresponding to 1,016 local rift faults and 633 regional rift faults (*Figure 4.3*).

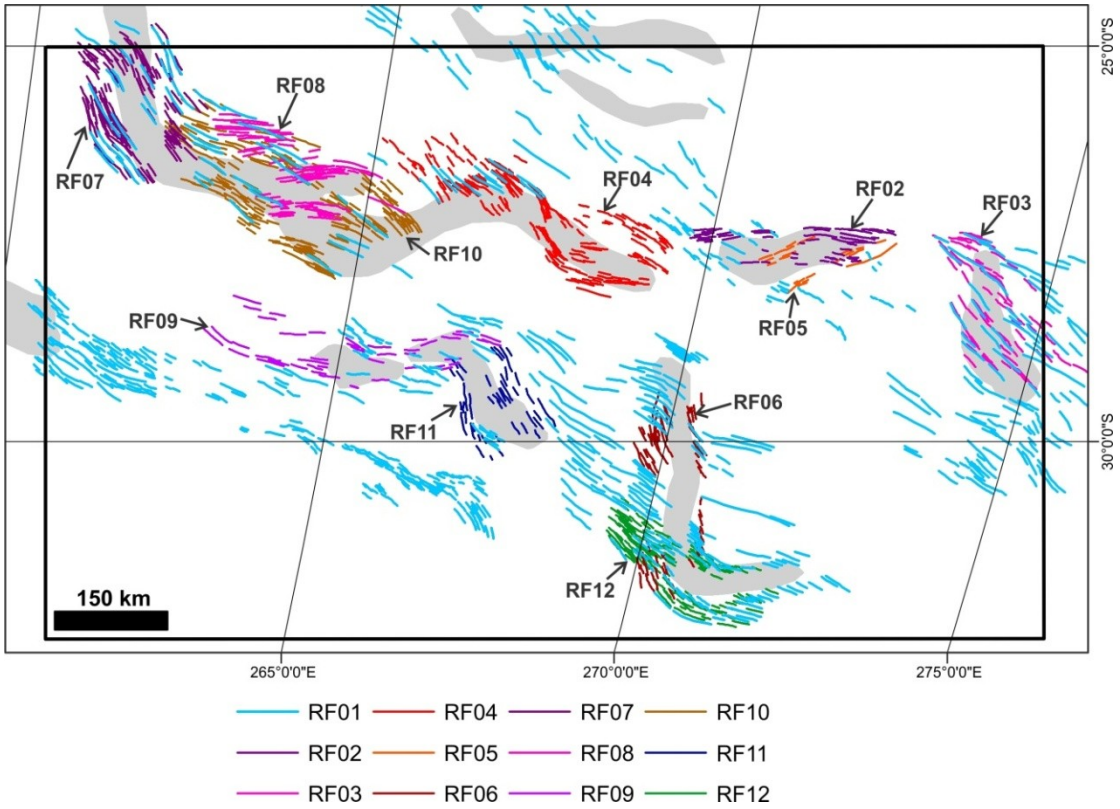

Figure 4.3. Distribution of rift-related lineaments within the study area. Topographic troughs are indicated in grey (Section 3.4).

4.2.3 Descriptions of Most Significant Graben-Fissure Systems

Within the study area, there are notable locations that are host to multiple graben-fissure systems and/or contain major geologic structures (i.e. coronae, large volcanoes, etc.). Specifically, ten of these notable locations have been selected (*Figure 4.4*) as representations of either the largest or most densely populated graben-fissure systems in the study area, or as locations of major geologic structures that often host a dense clustering of rift faults and/or multiple graben-fissure systems. These locations will herein be discussed in greater detail describing the physical characteristics, morphologies, and tectonic setting (where possible) of these notable graben-fissure systems and geologic structures. Also discussed will be cross-cutting relationships between interacting graben-fissure systems – later used to produce a relative chronology timeline (Section 4.3) and summary map (Section 4.4).

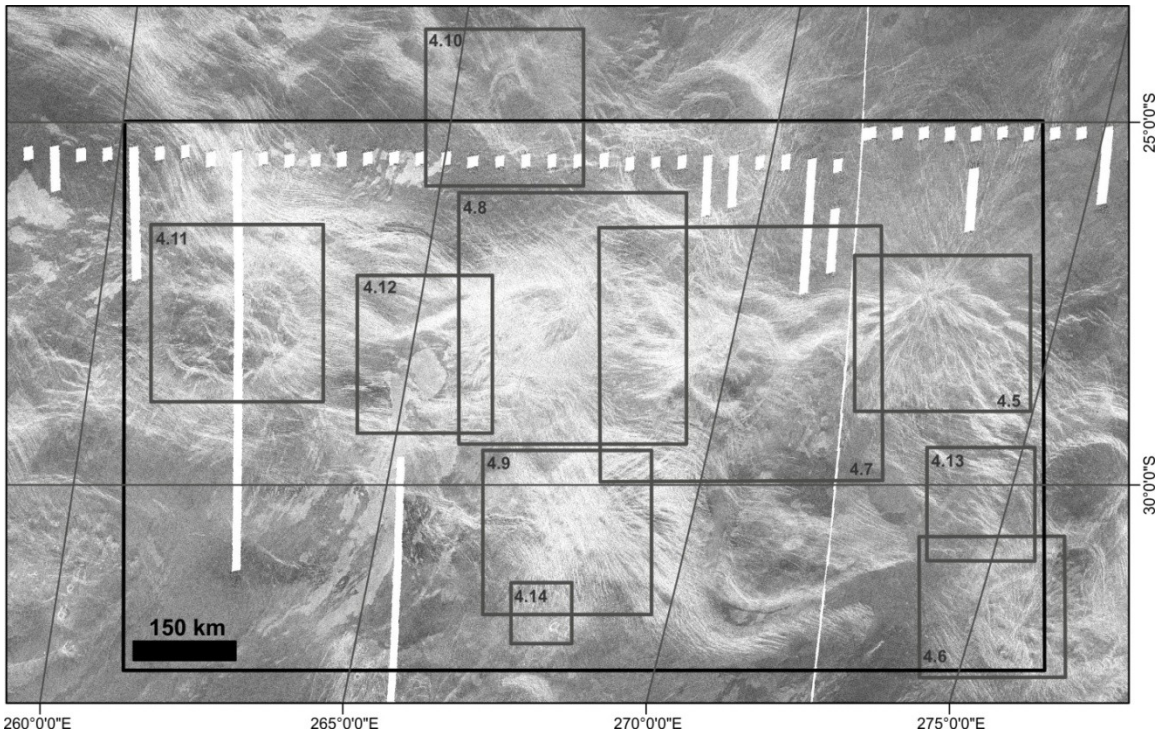

Figure 4.4. Designated locations for subsequent figures (*4.5 – 4.14*).

4.2.3.1 Systems R04, R09, R20: Ts'an Nu Mons

Ts'an Nu Mons (272.75°E, 27.25°S) is a large volcano, 310 km in diameter (*Figure 4.5*), in the northwestern corner of the V-53 Themis Regio quadrangle (270° – 300°E, 25° – 50°S). It reaches an elevation of 2.8 km above Mean Planetary Radius (MPR) and 1.6 km above the surrounding volcanic plains material composed of intermediate radar backscatter flow units, likely formed from the volcanic edifice itself (Stofan and Brian, 2012). Assuming that this large volcano is associated with a mantle plume, then domal uplift is expected and could result in local triple-junction rifting, creating two rift arms – one trending west (RF02) towards Xmukane Corona (and system R01); the other trending south-southeast (RF03) towards Gertjon Corona (and system L07) (*Figure 4.3*). These rift arms are associated with topographic troughs that also contain dense clusters of thick and sinuous radar-bright lineaments trending from Ts'an Nu Mons. The rift faults comprising the south-southeast trending rift arm towards Gertjon Corona are observed to be following previously established regional rift faults (RF01), produced from the large-scale regional NE-SW extension of Parga Chasma (Martin et al., 2007; Lopez and Hansen, 2008; Stofan and Brian, 2012). Both the regional and local rift fault lineaments (Section 4.2.2) are interpreted to be rift-related (associated with the overall formation of Parga Chasma). However, cross-cutting is observed between these prominent rift faults (local and regional) at the detailed scale of this mapping, resulting in the observation that the local rifting events – interpreted to be linked to separate magmatic centres (e.g. Ts'an Nu Mons) – are distinct from the older rifting associated with regional extension. Within the areal extent of Ts'an Nu Mons lie the radiating graben-fissure systems R04, R09, and R20.

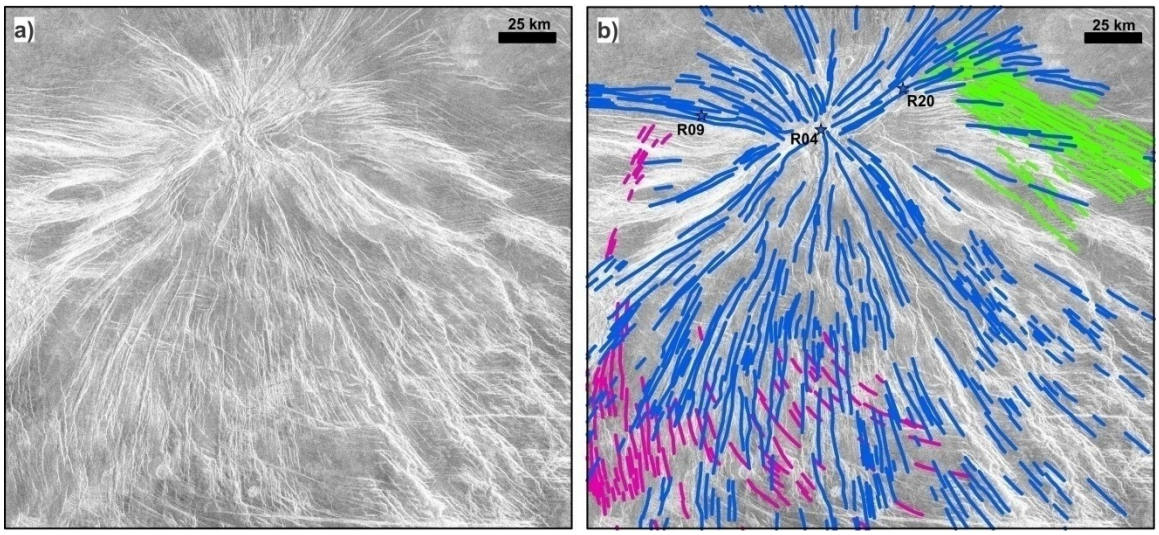

Figure 4.5. Graben-fissure systems R04 (blue), R09 (pink), and R20 (light green); Ts'an Nu Mons is situated surrounding the centre of R04. (a) Magellan SAR image. (b) SAR image superimposed with mapped systems. Graben-fissures from system R04 cut across those of R09 and R20, and are interpreted as being younger. See *Figure 4.4* for image location.

4.2.3.1.1 System R04

System R04 is a radiating graben-fissure system centred at 273°E, 27.25°S, and situated roughly 30-50 km southwest from the central high point of Ts'an Nu Mons (*Figure 4.5*). Due to its spatial proximity to the centre of Ts'an Nu Mons it is likely a product of the same underlying mantle source. It is interpreted to have been emplaced after the main constructional phase of the volcano and subsequent lava flow units, due to the graben and fissures that cross-cut the surrounding plains. This system contains 634 mapped lineaments of graben-fissures, with a maximum observed radius of 471 km, a near-perfect arc of 320°, and is elevated 2.2 km above MPR.

Systems directly interacting with R04 include: R01 (Xmukane Corona), R03 (Obiemi Corona), R09, R18, R20, L04, and L07, in addition to lineaments from both local (RF02, RF03) and regional (RF01) rifting (*Figure 4.3*). Age relationships are inferred between systems R04 and R14, as only indirect interactions are observed. Analysis of cross-cutting relationships between interacting graben-fissure systems reveals

R04 to be among the youngest based on well defined cross-cutting by many graben-fissure lineaments belonging to R04. However, ambiguous cross-cutting is observed between some interacting graben-fissures of systems R04 and R01, and so a degree of synchroneity between these systems is inferred.

Graben-fissures from R04 extend to within the radial extent of system R14, but direct cross-cutting between the lineaments is not observed, therefore relative age relationships can only be inferred from indirect interactions. The formation of Ts'an Nu Mons and subsequently system R04 itself is interpreted as the source point for local triple-junction rifting. System R14 is observed to cross-cut some of the surrounding plains material and the local rift faults, and is therefore inferred to be younger or partially synchronous to R04.

Due to its genetic link to the formation of Ts'an Nu Mons, system R04 is interpreted as coeval with the local rift faulting (RF02, RF03), but is observed to cross-cut the older regional NW-SE rift fault pattern (RF01) (*Figure 4.3*). Some cross-cutting is observed between the graben-fissures from R04 and the rift faults comprising the local south-southeast trending rift segment (RF03), however, this local rift segment follows the same orientation as the regional rift fault pattern (RF01), resulting in some ambiguity in the observed interactions.

4.2.3.1.2 System R09

System R09 is also a radiating system, centred at 272.25^{o}E, 27.25^{o}S, on the western flank of Ts'an Nu Mons, 53 km west of the centre of system R04. System R09 is elevated 1.5 km above MPR, consists of 162 mapped lineaments, has a maximum observed radius

of 230 km, and an arc of 75^{o} opening to the south. R09 is observed as an older system that is cross-cut by graben-fissures of R04, as well as both local (RF02, RF05) and regional (RF01) rift faulting. R09 displays a slightly arcuate geometry and may instead represent a small annular portion of an old or possibly cryptic circumferential graben-fissure system, unrelated to the formation of Ts'an Nu Mons.

4.2.3.1.3 System R20

System R20 is a radiating system located on the eastern flank of Ts'an Nu Mons, centred at 273.25^{o}E, 27.25^{o}S, and 40 km northeast of system R04. System R20 is 2.2 km above MPR, consists of 75 mapped lineaments, and forms a maximum observed radius of 152 km with an arc of 85^{o} opening to the southeast. System R20 interacts with graben-fissures from systems R04 and L04, and is observed to be cross-cut by both. Cross-cutting relationships reveal R20 to predate both the adjacent rift faulting (RF01, RF03) and the surrounding flooded plains material, within which the radar brightness of the lineaments diminish as they are covered by lava flows.

4.2.3.2 Systems R03, R18, L05: Obiemi Corona

Obiemi corona (*Figure 4.6*) is an obliquely shaped ellipsoidal corona in the southeast corner of the study area. It is situated in the northwest of Themis Regio and centred at approximately 276^{o}E, 31.75^{o}S. It features a maximum and minimum diameter of 276 km and 182 km, respectively. Obiemi corona has experienced a high amount of deformation, resulting in a heavily fractured interior rim with very sinuous and obliquely oriented circumscribing fractures; the observed exterior rim lacks well defined circumscribing fractures. This corona is spatially associated with graben-fissure systems R03, R18, and L05. System R03 is interpreted to be genetically related to the corona

formation, but is centred 21 km west of the Obiemi corona centre. Additionally, a smaller subcentre is located 12 km south of the R03 centre, containing prominent graben-fissures with possible genetic association to the formation of either or both system R03 and Obiemi Corona.

4.2.3.2.1 System R03

System R03 is a radiating system centred at 275.75°E, 31.75°S, approximately 21 km west of the centre of Obiemi Corona. A total of 751 lineaments have been mapped, exhibiting a maximum radius of 475 km and an arc of at least 330°; the remaining portion is outside the study area to the east and was not mapped (*Figure 4.6*). System R03 is elevated 1.5 km above MPR and interacts with many other mapped systems, including: R04, R08, R10, R18, L05, L07, L12, and a number of lineaments associated with both local (RF12) and regional (RF01) rifting of Parga Chasma (*Figure 4.3*). Observed to be cross-cut by most of the aforementioned systems, R03 is interpreted to be an older system that is also cut by regional (RF01) rifting. System R18 is observed as older or partially synchronous to R03, and is likely a precursor event to the corona-forming event and to the larger system R03. R03 is also observed to be either younger or partially synchronous to linear system L07.

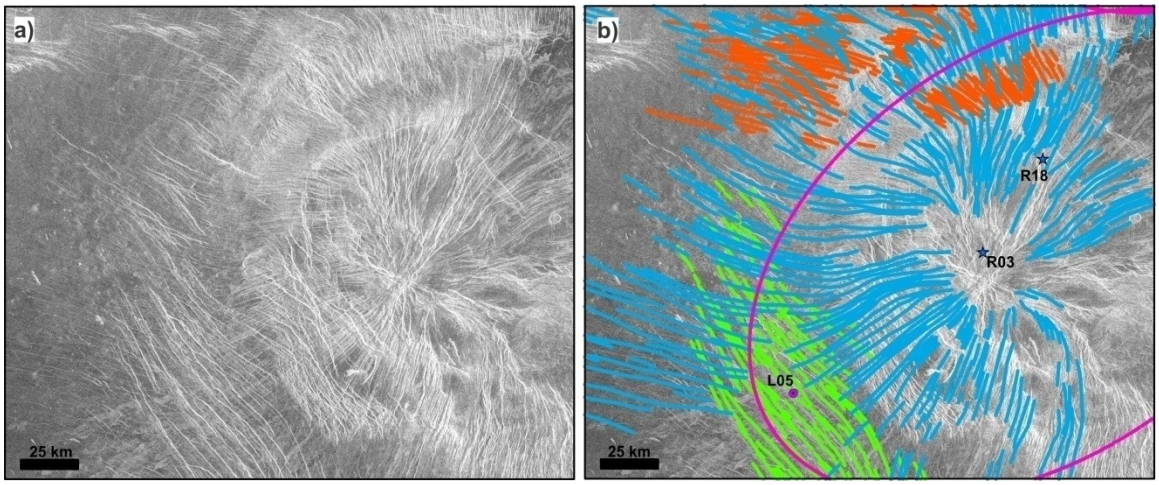

Figure 4.6. Graben-fissure systems R03 (light blue), R18 (orange), and L05 (light green); the rim of Obiemi Corona is outlined in magenta. (a) Magellan SAR image. (b) Image superimposed with mapped systems. Graben-fissures from R03 display a younger to synchronous cross-cutting relationship with R18, but are clearly cut by L05, interpreted as the youngest of the three. See *Figure 4.4* for image location.

4.2.3.2.2 System R18

System R18 is a small radiating system centred at 275.75^{o}E, 31.5^{o}S, near system R03. It extends outward to the northwest, but becomes completely flooded within the western plains after extending 175 km from its centre. System R18 consists of 302 mapped lineaments, with an arc of 80^{o} opening towards the northwest, and is elevated 1.6 km above MPR – likely a result of being situated near the raised rim of Obiemi Corona. System R18 directly interacts with systems R03, R04, and L07, and indirectly with L05. Cross-cutting relationships reveal R18 to be older than systems R03, R04, and L07. It is interpreted to also be older than system L05 as the observed cross-cutting relationships reveal that the development of Obiemi Corona preceded the formation of L05, but occurred after the formation of R18. System R18 is also covered extensively by lava flows interpreted to have originated from Obiemi Corona, providing further evidence of its earlier formation.

4.2.3.2.3 System L05

System L05 is a small linear system that passes through the southwestern flank of Obiemi Corona. System L05 may also be an extended portion of a larger graben-fissure system associated with Rigatona Corona, located to the southeast of Obiemi Corona and outside of the study area. System L05 contains 122 mapped lineaments, a maximum length of 187 km, and a width of 73 km. System L05 interacts only directly with system R03 and indirectly with system R18. Cross-cutting relationships reveal it to be younger than Obiemi Corona, and therefore younger than both systems R03 and R18. Graben-fissures of system L05 are also observed to clearly cross-cut the lineaments of these other systems, as well as the majority of the flooded plains and corona annulus material, indicating later formation.

4.2.3.3 System R01 and Xmukane Corona

Centred almost exactly on the borders between the V-52 and V-53 quadrangles of Helen Planitia and Themis Regio, respectively (270^{o}E, 28.25^{o}S), Xmukane Corona displays a near perfect circular geometry with a diameter of 140 km (*Figure 4.7*). It is located at the centre of a flooded rift valley and interpreted to be the locus of triple-junction rifting, producing individual rift segments extending in three directions: northwest (RF04), east-northeast (RF05), and south (RF06) (*Figure 4.3*).

The northwest rift segment (RF04) propagates sinuously towards system R02, and displays the characteristic normal faulting expected with rifting, but also displays transtensional characteristics by exhibiting a component of strike-slip faulting 250 km away from Xmukane Corona. This strike-slip component (observed as right-lateral or dextral) can be seen in the deformational offset pattern within the linear swarm of system

L01, to the northwest of system R02 (*Figure 4.8*). The trend of this rift segment is also interpreted to have been deformed around the eastern flank of system R02 due to local compressional stresses associated with the crustal relaxation (e.g. see model shown in Figure 8 in Lopez et al., 2008) beneath R02. This is observed in the rift fault pattern (RF04) as it exhibits different local trends along the length of the single rift segment, notably when observed to veer around the structure of system R02 (*Figures 4.3 and 4.8*).

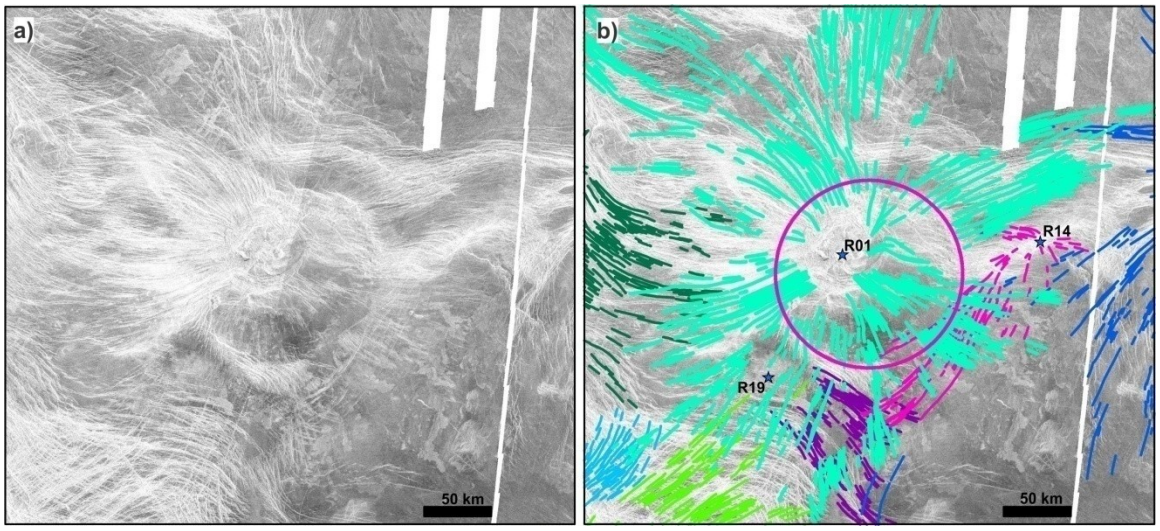

Figure 4.7. Graben-fissure systems R01 (turquoise), R02 (dark green), R04 (blue), R07 (light green), R14 (pink), R19 (purple), and R23 (light blue); the rim of Xmukane Corona is outlined in magenta. (a) Magellan SAR image. (b) SAR image superimposed with mapped systems. Graben-fissures from R01 cut across those from systems R02, R07, and R23, but are cut by graben-fissures from R04, R14, and R19. Some overlap in timing is observed to exist between systems R01, R02, R04, and R07. See *Figure 4.4* for image location.

The valley to the northeast of Xmukane Corona consists of a combination of the east-northeast rift segment (RF05) from Xmukane Corona, and the western rift segment (RF02) from Ts'an Nu Mons 300 km to the northeast (*Figures 4.3 and 5.3*). This interpretation comes from the detailed mapping of the rift fault lineament pattern and the appearance of two distinct trends contained within a single rift valley. The orientation of this rift valley is also oblique to the regional rift fault pattern associated with the regional extension of Parga Chasma.

The southern rift segment (RF06) contains a complex set of fault lineament orientations that is interpreted to consist of a combination of both the local and regional rift fault patterns (*Figure 4.3*). The formation of the local rift segment is likely a younger event compared to the regional rifting of Parga Chasma, because this local rift valley is almost completely flooded, obscuring the traces of nearly all radar-bright lineaments within, including local and regional rift faults, and graben-fissures.

4.2.3.3.1 System R01

Radiating system R01 (*Figure 4.7*) is centred at 269.75°E, 28°S, 24 km northwest of the centre of Xmukane Corona, and elevated 1.9 km above MPR. R01 consists of 733 mapped lineaments, extending as far as 747 km from their source centre, with a complete radial arc of 360°. There is also a small and confined system of circumscribing fractures surrounding the centre of R01, but offset from the corona centre – possibly associated with an interior rim of Xmukane Corona. R01 interacts directly with systems R02, R04, R07, R14, R17, R19, R23, L01, and indirectly with R21. Cross-cutting relationships reveal R01 to be younger than systems R02, R07, R23, L01, and regional rifting (RF01), but older than systems R04, R14, R17, R19. Graben-fissures from R01 and R21 both extend through the flooded southern rift valley, however, the graben-fissures from R21 are observed to be completely flooded, while the graben-fissures from R01 are only partially flooded. These lava flows are interpreted to be associated with Xmukane Corona, following the formation of the southern rift segment, which is also observed to cut across system R21, further leading to the interpretation of an earlier emplacement of R21. Graben-fissures from system R01 are also interpreted to be younger than the formation of Hervor Corona to the north (*Figure 4.1*), as many lineaments extend nearly

uninterrupted across the corona, in addition to cross-cutting a series of fractures circumscribing multiple annuli locations within Hervor Corona. Additionally, some graben-fissures from R01 are observed to be propagating within some circumferential fractures of Hervor Corona when their respective trends match up, providing further evidence of younger graben-fissures following previously established fracture zones.

4.2.3.4 System R02

System R02 is centred at 267.5°E, 27.5°S and elevated at 0.8 km above MPR. R02 contains 730 mapped lineaments, a maximum radius of 560 km, and an arc of 260°. Its arc may extend further towards the east, but the lineament trace becomes obscured by early lava flooding, graben-fissures from R01, and the local rift faults from the adjacent rift segment (RF04). R02 (*Figure 4.8*) interacts directly with systems R01, R06, R16, R26, L01, local (RF04, RF07 – RF10) and regional (RF01) rifting (*Figure 4.3*), and indirectly with system R17. The structure associated with R02 was likely in the gravitational relaxation stage producing local compressional stresses during local rift formation (e.g. see model shown in Figure 8 in Lopez et al., 2008), thereby causing the northwestward propagating rift segment from Xmukane Corona to veer around the structure of R02, and also leading to a right-lateral (dextral) strike-slip component within system L01 to the north of R02. Cross-cutting relationships reveal system R02 to be older than R01, R06, and RF04. Synchroneity is observed between R02 and the remaining local rift faults (RF07 – RF10). Graben-fissures from system R02 are observed to cross-cut those from systems R26 and L01, with synchroneity observed between R02 and R16 based on ambiguous cross-cutting relationships. Despite a lack of direct cross-cutting between R02 and R17, age relationships are inferred based on the age relationship

between R01 and R17. R01 is observed to cross-cut R02, but gets cross-cut by R17, and therefore, R02 is inferred to be older than R17.

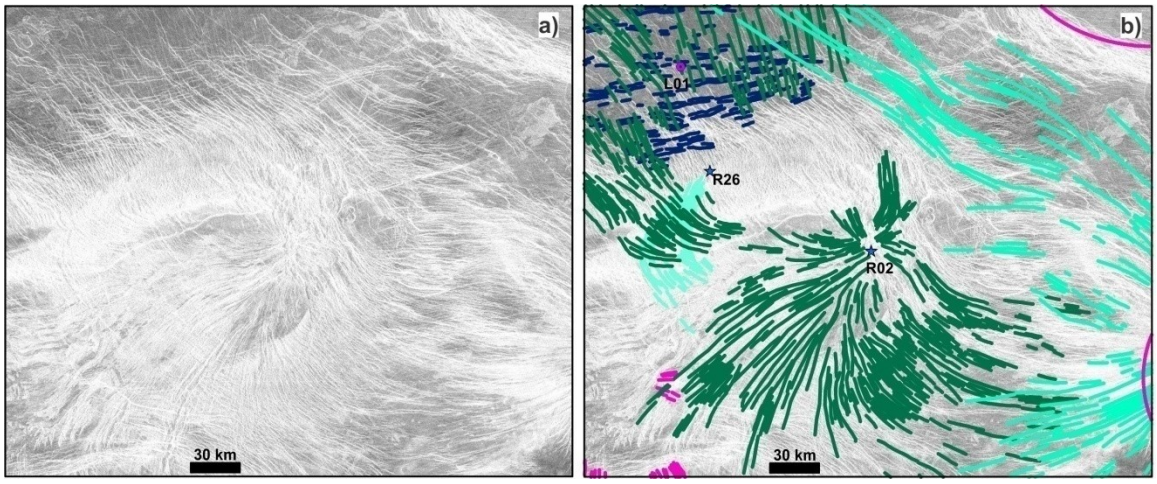

Figure 4.8. Graben-fissure systems R01 (turquoise), R02 (dark green), R16 (pink), R26 (aqua), and L01 (dark blue). (a) Magellan SAR image. (b) SAR image superimposed with mapped systems. Graben-fissures from R02 cross-cut those of R26 and L01, are synchronous with R16, and are cut by R01; R26 is observed to be the oldest of the five. See *Figure 4.4* for image location.

4.2.3.5 Systems R07, R11, R15, R23, R24, L09, L11

Collectively, the centres of graben-fissure systems R07, R11, R15, and R23 all fall within the spatial proximity of a hypothesized major mantle upwelling zone, providing a magma source for these multiple systems (*Figure 4.9*). There are also two interpreted rift segments (based on the local rift fault pattern) located to the northwest (RF11) and southeast (RF12) (*Figure 4.3*) of these graben-fissure systems – all of which are interpreted to have been formed from this underlying mantle upwelling. Within this broad zone of magmatism, there is a very dense clustering of radar-bright lineaments and an overall high radar backscatter signal throughout, indicating a high amount of tectono-magmatic activity. Some of these interpreted rift faults may also be linked to the magmatic centre of system R16, or could be linked to the regional extension of Parga Chasma, as they follow the NW-SE orientation of the regional rifting pattern (RF01).

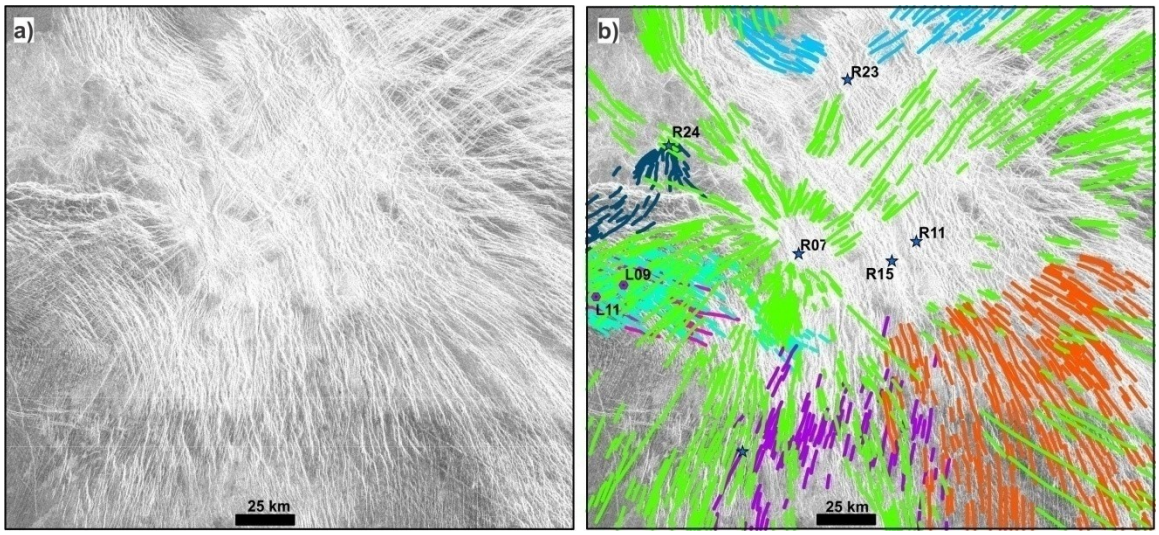

Figure 4.9. Graben-fissure systems R07 (light green), R11 (orange), R15 (purple), R23 (light blue), R24 (dark blue), L09 (turquoise), and L11 (pink). (a) Magellan SAR image. (b) SAR image superimposed with mapped systems. The dense clustering and abundance of radar-bright lineaments lead to the interpretation of a large mantle source underlying these graben-fissure systems. R07 cross-cuts systems R15, L09, and L11, and exhibits synchroneity with systems R23 and R24. R11 cross-cuts R07, thus is interpreted as the youngest. See *Figure 4.4* for image location.

4.2.3.5.1 System R07

System R07 is centred at 268°E, 30.5°S, 78 km south-southwest of R23 and similarly elevated at 0.7 km above MPR. R07 is much larger than R23, featuring a maximum radius of 280 km, with an arc of 335°. R07 also contains the highest number of mapped lineaments of all mapped systems in the study area at 834. This system is observed to be the largest magmatic pulse from the underlying mantle source beneath systems R07, R11, R15, R23, R24, R28, L09, and L11 (*Figure 4.9*). R07 interacts directly with neighbouring systems R01, R03, R08, R10, R11, R15, R23, R24, L09, L11, L12, and indirectly with R19 to the northeast. R07 is observed to be older than R07 and R11, and younger than systems R03, R10, R15, R23, R24, R28, L09, L11, and L12, with some partial synchroneity observed with R08 and R01. Despite a lack of directly observed cross-cutting relationships, R07 is inferred to be partially synchronous with R19 based on the age relationship between R01 and R19 (Section 4.2.3.3.1).

4.2.3.5.2 System R11

Centred at 268.25°E, 30.75°S, system R11 is only 40 km northeast of R15, and is interpreted to be the youngest pulse from the underlying mantle source. Likely due to its proximity to R15, it is also elevated 1.3 km above MPR, but displays a larger radius of 221 km and arc of 95°, consisting of 237 mapped lineaments. Many of its grouped lineaments also follow the trend direction of the NW-SE regional rift fault pattern (RF01) and so it is likely that many of the graben-fissures from this source had followed the already weakened and fractured crust. Within the vicinity of R11 is an abundance of densely clustered radar-bright lineaments with large thicknesses and sinuosity (likely rift-related). This clustering is interpreted to consist mostly of regional rift faults (RF01), with a lesser amount of local rift faults (RF12) (*Figures 4.3 and 4.9*). This provides further evidence in support of system R11 graben-fissures following the previously established zones of weakness associated with the older phase of regional rifting. R11 interacts with graben-fissures from systems R07, R08, R10, R15, and L09. Cross-cutting relationships reveal R11 to be the youngest of all interacting systems, coinciding with the interpretation of R11 representing the youngest magmatic pulse from the underlying source.

4.2.3.5.3 System R15

System R15, centred at 268.25°E, 30.5°S, is located 40 km east of system R07 and 14 km southwest of system R11. It is elevated 1.3 km above MPR, and is interpreted to be one of the major centres (along with systems R07, R11, and R23) produced by the hypothesized underlying mantle source – also interpreted as the focal point of local triple-junction rifting. R15 features a maximum radius of 197 km, extending southward with an

arc of 60° and consisting of 106 mapped lineaments. R15 interacts with systems R07, R11, and L09. Cross-cutting relationships reveal it to be older than systems R07 and R11, but younger than L09. System R15 is interpreted as the oldest pulse from the hypothesized mantle source feeding the centres of systems R07, R11, R15, and R23.

4.2.3.5.4 System R23

System R23 is centred at 268°E, 30.5°S, with its radial geometry split into two separate arc segments – one with an angle of 35° opening to the northwest, and the other opening 60° to the northeast. R23 is centred at an elevation of 0.7 km above MPR, consists of 110 mapped lineaments, and exhibits a maximum radius of 111 km. R23 interacts with systems R01, R07, R27, and the local rift faults from the interpreted northwest trending rift segment (RF11). Cross-cutting relationships reveal system R23 to be older than systems R01, R07, and the local rift faults. It is also inferred to be younger than R27, based on a lesser degree of partial flooding observed within the valley to the northwest of R23. The proposed local rift faults (RF11) and the regional rifting pattern (RF01) are both observed to cross-cut the graben-fissures of R23, thus making R23 older than both the local rifting and regional extension of Parga Chasma.

4.2.3.5.5 System R24

System R24 is a small and sinuous radiating system 73 km northwest of system R07. It is centred at 267°E, 30°S, and elevated at 1.8 km above MPR, which is significantly higher than R07. R24 features a maximum radius of 107 km and consists of 74 mapped lineaments with an arc of 90°. Graben-fissures from R24 trend south then southwest across an interpreted escarpment zone where topography drops sharply in elevation toward the south-southwest (~1 km over a lateral distance of 80 km). The top

"cliff edge" is densely clustered with thick and very sinuous radar-bright lineaments correlated to the regional rifting pattern (RF01) from the extension of Parga Chasma. Graben-fissures of R24 extend across zones of regional rift faulting and are observed to exhibit a degree of synchroneity with the regional rifting; however, some locations do exist where graben-fissures from system R24 are clearly overprinted by regional rift faults. R24 also interacts with lineaments from systems R07, L09, and L11. R24 exhibits well defined cross-cutting relationships with graben-fissures from L09 and L11, but is observed to be cut by graben-fissures of system R07.

4.2.3.5.6 Systems L09 and L11

Systems L09 and L11 are linear graben-fissure systems centred close together – 266.25^{o}E, 30.5^{o}S and 30.75^{o}S, and elevated only 0.6 and 0.7 km above MPR, respectively. L09 is the larger of the two, with a maximum length of 143 km, a width of 58 km, and consisting of a total of 236 mapped lineaments. System L11 exhibits a maximum length of 92 km, a width of 40 km, and consists of only 49 mapped lineaments. L11 displays interactions with graben-fissures from systems R07, R24, and L09, and is interpreted to be older than all three systems, and is one of the oldest systems within the study area. L09 interacts with systems R07, R11, R15, R24, and L11. Cross-cutting relationships reveal it to also be older than all interacting systems, except for L11, as previously stated. Aside from being younger than L11, L09 is also observed to be one of the oldest systems in the study area. Both systems are interpreted to predate the regional extension of Parga Chasma (RF01).

4.2.3.6 System R17 and Chuku Corona

The interpreted centre of Chuku Corona is located approximately 100 km north of the system R17 centre (*Figure 4.10*). Chuku Corona displays a deformed morphology represented by an oblique orientation of circumscribing fractures, most notably observed along its northern flank. It is catalogued as having a diameter of 380 km, but due to its deformed morphology, establishing its exact boundaries is difficult. The corona itself does not contain a central radiating system (only R17 which is offset by ~100 km from the corona centre), or any well defined circumscribing annular fractures. It is observed to be cut by regional rift faults, indicating an early formation that predates the regional extension of Parga Chasma. Additionally, gravitational relaxation has reduced its central topography, with observable flooding within many parts of its centre region.

R17 is centred at 266^{o}E, 24.5^{o}S and located 100 km south of the centre of Chuku Corona (*Figure 4.10*). Containing a well-established circumferential system of its own, R17 is interpreted to represent a younger magmatic pulse from the same or a nearby mantle source. Magmatism here has produced a radiating system with a maximum observed radius of 186 km, and 391 mapped lineaments creating an arc of a nearly-complete 330^{o}. Similar to the depressed centre of Chuku Corona, R17 is elevated only 0.7 km above MPR, despite being situated within the rim of Chuku Corona, along the southern flank. R17 displays interactions with graben-fissures from systems R01, R02, and the regional rift faulting of Parga Chasma north of the study area. R17 is observed to cross-cut the graben-fissures from both R01 and R02, as well as the regional rift faulting (RF01), and is consequently interpreted as one of the youngest mapped systems during this study.

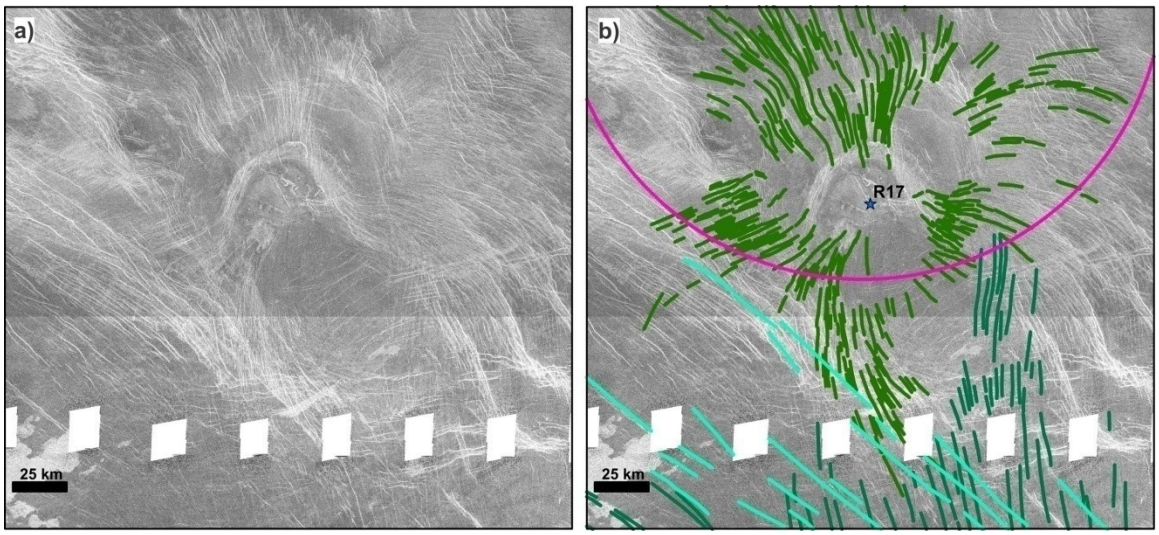

Figure 4.10. Graben-fissure systems R01 (turquoise), R02 (dark green), and R17 (green); the rim of Chuku Corona is outlined in magenta. (a) Magellan SAR image. (b) SAR image superimposed with mapped systems. Graben-fissures from R17 cross-cut both R01 and R02, and R17 is interpreted as the youngest. See *Figure 4.4* for image location.

4.2.3.7 Systems R05, R06, R12, R13, R22, L08: Kulimina Corona

Kulimina Corona is a deformed ellipsoidal corona with a minimum and maximum diameter of 160 km and 215 km, respectively. It is located in the northwestern corner of the study area and centred approximately at 262°E, 27.5°S (*Figure 4.11*). Within the boundaries of its deformed and ellipsoidal annulus lie the centres of systems R05, R06, R12, and R13, with system R22 situated just outside its eastern flank. Linear system L08 passes across its northwestern border. Kulimina Corona is interpreted to be the source of triple-junction style rifting, forming three separate rift segments, extending to the north-northwest (RF07), east (RF08), and southeast (RF09) (*Figures 4.3 and 4.11*). The rift valley to the east (RF08) contains rift faults in an east-west orientation, but also displays rift faults in a northwest-southeast orientation. This indicates the possibility of multiple local rifting events, with the NW-SE trending segment (RF10) having formed from either the hypothesized magmatic centre to the southeast underlying systems R07, R11, R15, R23, or from a cryptic centre interpreted to underlie radiating system R16, 323 km east of

Kulimina Corona. These NW-SE trending rift faults may also comprise part of the regional rifting (RF01) from Parga Chasma extension. Systems R05, R06, R12, and R13 are linked to the main building stage of Kulimina Corona (*Figure 4.11*), and all three are interpreted to postdate the regional extension of Parga Chasma (with some synchroneity observed in R05 and R12 in comparison with the regional rifting). Additionally, R06 cross-cuts all of these systems and its associated graben-fissures are observed to follow the weakened crustal zones from established local and regional rift faulting, and so R06 is interpreted as the youngest and largest magmatic pulse from the mantle source underlying Kulimina Corona.

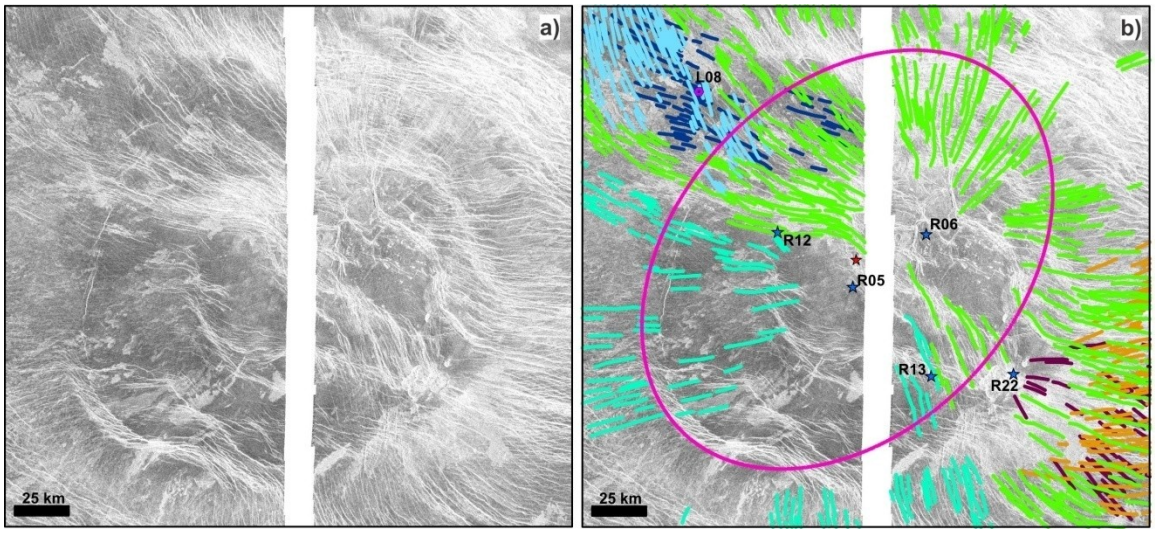

Figure 4.11. Graben-fissure systems R05 (turquoise), R06 (light green), R12 (light blue), R13 (orange), R22 (purple), and L08 (dark blue); the rim of Kulimina Corona is outlined in magenta. (a) Magellan SAR image. (b) SAR image superimposed with mapped systems. R06 cross-cuts all interacting systems and is interpreted as the youngest. See *Figure 4.4* for image location.

4.2.3.7.1 System R05

R05 is centred at 262°E, 28°S, only 42 km southwest of R06. It is elevated 1.5 km above MPR, features a maximum radius of 448 km from 344 mapped lineaments, and an arc split into two separate directions – west-southwest and southeast at 50° and 45° angles, respectively (*Figure 4.11*). R05 is located only 12 km south of the Kulimina

Corona centre, but interacts only with graben-fissures from R06. However, some graben-fissures from system R12 may belong to the centre of R05 – based on the spatial proximity of R12 and the orientation of its graben-fissures – which in turn would imply interactions with system L08. If this is the case, then R05 would be observed to postdate L08. Cross-cutting relationships reveal R05 to be older than R06.

4.2.3.7.2 System R06

Centred within Kulimina Corona at 262.5°E, 27.5°S, system R06 is a large radiating system elevated 1.2 km above MPR with 711 mapped lineaments and features a maximum observed radius of 352 km, with a 250° arc (*Figure 4.11*). R06 interacts with graben-fissures from systems R05, R12, R13, R16, R22, L06, L08, and L10. It is also interpreted to postdate local and regional rifting (RF01, RF07 – RF10) and its associated graben-fissures are observed to follow the trend of established local and regional rift faults from the formation of Parga Chasma. R06 is observed to cross-cut all systems interacting with it, and is therefore interpreted to be the youngest event within the immediate vicinity.

4.2.3.7.3 Systems R12 and L08

R12 is a radiating system centred at 262.75°E, 27.5°S, and 38 km west-northwest from the centre of Kulimina Corona (*Figure 4.11*). R12 consists of 136 mapped lineaments, a maximum observed radius of 213 km, and an arc of 50° opening towards the north. L08 is a linear system centred at 262.25°E, 27°S, extending across the northern flank of Kulimina Corona. L08 features a maximum length measured at 150 km, a width of 54 km, and consists of 84 mapped lineaments. Both systems, R12 and L08, have similar elevations of 1.6 km and 1.8 km above MPR, respectively. R12 interacts with

graben-fissures from R06 and L08. R12 is observed to cross-cut graben-fissures from L08, and be cross-cut by those from R06. L08 interacts with graben-fissures from R06 and R12, and is observed to be cross-cut by both. Additionally, the graben-fissures from L08 are observed to be partially flooded by lava flows from Kulimina Corona – both within and outside the corona centre – and therefore, L08 is interpreted to be older.

4.2.3.7.4 Systems R13 and R22

Systems R13 and R22 are only 38 km apart and centred at 262.5°E and 263°E, 28°S, respectively (*Figure 4.11*). Each system is situated at similar elevations of 1.5 km and 1.3 km above MPR, respectively. System R13 is the larger and younger of the two, consisting of 172 mapped lineaments, a maximum radius of 203 km, and an arc of 90°; R22 consists of 63 mapped lineaments, a maximum radius of 114 km, and an arc of 65°. R22 is observed to be cross-cut by graben-fissures from R13, and local rift faults (RF09). R22 is also observed to be partially flooded by lava flows from Kulimina Corona, further indicating an early formation. Both systems interact with the large system R06, while R13 also interacts with R16 and L10. Cross-cutting relationships reveal R13 to be younger than R22, L10 and regional rift faulting (RF01); synchronous with R16; and older than R06.

4.2.3.8 System R16

R16 is located at 265.5°E, 27.5°S, features a maximum radius of 196 km, three separate arcs of 85°S, 70°NW, and 25°E, and consists of 309 mapped lineaments (*Figure 4.12*). R16 is interpreted as the source for graben-fissures propagating primarily to the northwest, and a lesser amount propagating to the south and to the east. The location of R16 as a magmatic centre suggests a link to local rift faults trending to the northwest

(RF10) and southeast (RF11) of R16 (*Figure 4.3*), as well as explaining the presence of adjacent and surrounding lava flows to the southwest.

R16 interacts with systems R02, R06, R13, L02, and L10 (*Figure 4.12*). Cross-cutting relationships reveal R16 to be younger than L02 and L10; synchronous with R02 and R13; and either older or partially synchronous with R06. Cross-cutting relationships are difficult to resolve between R16 and the regional rifting (RF01), but lava flows associated with R16 are observed to both cross-cut and be cross-cut by regional rift faults, and so some degree of synchroneity is inferred.

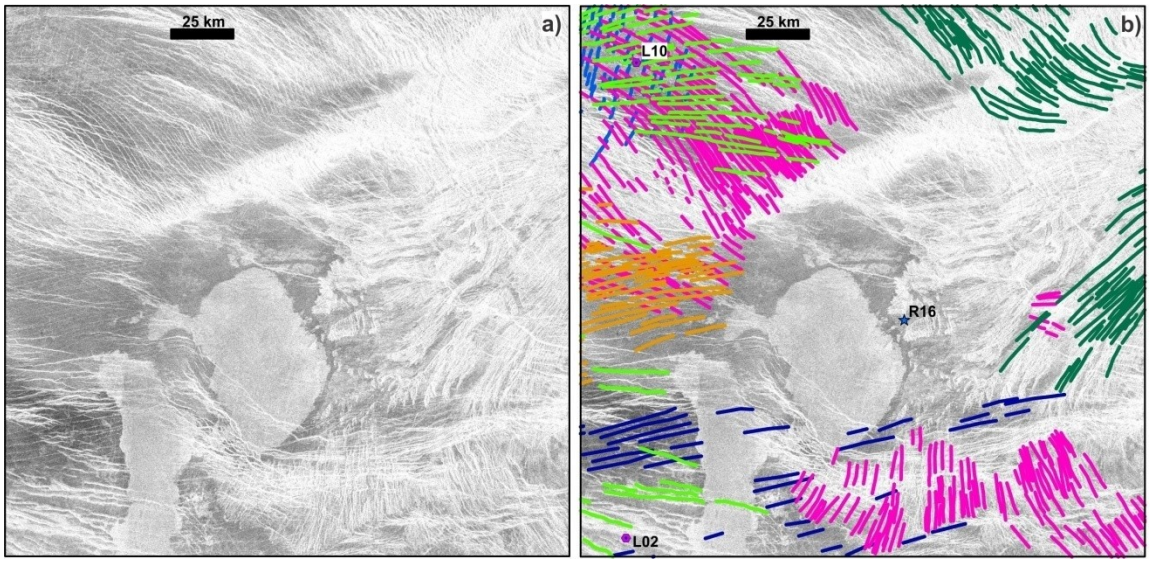

Figure 4.12. Graben-fissure systems R02 (dark green), R06 (light green), R13 (orange), R16 (pink), L02 (dark blue), and L10 (blue). (a) Magellan SAR image. (b) SAR image superimposed with mapped systems. Graben-fissures from R16 cross-cut those from L02 and L10; are relatively synchronous with those from R02 and R13; and are cut by R06 – indicating R06 as the youngest system. See *Figure 4.4* for image location.

4.2.3.9 System L07 and Gertjon Corona

Gertjon Corona is an ellipsoidal corona situated at 266°E, 30°S along the eastern border of the study area. It has a maximum diameter of 210 km and a minimum diameter of 165 km (*Figure 4.13*). Gertjon Corona contains heavily deformed annulus of circumscribing fractures and lacks a radiating system focussed on its centre. It is located at a possible junction point for the local southeast trending rift segment (RF03) from Ts'an Nu Mons (*Figure 4.3*).

L07 is a small linear system that extends from the southwestern flank of Gertjon Corona to the western plains. L07 is situated at 275.5°E, 30.5°S, and consists of 194 mapped lineaments with a length of 152 km and width of 54 km (*Figure 4.13*). The central area is located at an elevation of 1.2 km above MPR. L07 interacts with graben-fissures from R03, R04, R18, and the regional rifting of Parga Chasma. Graben-fissures from L07 are observed to be cross-cut by the regional rift faults (RF01), and so are interpreted to predate Parga Chasma extension. Ambiguous cross-cutting relationships are observed between the graben-fissures of L07 with those from R03 and R18 – which are also cut by regional rift faults – and so synchroneity between these systems is inferred. Cross-cutting relationships between L07 and R04 are difficult to resolve; however, graben-fissures from R04 postdate the regional rifting. Therefore, L07 is interpreted to be older than R04.

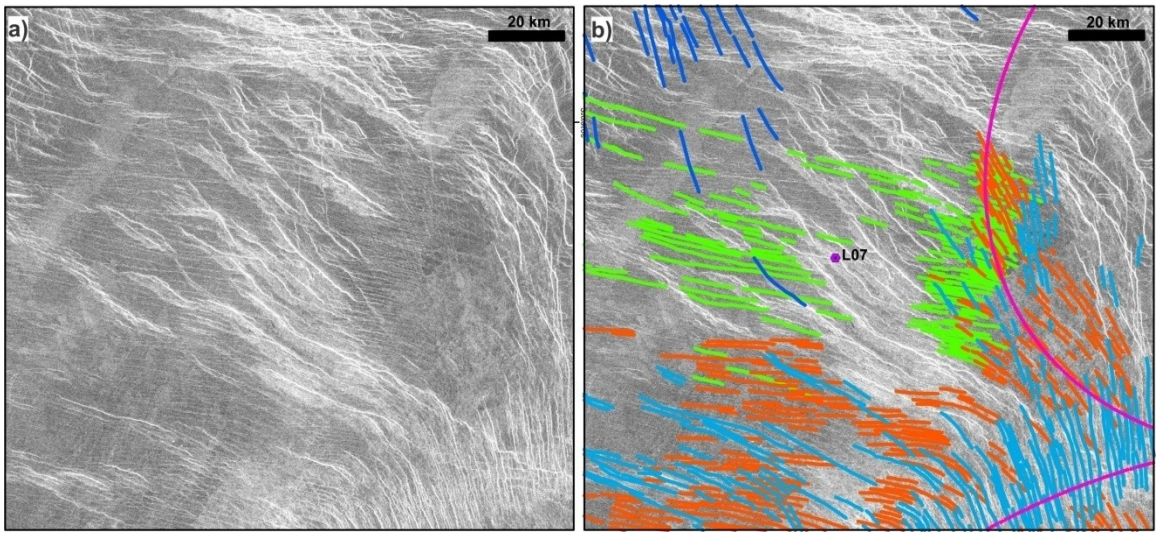

Figure 4.13. Graben-fissure systems R03 (light blue), R04 (blue), R18 (orange), and L07 (light green); the western rim of Gertjon Corona is outlined in magenta. (a) Magellan SAR image. (b) SAR image superimposed with mapped systems. Cross-cutting reveals L07 to be older than R04, and synchronous with R03 and R18. See *Figure 4.4* for image location.

4.2.3.10 System R25 and Otohime Tholus

Otohime Tholus is a small circular domal structure, roughly 20 km in diameter, located at 268.25°E, 32°S (*Figure 4.14*). Graben-fissures belonging to systems R07, R15, and R25 all extend towards and past Otohime Tholus but cannot be tracked across the structure. Because of this observation the formation of Otohime Tholus is interpreted to postdate systems R07, R15, and R25.

R25 is a small radiating system that propagates southeast towards Otohime Tholus, centred at 267.75°E, 31.5°S (*Figure 4.14*), and situated at an elevation of 0.7 km above MPR. R25 consists of 104 mapped lineaments, spreading over an arc of 60° opening towards the southeast, and extending to a maximum radius of 99 km. R25 (*Figure 4.14*) interacts only with graben-fissures from systems R07 and R15, with cross-cutting relationships revealing it to be the oldest of these systems.

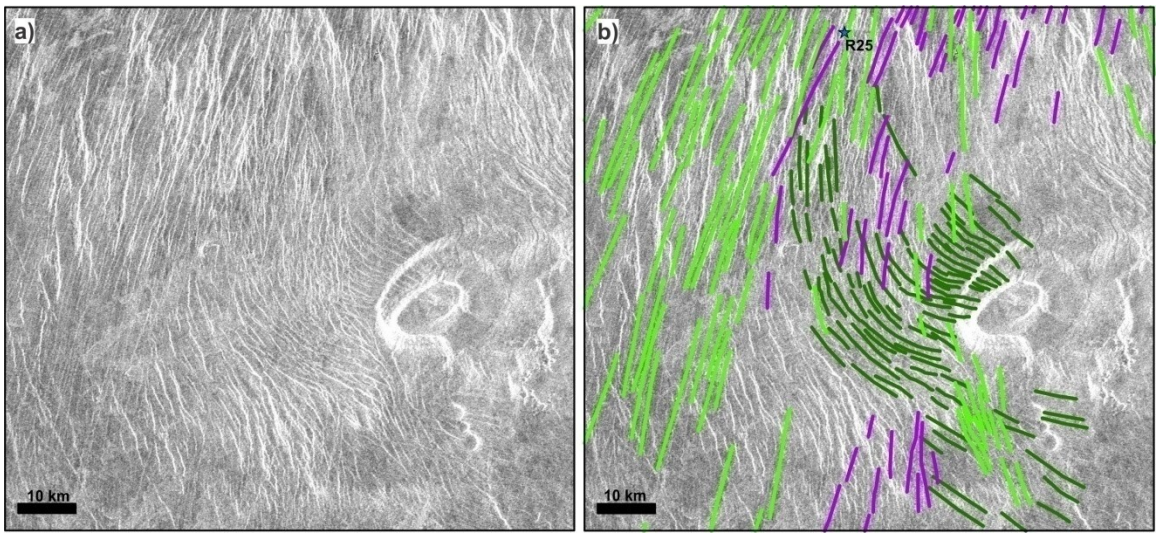

Figure 4.14. Graben-fissure systems R07 (light green), R15 (purple), and R25 (green); Otohime Tholus is the circular structure to the east lacking graben-fissures. (a) Magellan SAR image. (b) SAR image superimposed with mapped systems. Graben-fissures from R25 are observed to be cut by those of R07 and R15, and R25 is interpreted as the oldest. See *Figure 4.4* for image location.

4.2.4 System Size Distribution throughout the Study Area

Of the 47 grouped systems, the majority (37) have maximum radii/lengths less than 250 km, while the remaining systems (10) extend to greater distances (*Figure 4.15*). Two systems (R01 and R02) extend more than 550 km from their source. The smaller sizes of most observed graben-fissure systems (< 500 km) – compared to previous mapping work (e.g. Ernst et al., 2003; Studd et al., 2011) in which multiple radiating systems had been observed with maximum radii exceeding 1,000 km – could be attributed to the detailed mapping of a larger number of separate systems within a smaller study area (1.5 million km^2 compared to > 10 million km^2 study areas in Ernst et al., 2003 and Studd et al., 2011). There is also the possibility that some linear graben-fissure systems could actually be distal parts of larger radiating and/or circumferential systems (e.g. Ernst et al., 2003).

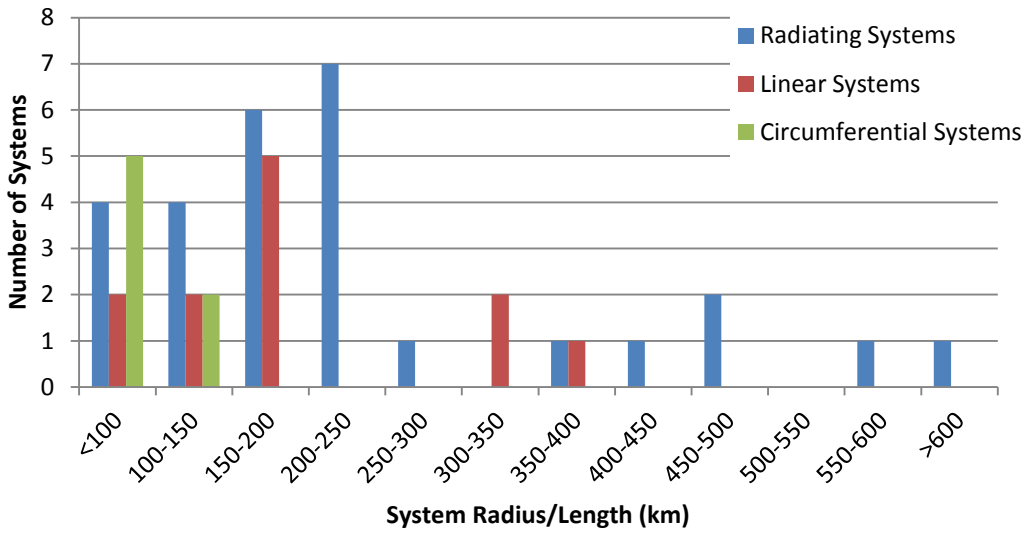

Figure 4.15. Histogram of the maximum radius (radiating/circumferential systems) or length (linear systems) of all mapped graben-fissure systems. Values come from the data catalogued in *Tables 4.1 – 4.3*.

4.2.5 Topographic Variations throughout the Study Area

The relationship between system size and central elevation was also obtained for all systems (*Figure 4.16*). Within the study area, all systems are situated at elevations above MPR. This result coincides with the tectonic setting of the study area as part of the uplifted volcanic plateau that largely defines Themis Regio. The southern boundaries of this plateau are present within the study area – marked by the southwestern regional rift faults (RF01) (*Figure 4.3*) and an escarpment – which exhibits a ~1 km drop in a south-southwest direction across a lateral distance of ~80 km.

A cluster of variable system elevations (0.5 – 2.5 km above MPR) is observed for the majority of systems with maximum sizes < 300 km. The largest systems (> 400 km) are observed to reach elevations no higher than 1.5 km above MPR. Many systems associated with major geologic structures – notably coronae and large volcanoes – are situated at higher elevations. Additionally, graben-fissure systems that are centred within a single corona often exhibit distinct central elevations for their respective centres. This

could imply an unequal distribution of topography variation during the early constructional uplift and later gravitational relaxation stages of corona formation, or a time-transgressive formation of graben-fissure systems from a singular mantle source.

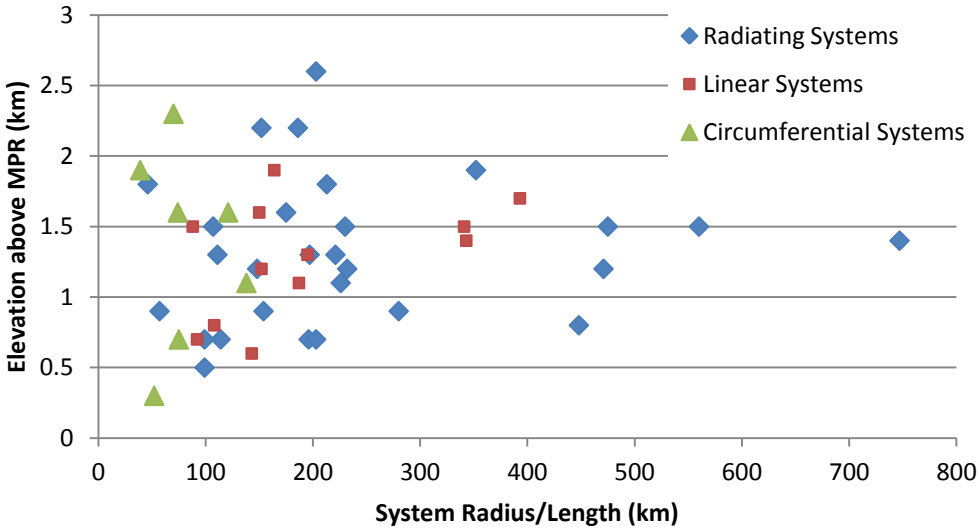

Figure 4.16. Relationship between the elevation above MPR and the maximum sizes of associated graben-fissure systems. Values come from data catalogued in *Tables 4.1 – 4.3*.

4.3 Relative Chronology of Tectono-Magmatic Events

Using similar methods employed by Studd et al. (2010), a relative chronology of the tectono-magmatic events within the study area has been created (*Figure 4.17*). This method utilized the analysis of cross-cutting relationships to interpret the temporal emplacement of graben-fissure systems with respect to rifting. For this study it has also been assumed that the time period of emplacement for each graben-fissure system was short (~ a few Myr), based on terrestrial studies of dyke swarm emplacement (e.g. Ernst et al., 2001; Ernst, 2014). The initial regional extension and rifting of Parga Chasma is interpreted to have occurred over a relatively short time span of 10 – 50 Myr, based on the terrestrial rift review and catalogue by Sengör and Natal'in (2001), and is placed in the centre of the produced timeline. For the purposes of this study, the regional rifting of

Parga Chasma is assumed to have temporal synchroneity. However, the timing of local triple-junction rifting events have variable timing and are linked to the localized magmatic centres from which they are interpreted to be focussed on.

To build this chronology, the relationships between neighbouring radiating and linear graben-fissure systems and/or the local/regional rifting of Parga Chasma (*Table 4.4*) were integrated to produce a timeline of tectono-magmatic events in the study area (*Figure 4.17*). The criteria used for determining the relative age relationships were presented in Section 4.1, and is summarized herein.

Graben-fissure lineaments that clearly cross-cut rift-related lineaments are interpreted to have been emplaced after rifting, whereas graben-fissure lineaments that are clearly cross-cut by rifting are interpreted to have been emplaced prior to rifting. When there is ambiguity between interacting graben-fissure and/or rift-related lineaments, or contradictory cross-cutting is observed, synchronous emplacement is interpreted to have occurred. Age relationships were further constrained when the presence of lava flooding (partially or completely) obscures the radar signal of graben-fissures and/or rift faults. In this timeline, horizontal lines are used to schematically represent the time span of possible age ranges of each system, with time moving from left to right (older to younger). When graben-fissures interacted with regional rift faults from Parga Chasma, age relationships relative to rifting could be determined and the system was provisionally placed on the left, centre, or right side of the timeline. When the graben-fissures from different systems were observed to intersect, age relationships between neighbouring systems could be obtained and the relative positioning of these systems on the timeline could be refined.

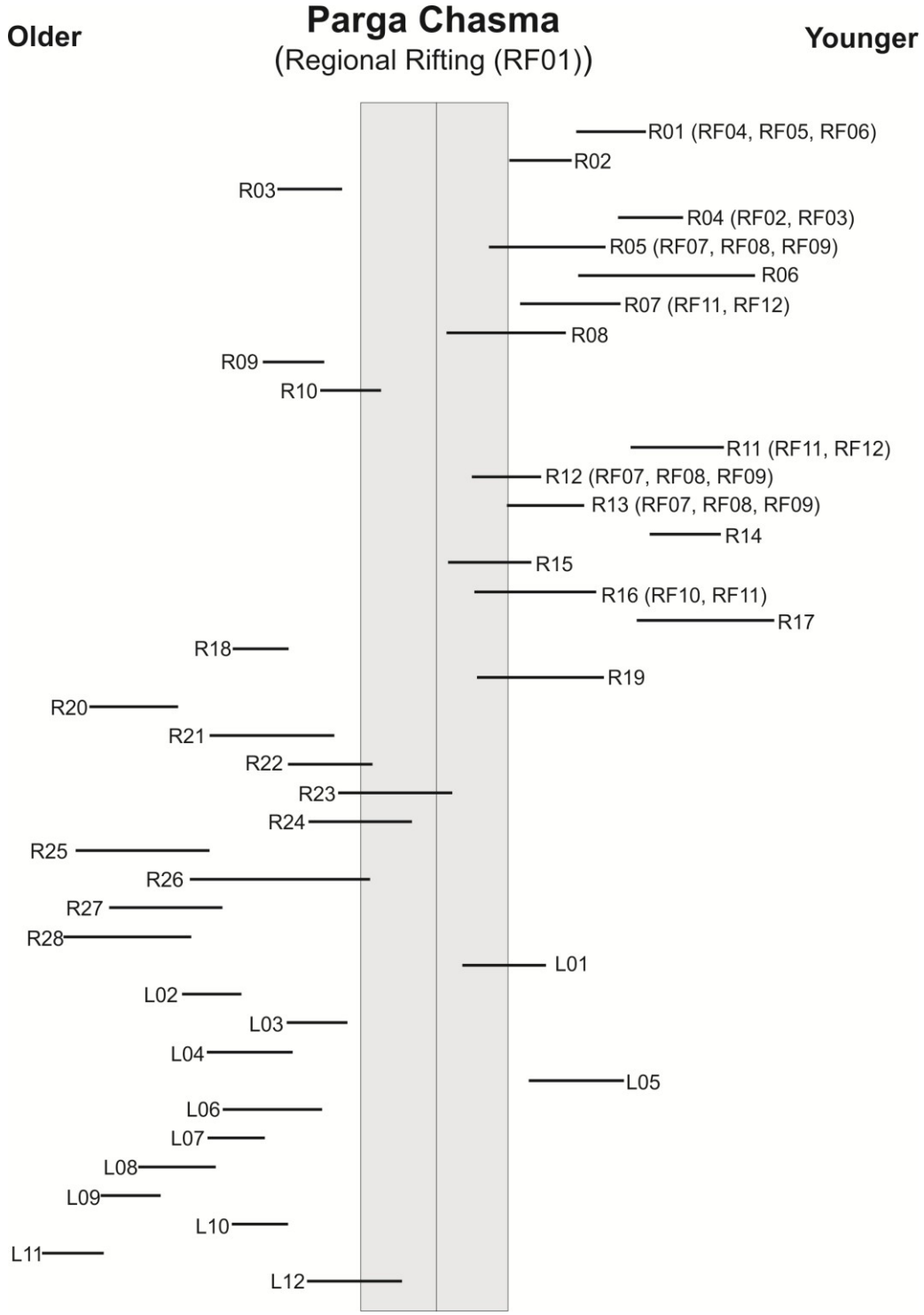

Figure 4.17. Timeline of the tectono-magmatic events within the study area. The regional rifting of Parga Chasma is taken as the baseline, with the interpreted temporal formation of each graben-fissure system relative to regional rifting (RF01). Older systems are placed towards the left side; younger towards the right. Systems interpreted to be synchronous with regional rifting intersect the baseline. Systems are numbered from top to bottom with horizontal lines representing their interpreted age ranges relative to each other and to the regional extension (*Table 4.4*). Local rift fault segments are listed in parentheses next to the system(s) they are genetically linked to.

Table 4.4. Summary of cross-cutting relationships between radiating and linear graben-fissure systems catalogued in the study area. Systems in the first column are compared to all interacting systems or regional rift faults in subsequent columns as younger (<), coeval (=), older (>), or a combination thereof. Types of cross-cutting observed are colour-coded based on either direct (blue) or indirect (green) interactions.

	R01	R02	R03	R04	R05	R06	R07	R08	R09	R10	R11	R12	R13	R14
R01		<		>/=			<							>
R02	>					>								
R03				>				>		>				
R04	</=		<						<					>
R05						>/=						=		
R06		<			</=							<	</=	
R07	>		<					>		<	<			
R08			<				>/=			<	>			
R09				>										
R10			</=				>	>			>			
R11							<	<		<				
R12						>								
R13						>/=								
R14	</=			=										
R15							>				>			
R16		=				>/=							=	
R17	</=	<												
R18			>/=	>										
R19	>/=						=							>
R20				>										
R21														
R22						>							>	
R23	>						>							
R24							>							
R25							>							
R26		>												
R27							>							
R28		>					>							
L01	>	>												
L02					>									
L03					>									
L04				>										
L05			<											
L06						>								
L07			>/=	>										
L08						>						>		
L09							>				>			
L10						>							>	
L11							>							
L12			</=				>	>						

Table 4.4. continued.

	R15	R16	R17	R18	R19	R20	R21	R22	R23	R24	R25	R26	R27	R28
R01			>		>		<		<					
R02		<	>									<		
R03				</=										
R04				<		<								
R05														
R06		</=						<						
R07	<				>				<	<				<
R08														
R09														
R10														
R11	<													
R12														
R13		=						<						
R14					<									
R15														
R16								<					<	
R17														
R18														
R19														
R20														
R21														
R22		>												
R23													<	
R24														
R25	>													
R26														
R27		>							>					</=
R28														
L01														
L02		>												
L03														
L04						<								
L05				<										
L06														
L07				>/=										
L08														
L09	>									>				
L10		>												
L11										>				
L12														

Table 4.4. continued.

	L01	L02	L03	L04	L05	L06	L07	L08	L09	L10	L11	L12	RF01
R01	<												<
R02	</=												<
R03					>		<					>	>
R04				<			<						<
R05			<					<					</=
R06		<				<				<			<
R07									<		<	>	<
R08												<	</=
R09													>
R10													>/=
R11									<				<
R12								<					</=
R13										<			
R14													<
R15									<				</=
R16		<								<			</=
R17													<
R18					>		</=						>
R19													</=
R20				>									>
R21												>/=	>
R22													
R23													>/=
R24									<		<		>/=
R25													
R26													>/=
R27													
R28													>
L01													</=
L02			>										>
L03		<											>
L04													>
L05													
L06													>
L07													>
L08													
L09											<		>
L10													>
L11									>				>
L12													>/=

Results derived from this timeline (*Figure 4.17*) are: 17 / 40 (42.5 %) of systems are observed to directly predate regional rifting; 13 / 40 (32.5 %) exhibit synchroneity with regional rifting, and 10 / 40 (25 %) of all systems directly postdate regional rifting. Of the 13 systems that exhibit synchroneity to regional rifting, 7 / 13 (54 %) exhibit a combination of younger and synchronous relationships, while the remaining 6 / 13 (46 %) exhibit a combination of older and synchronous relationships.

4.4 Implications of the Relative Chronology

The main results from this relative chronology (*Figure 4.17*) have been superimposed onto a SAR image of the study area, with detailed linework mapping (*Figure 4.18*). From this figure it can be seen that graben-fissure systems of all sizes are evenly distributed throughout the study area, but the largest ones – notably systems R01-R05 – are situated within the centres of coronae (R01-R03, R05) or large volcanoes (R04). There are also some locations, such as within the areal extent of Kulimina Corona (e.g. systems R05 and R06) and in the vicinity of the hypothesized centre that likely underlies system R07 that contain dense clusters of (mostly) smaller systems. These aforementioned locations also host the majority of young systems interpreted to postdate regional rifting. Many of the largest radiating systems are also among the youngest systems (with R03 as a notable exception) in the study area. Additionally, all local magmatic centres that are interpreted as the focal points for local triple-junction rifting contain graben-fissure systems that are observed to cross-cut regional rift faults. These age relationships provide further evidence in support of multiple stages of Parga Chasma rifting – beginning from regional NE-SW extension between Atla and Themis Regiones and following with local rifting events from isolated magmatic centres.

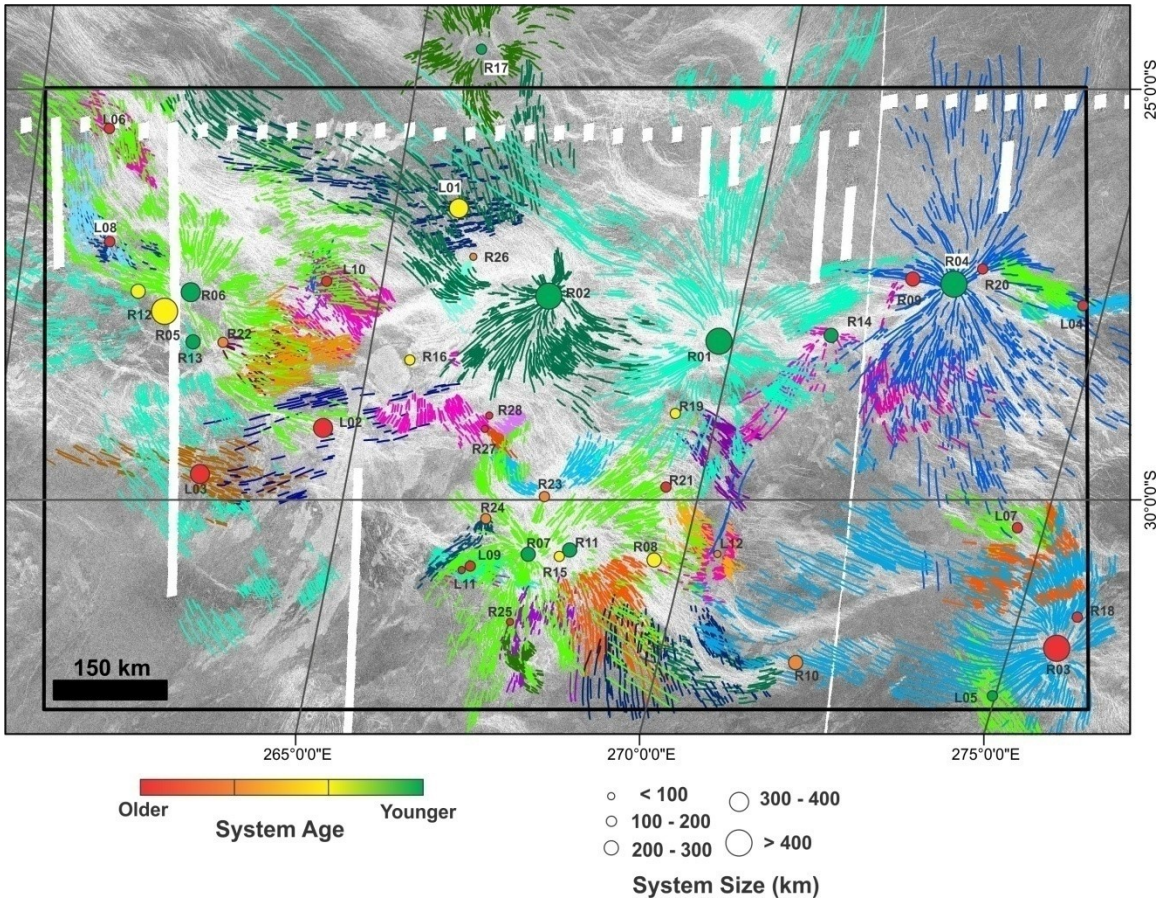

Figure 4.18. Magellan SAR image of the study area, superimposed with detailed linework of all radiating and linear graben-fissure systems. All system centres are identified by circles which are sized and coloured according to maximum system radius/length and relative age, respectively.

5 Chapter: Relationship between Rifting and Magmatic Centres

5.1 Regional and Local Rifting within the Study Area

Prominent rifting has taken place throughout the study area (*Figure 4.3*), interpreted to be associated with both regional and local rifting of the Parga Chasma rift system. The regional rifting is observed as a pattern of NW-SE trending rift faults extending across the study area (*Figure 5.1*), while local rifting is observed as individual segments (also marked by topographic troughs) extending from isolated magmatic centres (*Figure 5.2*). Lineaments associated with both the regional and local rifting of Parga Chasma are rift-related and thus exhibit the same morphological characteristics that distinguish them from graben-fissures (Section 3.4). Detailed mapping in the study area has revealed over 1,500 rift-related lineaments, grouped into 1,016 local and 633 regional rift faults, respectively (*Figure 4.3*).

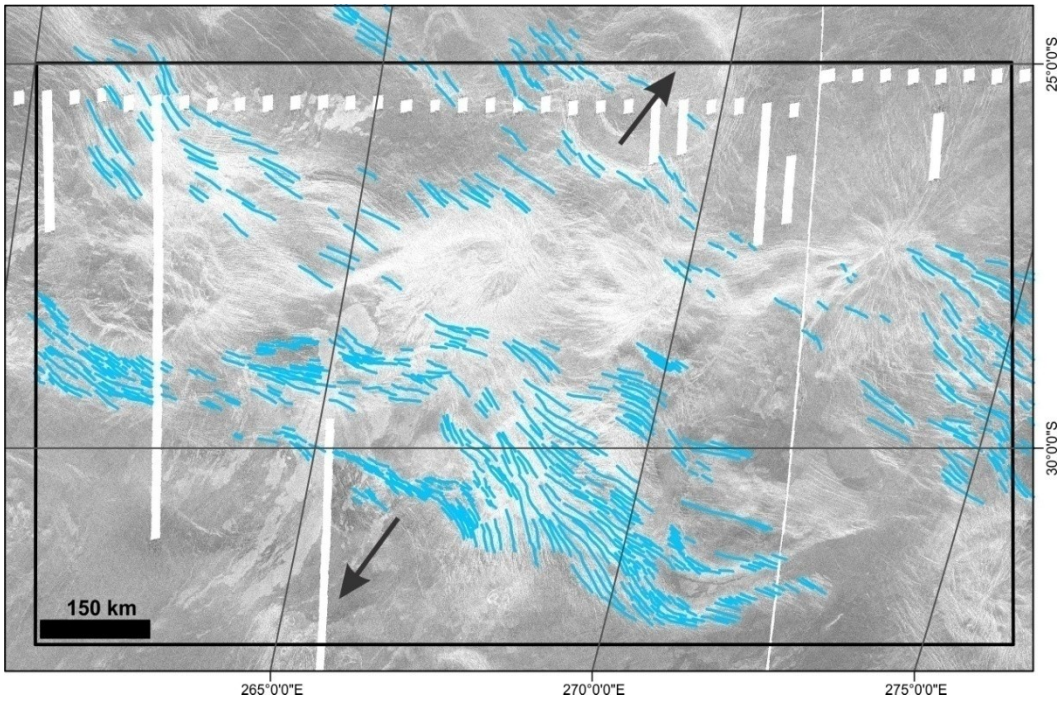

Figure 5.1. Magellan SAR image of the study area superimposed with mapping of the regional rift fault pattern (light blue). The arrows denote the regional NE-SW extension of Parga Chasma.

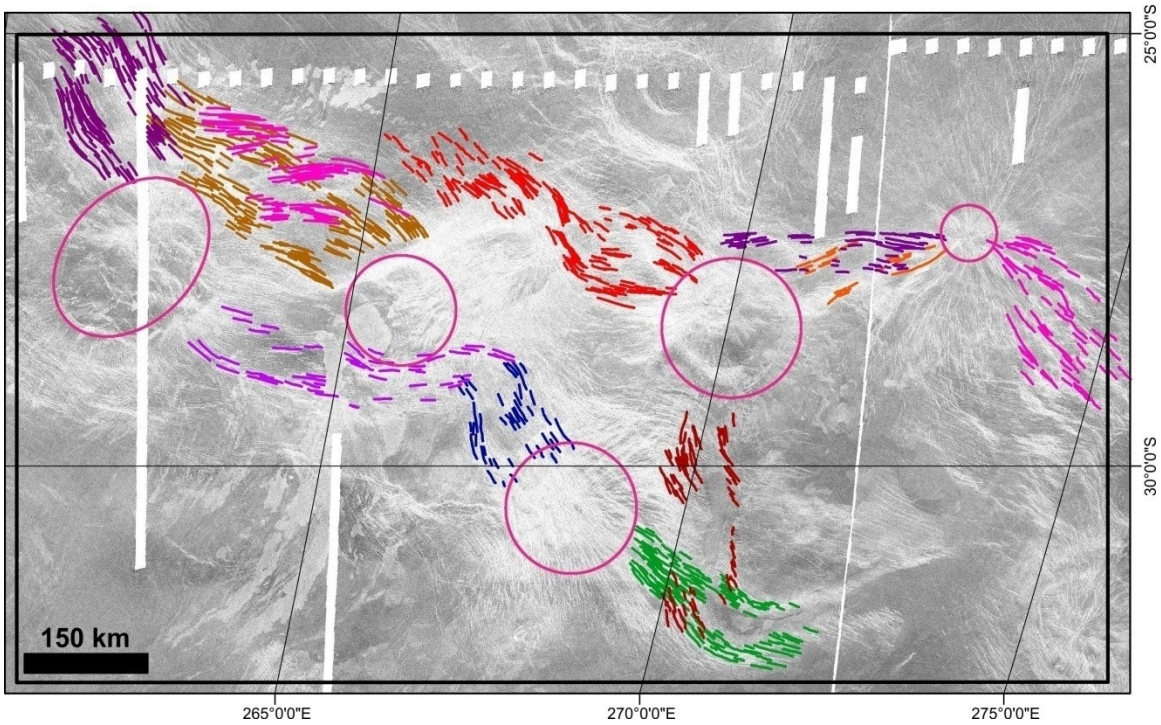

Figure 5.2. Magellan SAR image of the study area superimposed with mapping of local rift faults. The various orientations of these lineaments have been grouped into individual rift segments (*cf. Figure 4.3*), each of which has been linked to a specific magmatic centre (pink circles) as a focal point.

Within the study area, all of the interpreted local rift segments can be linked to individual magmatic centres acting as the focal points of local triple-junction rifting. Some of these centres are coronae, while the rest are linked to large volcanoes or cryptic centres only recognized as the locus of radiating graben-fissure systems – each of which are understood to be formed from mantle upwellings (Ernst and Buchan, 1997a; Herrick, 1999; Ernst et al., 2001). These upwellings may be linked to rising mantle plumes or from lithospheric delamination (e.g. Sengör, 2001; Sengör and Natal'in, 2001; Ernst, 2014) – with plume-generated triple-junction rifting well observed in terrestrial settings (Burke and Dewey, 1973)

From detailed mapping, 11 local rift segments have been identified and are interpreted to extend directly from 5 individual magmatic centres (*Table 5.1; Figure 5.3*). These centres include 1 large volcano – Ts'an Nu Mons, 2 coronae – Xmukane Corona and Kulimina Corona, and 2 unnamed magmatic centres, interpreted as the sources of radiating graben-fissures systems. These two magmatic centres are associated with system R16 (*Figure 4.12*) and system R07 (*Figure 4.9*).

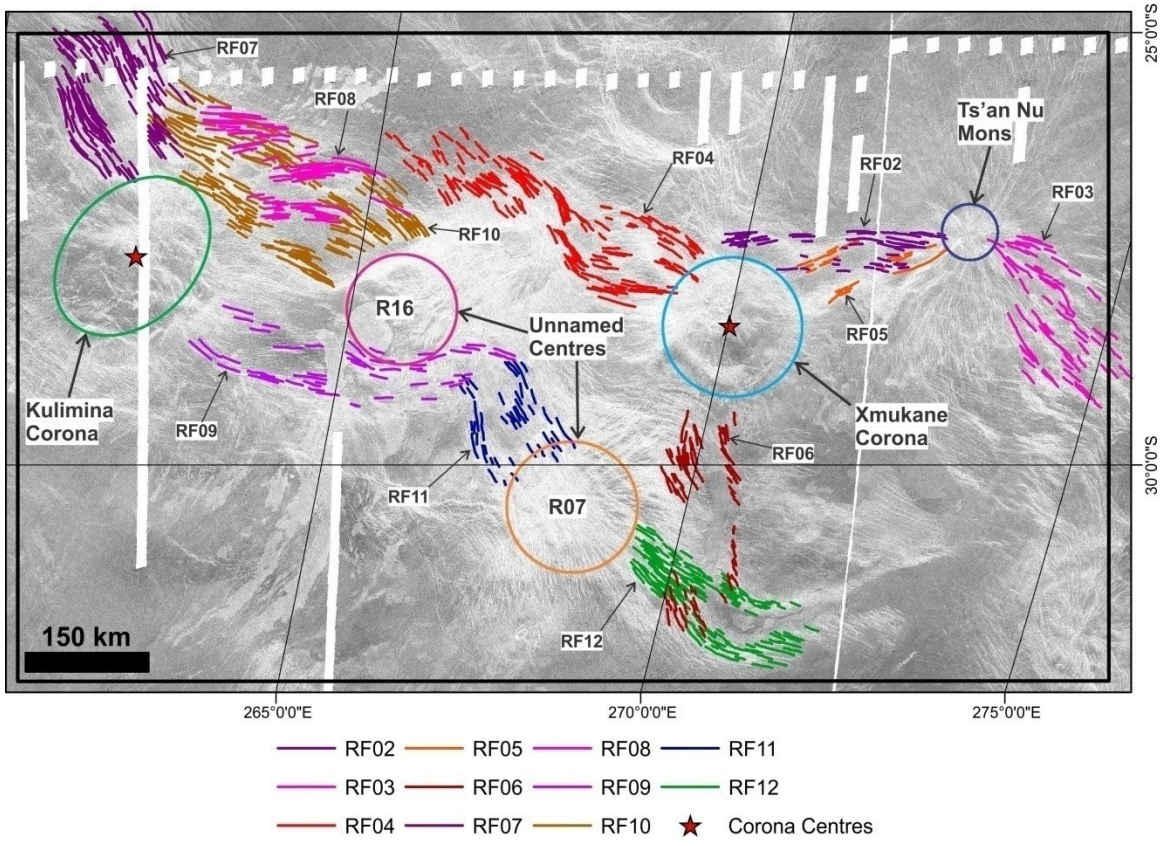

Figure 5.3. Magellan SAR image of the study area superimposed by mapping of the local rift faults which are further grouped into separate rift segments based on lineament orientation. These local rift segments are colour-coded to refer to the specific magmatic centre they are linked with. Corona centres are denoted by red stars. Local rift segments are labelled based on the data catalogued in *Table 5.1*.

Table 5.1. Local rift segments catalogued in the study area.

Rift Segment	Number of Rift Faults	Associated Magmatic Centre	Extension Direction	Colour-Coded Association
RF02	52	Ts'an Nu Mons	West	Dark Blue
RF03	64	Ts'an Nu Mons	Southeast	Dark Blue
RF04	202	Xmukane Corona	Northwest	Turquoise
RF05	23	Xmukane Corona	Northeast	Turquoise
RF06	75	Xmukane Corona	South	Turquoise
RF07	136	Kulimina Corona	Northwest	Green
RF08	67	Kulimina Corona	East	Green
RF09	51	Kulimina Corona	East-southeast	Green
RF10	174	System R16	Northwest	Pink
RF11	43	System R16 / R07	Southeast / northwest	Pink / Orange
RF12	129	System R07	Southeast	Orange

Ts'an Nu Mons (*Figure 5.4*) is the source of two separate rift segments, propagating to the west (RF02) and to the southeast (RF03) of the volcano. Xmukane Corona (*Figure 5.5*) contains 3 separate rift segments – propagating to the northeast (RF04), northwest (RF05), and to the south (RF06) of the corona. Kulimina Corona (*Figure 5.6*) also contains 3 rift segments – propagating to the northwest (RF07), east (RF08), and east-southeast (RF09) of the corona. The unnamed magmatic centres are interpreted based on the local rift fault pattern, coupled with the presence of multiple graben-fissure systems. System R16 (*Figure 5.7*) is centred on a northwest trending rift segment (RF10), in addition to a segment trending to the southeast (RF11) – this latter segment also connects with the other magmatic centre at system R07. The magmatic centre at system R07 (*Figure 5.7*) is also interpreted to be the source of a rift segment trending to the southeast (RF12), in addition to having a connection with the rift segment (RF11) in between the magmatic centres at systems R16 and R07 (*Figure 5.7*). Combining these observations yields a summary map of the study area that displays the distribution of the 5 major magmatic centres interpreted to each be the locus for

associated local triple-junction rifting (*Figure 5.8*) – distinct from the regional NW-SE rift pattern (*Figure 5.1*).

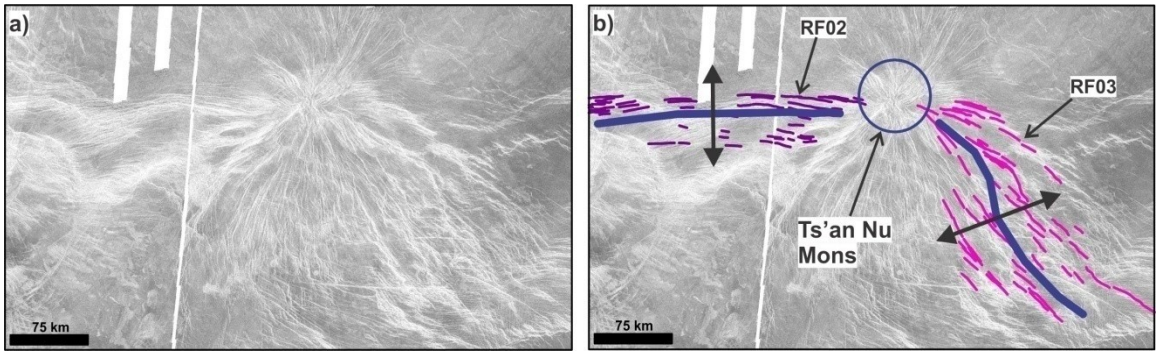

Figure 5.4. Local rifting associated with Ts'an Nu Mons. (a) Magellan SAR image. (b) Image overlain with mapping of local rift faults and segment lines (RF02, RF03) extending from Ts'an Nu Mons (dark blue). Arrows denote direction of opening.

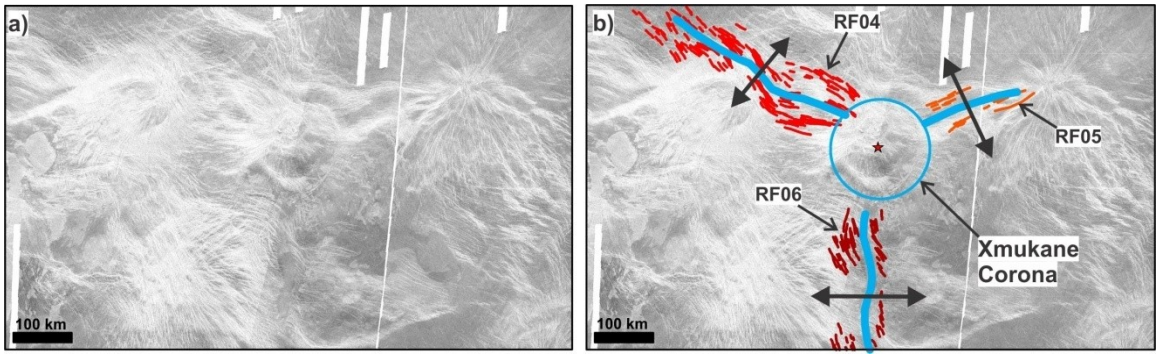

Figure 5.5. Local rifting associated with Xmukane Corona. (a) Magellan SAR image. (b) Image overlain with mapping of local rift faults and segment lines extending from Xmukane Corona (turquoise). Arrows denote direction of opening.

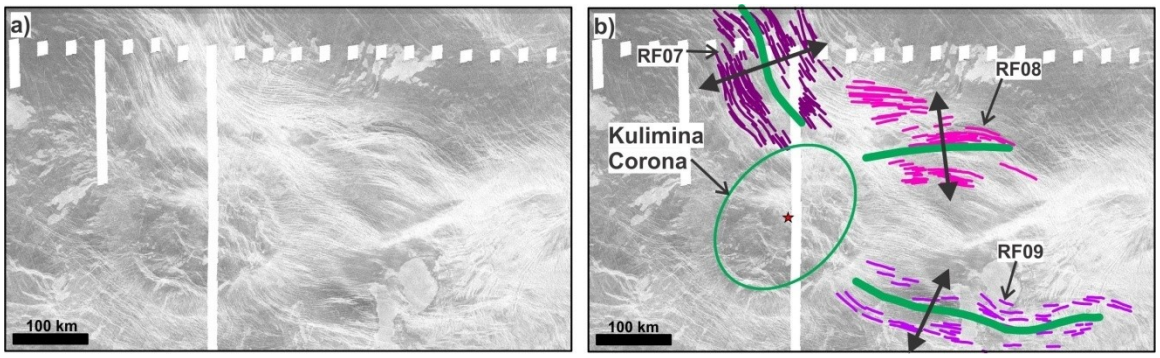

Figure 5.6. Local rifting associated with Kulimina Corona. (a) Magellan SAR image. (b) Image overlain with mapping of local rift faults and segment lines extending from Kulimina Corona (green). Arrows denote direction of opening.

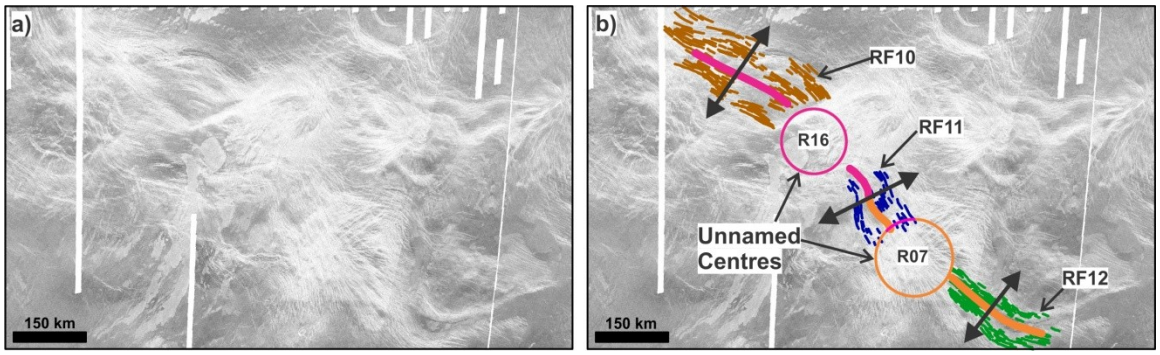

Figure 5.7. Local rifting associated with the two unnamed magmatic centres. (a) Magellan SAR image. (b) Image overlain with mapping of local rift faults segment lines extending from R16 (magenta) and R07 (orange). The rift segment RF11 is observed connecting the two centres and is coloured in both magenta and orange. Arrows denote direction of opening.

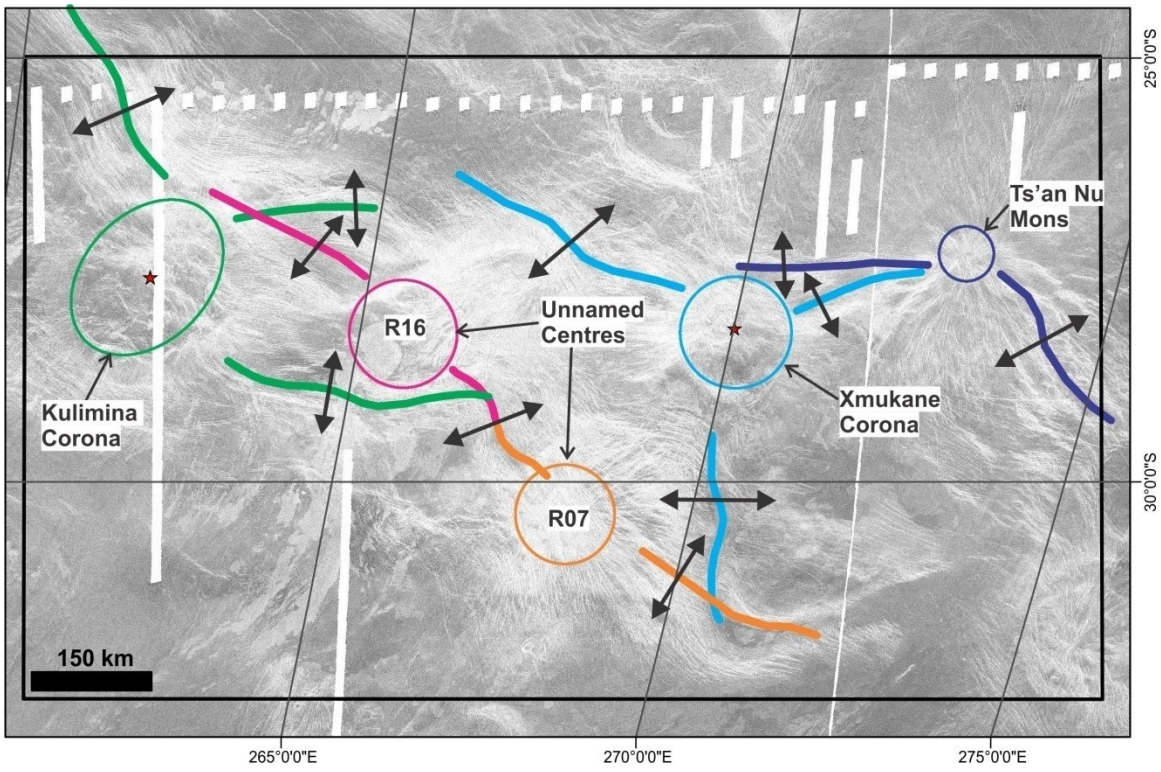

Figure 5.8. Magellan SAR image of the study area superimposed by a summary of all magmatic centres interpreted to be the locus of an individual triple-junction rifting event; rift segments and centres are coloured-coded based on this interpreted association. Arrows denote direction of local opening.

In summary, the detailed mapping and analysis of the local rift fault pattern throughout the study area has revealed numerous local trends and provided the necessary information to group these rift faults into individual rift segments. Grouping these local rift segments allowed them to be linked to specific magmatic centres from which they

extend. The magmatic centres are typically marked by coronae, large volcanoes, or radiating and/or circumferential graben-fissure system. When enough of these mantle upwellings occur in a zone of regional extension and crustal thinning, these isolated magmatic centres can collectively produce the appearance of a large, but often discontinuous rift system. Examining the relative age relationships between the graben-fissure systems focussed at these isolated magmatic centres (Section 4.3; *Figures 4.17 and 4.18*) reveals a temporal link between local triple-junction rifting and graben-fissure system formation – different from (and postdating) the timing of regional extension.

5.2 BAT Region Rift Systems as Collections of Local Rifting

From the previous section it was observed that a major section of Parga Chasma can be interpreted as a collection of separate local rift segments, formed via triple-junction rifting from isolated magmatic centres. This section explores the possibility that isolated magmatic centres (coronae, volcanoes, centres of graben-fissure systems) can act as similar loci of triple-junction rifting along other parts of Parga Chasma and along the other major rift systems of the BAT region. This hypothesis is applied to explain the observed discontinuities in the rift zone morphologies throughout Hecate and Parga Chasmata (*Figures 2.8 and 2.10*). By contrast, Devana Chasma can most easily be explained as the result of triple-junction rifting extending from only the two major volcanic rises of Beta and Phoebe Regiones at the ends of the rift system (*Figures 2.7b-f and 2.9*). The southern rift segment from Beta Regio extends to the south, where it is met by a segment from Phoebe that extends to the north.

Hecate and Parga Chasmata (*Figures 2.8 and 2.10*) extend from major volcanic rises located at the ends of each respective rift system and are responsible for zones of regional extension. However, both Hecate and Parga contain numerous additional local rift segments. Applying the results from detailed mapping in the study area, I interpret that Hecate Chasma is composed of 13 local rift segments (*Figure 5.9*), including those extending directly from the main triple-junction rifting of Atla and Beta Regiones. For Parga Chasma, I interpret to contain as many as 45 local rift segments throughout its full length (*Figure 5.10*). Most of these local rift segments are linked to a corona or large volcano, but some segments are observed to be isolated from any corona of volcano. However, in such cases, graben-fissure systems (often radiating and/or circumferential geometries) are observed which mark a cryptic magmatic centre. On the following figures of Hecate and Parga Chasmata (*Figures 5.9 and 5.10*), the interpreted local rift segments and associated magmatic centres are grouped together and numbered as *rift segment groups* (RGS), and are catalogued with respect to each rift system (*Tables 5.2 and 5.3*).

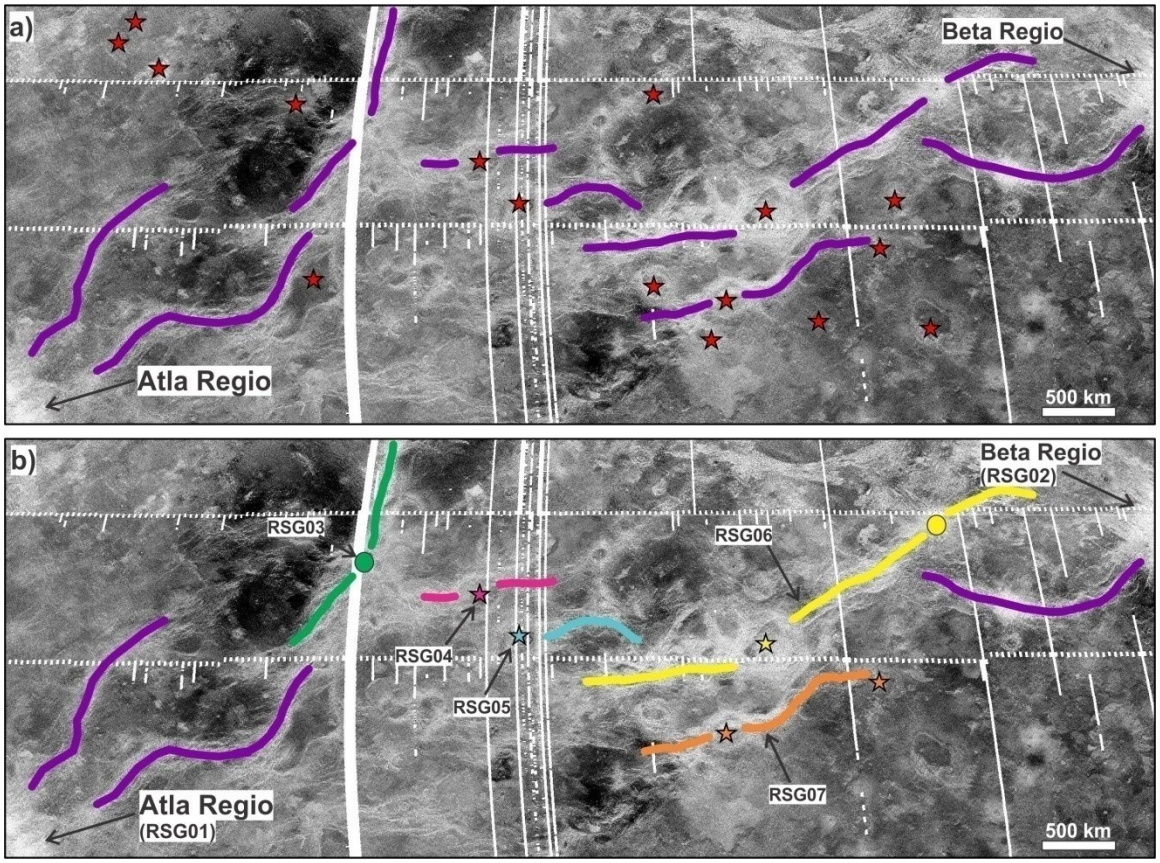

Figure 5.9. Magellan SAR images of Hecate Chasma (centred at 240°E, 16°N). (a) Image overlain by ungrouped local rift segments (purple lines) and corona locations (red stars). (b) Local rift segments and magmatic centres organized into *rift segment groups* (RGS) and colour-coded to represent genetic association. Stars represent coronae, while circles denote radiating and/or circumferential graben-fissure systems as either volcanoes or cryptic centres. Rift segment groups are catalogued in *Table 5.2*.

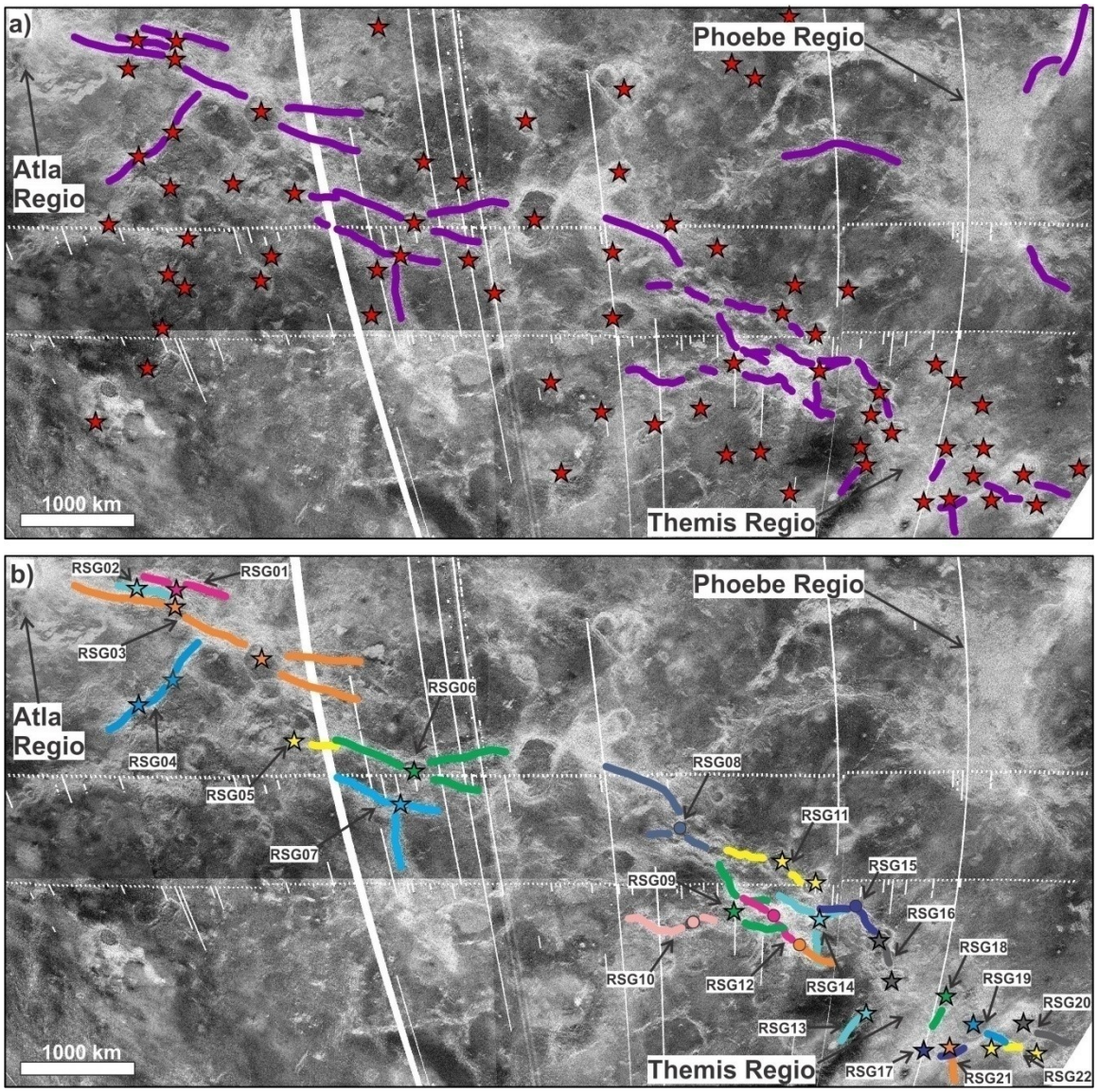

Figure 5.10. Magellan SAR images of Parga Chasma (centred at 245°E, 20°S). (a) Image overlain by ungrouped local rift segments (purple lines) and corona locations (red stars). (b) Local rift segments and magmatic centres organized into *rift segment groups* (RGS) and colour-coded to represent genetic association. Stars represent coronae, while circles denote radiating and/or circumferential graben-fissure systems as either volcanoes or cryptic centres. Rift segment groups are catalogued in *Table 5.3*.

Table 5.2. Rift segment groups catalogued along Hecate Chasma. Volcanic rises of Atla and Beta Regiones are labelled as such in the first column.

Rift Segment Group	# of Local Segments	# of Associated Magmatic Centres	Type(s) of Centre(s)
RGS01 (Atla Regio)	2	1	Volcanic rise
RGS02 (Beta Regio)	1	1	Volcanic rise
RGS03	2	1	Graben-fissure system
RGS04	2	1	Corona
RGS05	1	1	Corona
RGS06	3	2	Corona & graben-fissure system
RGS07	2	2	Corona

Table 5.3. Rift segment groups catalogued along Parga Chasma. RGS09, RGS12, RGS14, and RGS15 are the groups associated with the local centres mapped in the study area, and are labelled as such in the first column. Atla Regio is similarly labelled under RGS03.

Rift Segment Group	# of Local Segments	# of Associated Magmatic Centres	Type(s) of Centre(s)
RGS01	2	1	Corona
RGS02	2	1	Corona
RGS03 (Atla Regio)	4	3	Corona & volcanic rise
RGS04	3	2	Corona
RGS05	1	1	Corona
RGS06	3	1	Corona
RGS07	3	1	Corona
RGS08	3	1	Graben-fissure system
RGS09 (Kulimina)	3	1	Corona
RGS10	2	1	Graben-fissure system
RGS11	2	2	Corona
RGS12 (R16 and R07)	3	2	Graben-fissure system
RGS13	1	1	Corona
RGS14 (Xmukane)	3	1	Corona
RGS15 (Ts'an Nu Mons)	2	1	Volcano
RGS16	2	2	Corona
RGS17	1	1	Corona
RGS18	1	1	Corona
RGS19	1	1	Corona
RGS20	1	1	Corona
RGS21	1	1	Corona
RGS22	1	2	Corona

5.3 Terrestrial Analogue to Hecate and Parga Chasmata

The discontinuous morphology of rift systems, coupled with the interpretation of regional formation via a combination of local rifting from multiple magmatic centres, is not confined only to Venus. On Earth, the pre-spreading orientation of the Atlantic Rift System (*Figure 5.11*) exhibits discontinuities along its full extent, that are similar to those observed along both Hecate and Parga Chasmata. In addition, the rifting and subsequent opening of the Atlantic Ocean is linked to the arrival of three large mantle plumes, each of which resulted in the formation of a Large Igneous Province (LIP) (Ernst, 2014). Many similarities between the terrestrial rifting of the Atlantic Rift System and the Venusian rifting of Hecate and Parga Chasmata can be observed. Specifically, each rift system: (1) exhibits similar discontinuous morphology; (2) contains major plume-related magmatic centres, likely acting as a primary cause of rifting; and (3) contain smaller centres that display localized triple-junction rifting.

It is interesting to note that Hecate Chasma is observed to exhibit a more continuous morphology with a lesser number of local rift segments than the Atlantic Rift System (*Figure 5.12*). Parga Chasma, however, remains as a very complex and discontinuous rift system, and exhibits many similarities in morphology to the Atlantic Rift System (*Figure 5.13*). Both of these rift systems are observed to extend between major primary centres and similarly contain an abundance of local triple-junction rifting events from smaller magmatic centres along their full extent.

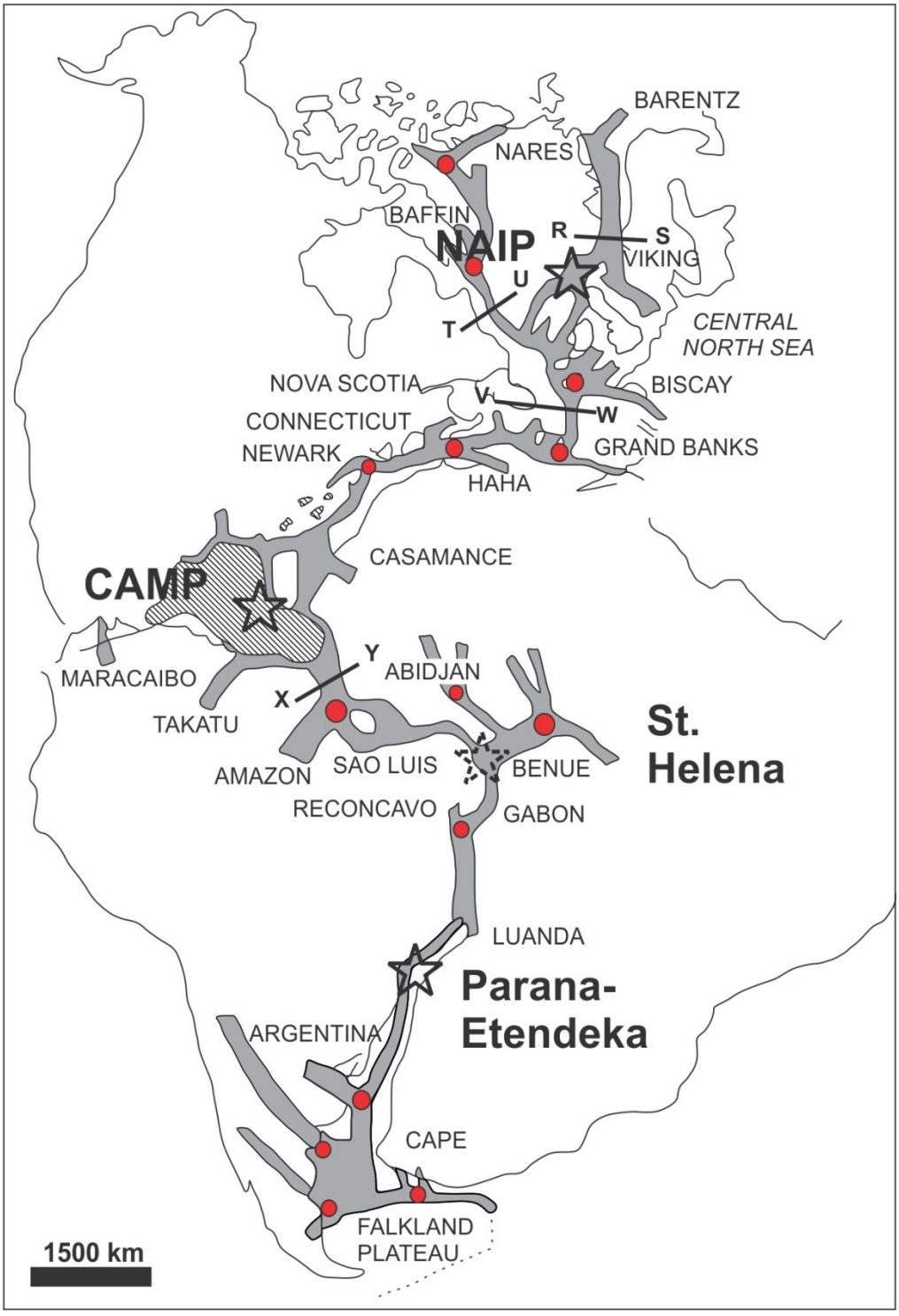

Figure 5.11. Rifting associated with the opening of the Atlantic Ocean and relationship to plumes and LIPs. See text for details. Interpreted centres of local triple-junction rifting superimposed (red circles). Background rift diagram is from Sengör (1995) with the mantle plume centres (stars) superimposed (from Figure 11.2 in Ernst, 2014).

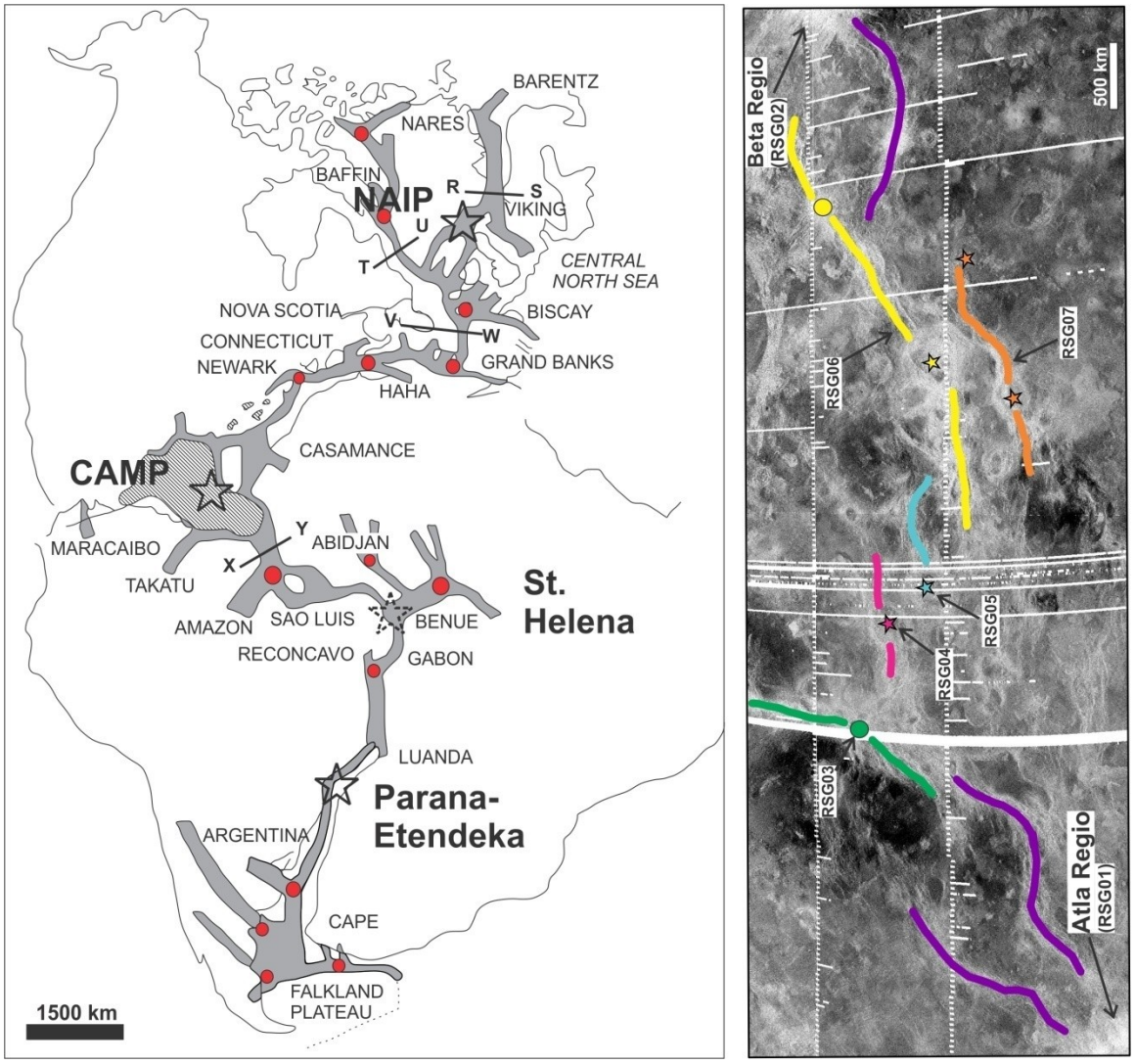

Figure 5.12. Comparison between the rifting along the Atlantic Rift System on Earth with the rifting of Hecate Chasma on Venus, rotated 90°. Note the difference in scale.

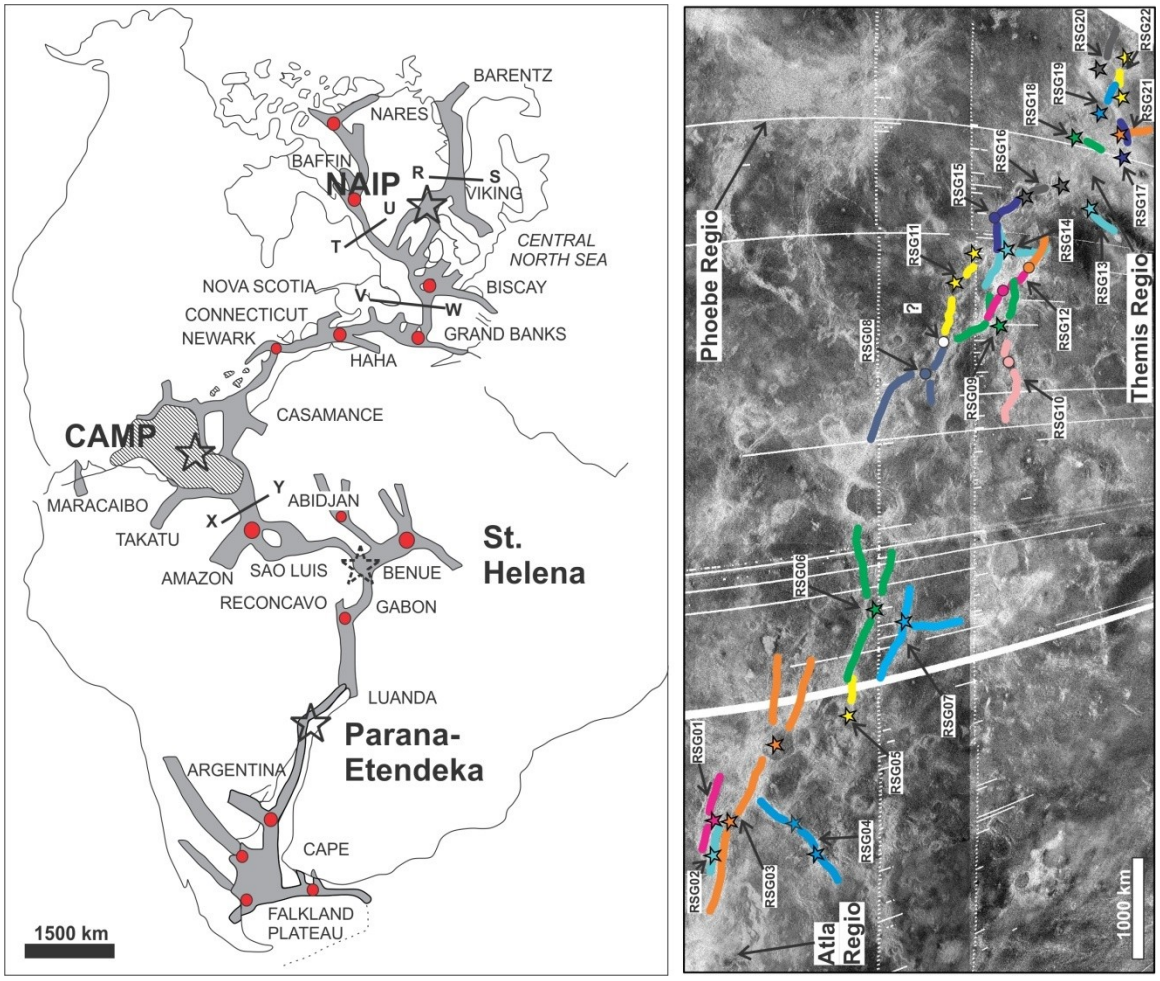

Figure 5.13. Comparison between the rifting along the Atlantic Rift System on Earth with the rifting of Parga Chasma on Venus, rotated 90°. Note the difference in scale.

Drawing further comparisons between terrestrial and Venusian rifting involves the age relationships between the rifting events and their interpreted magmatic centres. In the case of the Atlantic Rift System, while the main plume centres were emplaced at different times over a range of ~140 million years (200, 135, and 62 Ma; see Figure 11.2 in Ernst, 2014 for details), the individual rifts are interpreted to have formed synchronously (+/- ~10 – 20 Ma) with their associated plume centre (Ernst, 2014). With respect to Venusian rifting, the relative chronology of magmatic events within the study area (Chapter 4) reveals a comparable result. Specifically, the magmatic centres (and associated graben-fissure systems) that have been linked to local rift segments are as follows: Ts'an Nu

Mons (R04); Xmukane Corona (R01); Kulimina Corona (R05); and two unnamed centres, one located at R16 and another at R07. These systems have been dated via cross-cutting relationships, resulting in a relative chronology that places them as younger than the regional rifting of Parga Chasma. Additionally, the graben-fissure systems interpreted to be linked with the formation of local rift segments exhibit synchronous cross-cutting relationships with the individual rift faults comprising these segments. This result further supports a comparison to the Atlantic Rift System as a terrestrial analogue for understanding Venusian rifting.

In summary, each magmatic centre interpreted as the centre for local triple-junction rifting within the study area contains at least one primary graben-fissure system that exhibits synchronous age relationships to the associated local rift segments. The age relationships (*Figure 4.17*) of these same graben-fissure systems are also almost exclusively younger than the regional rift fault pattern marking the regional NE-SW extension of Parga Chasma (*Figure 4.3*). This result shows that while Venusian rift systems may appear as a single structure stretching over 1,000's of kilometres, they can be better understood as collections of local rifting events focussed on isolated magmatic centres along a regional system.

6 Chapter: Conclusions

The Beta-Atla-Themis (BAT) region of Venus is enclosed by three major rift systems – Hecate, Devana, and Parga Chasmata – with lengths up to 10,000 km (*Figure 1.3*). Each rift system is associated with numerous tectono-magmatic structures, including: coronae (circular volcanic structures typically ~200 – 500 km in diameter), *mons* (individual volcanoes >100 km in diameter) and graben-fissure systems (marking underlying dyke swarms). A 1,500 km section of the Parga Chasma rift system was mapped in detail, and cross-cutting relationships assessed in order to reconstruct the tectono-magmatic history of the study area. The insights obtained from the study area were then applied to the BAT region as a whole.

The study area located within the coordinates of 260^{o} – 275^{o}E, 25^{o} – 33^{o}S is 1,500 km long and 800 km wide, covering an area of ~1.2 million km^2. A general review of Venusian characteristics and its geology with a focus on the BAT region is provided in Chapters 1 and 2. This is followed by development and discussion of methodologies used (Chapter 3). ArcMap was used to map lineaments from the high resolution Synthetic Aperture Radar (SAR) images obtained from the Magellan mission (1990 – 1994). Criteria were presented to distinguish graben-fissure lineaments (thought to overlie laterally propagating dykes) from rift faults (Section 3.4), in addition to presenting criteria to determine relative age relationships between systems of grouped of lineaments (Section 4.1).

Relative chronology (*Figure 4.17*) was determined through the analysis of cross-cutting relationships between interacting graben-fissure and/or rift fault lineaments (Section 4.2). While previous studies primarily focussed on mapping graben-fissure

systems (e.g. Grosfils and Head, 1994a,b; Ernst et al., 2003; Studd et al., 2011), this mapping further included the identification of separate rift segments and detailed mapping of the associated individual rift faults. However, this presented the first challenge of this detailed mapping, as the radar-bright lineaments representing graben-fissures and rift faults can often appear very similar on SAR images.

Rift-distinguishing criteria was initially developed by Graff et al. (2014) and was further expanded upon using a terrestrial analogue during this research, the results of which are presented in Graff et al. (2015) and summarized in Section 3.4. Following these methods, rift faults were distinguished from graben-fissures on the basis of lineament thickness and sinuosity. Clusters of these rift fault and graben-fissure lineaments were then grouped into specific local rift segments and graben-fissure systems. Grouping rift fault lineaments into specific local segments also allowed them to be distinguished from regional rift faults. The regional rift faults are linked to the regional rifting along Parga Chasma, a process that is interpreted – on the basis of cross-cutting relationships – to have preceded local rifting events that are observed to extend from individual magmatic centres (marked by graben-fissure systems, often centred on coronae or large volcanoes). This interpretation of Parga Chasma is of particular importance to the development of a relative chronology because only the regional rifting can be considered as a singular event in time. This result can also have notable implications for further studies on Venus by providing a more detailed understanding of the tectono-magmatic history from the analysis of a greater diversity of geologic structures.

Applying the results from the generated chronology it is interpreted that Parga Chasma developed as a combination of two distinct rifting stages, beginning from a

precursor NE-SW regional extension (*Figure 5.1*) and followed by multiple local events of triple-junction rifting extending from individual magmatic centres (*Figure 5.8*). This model of local triple-junction rifting events from isolated centres – as mapped in the study area along Parga Chasma – was then applied to the rest of Parga Chasma and the entirety of Hecate Chasma. Hecate Chasma was observed to contain 13 local rift segments (*Figure 5.9*), while Parga Chasma contained as many as 45 local rift segments (*Figure 5.10*).

A similar complex rift morphology can also be observed in examples from Earth, notably along the Atlantic Rift System (*Figure 5.11*), which is ~15,000 km long – comparable to Venusian rift systems. Along its full extent, the pre-spreading morphology of this giant terrestrial rift system exhibits similar discontinuities to those observed along the full extent of Hecate and Parga Chasmata (*Figures 5.12 and 5.13*). The rifting of the Atlantic Rift System can also be observed to have formed from the arrival of three separate major upwelling events (in this case, mantle plumes with ages of 200, 130, and 62 Ma) and several minor upwellings, each causing local triple-junction rifting that collectively develop the full morphology of a complete rift system. This observation supports our hypothesis, implying that major Venusian and terrestrial rift systems can be identified as a collection of local triple-junction rifting events from individual magmatic centres and can develop over a range of time (at least 10's of Myr). This demonstrates that the model developed to explain the complex morphologies of Venusian rift systems is also supported by a terrestrial analogue.

References

Arvidson, R.E., Baker, V.R., Elachi, C., Saunders, R.S., Wood, J.A. 1991. *Magellan: Initial analysis of Venus surface modification*. Science, **252**, 270-275.

Baer, G., Schubert, G., Bindschadler, D.L., Stofan, E.R. 1994. *Spatial and Temporal Relations between Coronae and Extensional Belts, Northern Lada, Venus*. Journal of Geophysical Research **99**, 8355-8369.

Basaltic Volcanism Study Project. 1981. *Basaltic Volcanism on the Terrestrial Planets*. Pergamon Press, New York, N.Y. 1286p.

Bethell, E., Ernst, R.E., Samson, C., Buchan, K.L. 2016. *Circumferential Graben-Fissure Systems of Venusian Coronae as Possible Analogues of Giant Circumferential Dyke Swarms on Earth*. Lunar and Planetary Science XXXXVII (2016). Abstract 1471.

Buchan, K.L., Ernst, R.E. 2016. *Giant Circumferential Dyke Swarms on Earth as Possible Analogues of Coronae on Venus*. Lunar and Planetary Science XXXXVII (2016). Abstract 1183.

Burke, K., Dewey, J. 1973. *Plume-Generated Triple Junctions: Key Indicators in Applying Plate Tectonics to Old Rocks*. Journal of Geology **81**, 406-433.

Chaisson, E., McMillan, S. 2010. *Astronomy Today, Vol. 1 – The Solar System, 7th Edition*. Addison-Wesley Publishing, San Francisco, CA. Ch. 9, pp. 211-229.

Chapman, M.G., Kirk, R.L. 1996. *A Migratory Mantle Plume on Venus. Implications for Earth?*. Journal of Geophysical Research **101**, 15953-15967.

Crumpler, L.S., Head, J.W., Aubele, J.C. 1993. *Relation of Major Volcanic Center Concentration on Venus to Global Tectonic Patterns*. Science **261**(5121), 591-595.

Crumpler, L.S., Aubele, J.C. 2000. *Volcanism on Venus*. *In* Encyclopedia of Volcanoes. Academic, San Diego, California, pp. 727-770.

Davey, S.C., Ernst, R.E., Samson, C., Grosfils, E.B. 2013. *Hierarchical Clustering of Pit Crater Chains on Venus*. Canadian Journal of Earth Science **50**, 109-126.

Davies, M.E., Colvin, T.R., Rogers, P.G., Chodas, P.W., Sjogren, W.L., Akim, E.L., Stepanyantz, V.A., Vlasova, Z.P., Zakharov, A.I. 1992. *The Rotation Period, Direction of the North Pole, and Geodetic Control Network of Venus*. Journal of Geophysical Research **97**, 13141-13151.

Dombard, A.J., Johnson, C.L., Richards, M.A., Solomon, S.C. 2007. *A Magmatic Loading Model for Coronae on Venus*. Journal of Geophysical Research **112**, E04006, doi: 10.1029/2006JE002731.

Donahue, T.M., Russell, C.T. 1997. *The Venus Atmosphere and Ionosphere and Their Interaction with the Solar Wind: An Overview*. In Bougher, S.W., Hunten, D.M., & Phillips, R.J. (eds), *Venus II: Geology, Geophysics, Atmosphere, and Solar Wind Environment*. Tucson, AZ: University of Arizona Press, pp. 3-31.

Ernst, R.E. 2014. *Large Igneous Provinces*. Cambridge University Press, 653p.

Ernst, R.E., Buchan, K.L. 1997a. *Giant Radiating Dyke Swarms: Their Use in Identifying Pre-Mesozoic Large Igneous Provinces and Mantle Plumes*. AGU Geophysical Monograph **100**, 297-333.

Ernst, R.E., Buchan, K.L. 1997b. *Layered Mafic Intrusions: A Model for Their Feeder Systems and Relationship with Giant Dyke Swarms and Mantle Plume Centers*. South African Journal of Geology **100**, 319-334.

Ernst, R.E., Buchan, K.L. 2001. *The Use of Mafic Dyke Swarms in Identifying and Locating Mantle Plumes*. In Ernst, R.E. & Buchan, K.L. (eds), Mantle Plumes: Their Identification Through Time. Boulder, CO: Geological Society of America, Special Paper **352**, pp. 483-575.

Ernst, R.E., Buchan, K.L., Palmer, H.C. 1995a. *Giant Dyke Swarms: Characteristics, Distribution and Geotectonic Applications*. In Baer, G. & Heimmann, A. (eds), Physics and Chemistry of Dykes. Rotterdam: Balkema, pp. 3-21.

Ernst, R.E., Desnoyers, D.W. 2004. *Lessons from Venus for Understanding Mantle Plumes on Earth*. Physics of the Earth and Planetary Interiors **146**, 195-229.

Ernst, R.E., Desnoyers, D.W., Head, J.W., Grosfils, E.B. 2003. *Graben-Fissure Systems in Guinevere Planitia and Beta Regio (264^o-312^oE, 24^o-60^oN), Venus, and Implications for Regional Stratigraphy and Mantle Plumes*. Icarus **164**, 282-316.

Ernst, R.E., Head, J.W., Parfitt, E., Grosfils, E.B., Wilson, L. 1995b. *Giant Radiating Dyke Swarms on Earth and Venus*. Earth Science Reviews **39**, 1-58.

Ernst, R.E., Grosfils, E.B., Mege, D. 2001. *Giant Dyke Swarms: Earth, Venus, Mars*. Annual Review of Earth and Planetary Sciences **29**, 489-534.

ESA Venus Express 2007a. *Venus: Earth's Twin Planet*. Updated on Nov. 28, 2007. http://www.esa.int/Our_Activities/Space_Science/Venus_Express/Venus_Earth_s_twin_planet2.

ESA Venus Express 2007b. *Caught in the Wind from the Sun*. Updated on Nov. 28, 2007. http://www.esa.int/Our_Activities/Space_Science/Venus_Express/Caught_in_the_wind_from_the_Sun.

Graff, J.R., Ernst, R.E., Samson, C. 2014. *Mapping and Analysis of the Tectono-Magmatic Features Along the Hecate Chasma Rift System, Venus*. B.Sc. Thesis. Department of Earth Sciences. Carleton University.

Graff, J.R., Ernst, R.E., Samson, C. 2015. *Delineating Rift Faults on Radar Images in Hecate Chasma, Venus*. Lunar and Planetary Science XXXXVI (2015), Abstract 2217.

Grosfils, E.B., Ernst, R.E., Galgana, G.A. 2014. *Radiating Lineament System*. Encyclopedia of Planetary Landforms, pp 1-10.

Grosfils, E.B., Head, J.W. 1994a. *The Global Distribution of Giant Radiating Dike Swarms on Venus: Implications for the Global Stress State*. Geophysical Research Letters **21**, 701-704.

Grosfils, E.B., Head, J.W. 1994b. *Emplacement of a Radiating Dike Swarm in Western Vinmara Planitia, Venus: Implication of the Regional Stress Field Orientation and Subsurface Magmatic Configuration*. Earth, Moon and Planets **66**, 153-171.

Hamilton, V.E., Stofan, E.R. 1996. *The Geomorphology and Evolution of Hecate Chasma,Venus.* Icarus **121**, 171-194.

Hansen, V.L., Olive, A. 2010. *Artemis, Venus: The Largest Tectonomagmatic Feature in the Solar System?*. Geology **38**, 467-470, doi: 10.1130/G30643.1

Hansen, V.L., Young, D.A. 2007. *Venus' Evolution: A Synthesis*. *In* Convergent margin terranes and associated regions: a tribute to W.G. Ernst. *Edited by* M.Cloos, W.D. Carlson, M.C. Gilbert, J.G. Liou, and S.S. Sorensen. Geological Society of America Special Paper **419**, pp. 255-273.

Head, J.W., Crumpler, L.S., Aubele, J.C., Guest, J.E., Saunders, R.S. 1992. *Venus Volcanism: Classification of volcanic features and structures, associations, and global distribution from Magellan data*. Journal of Geophysical Research **97**, 13153-13197.

Herrick, R.R. 1999. *Small Mantle Upwellings are Pervasive on Venus and Earth*. Geophysics Research Letters **26**, 803-806.

Ivanov, M.A., Head, J.W. 2011. *Global Geological Map of Venus*. Planetary and Space Science **59**, 1559-1600.

Ivanov, M.A., Head, J.W. 2013. *A History of Volcanism on Venus*. Planetary and Space Science **84**, 66-92.

Kiefer, W.S., Peterson, K. 2003. *Mantle and Crustal Structure in Phoebe Regio and Devana Chasma, Venus*. Geophysical Research Letters **30** (1), 1005.

Kiefer, W.S., Swafford, L.C. 2004. *Rift System Architecture on Venus*. 35th Lunar and Planetary Science XXXV (2004), Abstract 1607.

Kiefer, W.S., Swafford, L.C. 2006. *Topographic Analysis of Devana Chasma, Venus: Implications for Rift System Segmentation and Propagation*. Journal of Structural Geology **28**, 2144-2155.

Kiefer, W.S. 2013. *Making Ishtar Terra, Venus: Mobile Lid Tectonics, Continental Crust, and Implications for Liquid Water and Planetary Evolution*. Lunar and Planetary Science XXXXIV (2013), Abstract 2541.

Leung, A., Ernst, R.E., Samson, C. 2013. *Mapping Graben-Fissure Systems in the Tassig and Galindo Regions of Venus*. B.Sc. Thesis. Department of Earth Sciences. Carleton University.

Lopez, I., Hansen, V.L. 2008. *Geologic Map of the Helen Planitia Quadrangle (V-52), Venus*. U.S. Geological Survey Scientific Investigations Map 3026, http://pubs.usgs.gov/sim/3026/.

Lopez, I., Lillo, J., Hansen, V.L. 2008. *Regional Fracture Patterns Around Volcanoes: Possible Evidence for Volcanic Spreading on Venus*. Icarus **195**, 523-536.

Martin, P., Stofan, E.R. 2004. *Coronae of Parga Chasma, Venus.* Lunar and Planetary Science XXXV (2004), Abstract 1576.

Martin, P., Stofan, E.R., Glaze, L.S., Smrekar, S. 2007. *Coronae of Parga Chasma, Venus*. Journal of Geophysical Research **112**, E04S03.

Masursky, H., Eliason, E., Ford, P.G., M^{c}Gill, G.E., Pettengill, G.H., Schaber, G.G., Schubert, G. 1980. *Pioneer-Venus Radar Results: Geology from the Images and Altimetry*. Journal of Geophysical Research **85**, 8232-8260.

McGill, G.E., Steenstrup, S.J., Barton, C., Ford, P.G. 1981. *Continental Rifting and the Origin of Beta Regio, Venus*. Geophysical Research Letters **8**, 737-740.

McKinnon, W.B., Zahnle, K.J., Ivanov, B.A., Melosh, H.J. 1997. *Cratering on Venus: Models and Observations*. In Bougher, S.W., Hunten, D.M., & Phillips, R.J. (eds), *Venus II: Geology, Geophysics, Atmosphere, and Solar Wind Environment*. Tucson, AZ: University of Arizona Press, pp. 969-1014.

Nimmo, F., McKenzie, D. 1998. *Volcanism and Tectonics on Venus*. Annual Reviews of Earth and Planetary Science **26**, 23-51.

Phillips, R.J., Hansen, V.L. 1994. *Tectonic and Magmatic Evolution of Venus*. Annual Review of Earth and Planetary Sciences **22**, 597-654.

Saunders, R.S., Pettengill, G.H., Arvidson, R.E., Sjogren, W.L., Johnson, W.T.K., Pieri, L. 1990. *The Magellan Venus Radar Mapping Mission*. Journal of Geophysical Research **95**, 8339-8355.

Saunders, R.S., Pettengill, G.H. 1991. *Magellan Mission summary*. Science **252**, 247-249.

Saunders, R.S., Spear, A.J., Allin, P.C., Austin, R.S., Berman, A.L., Chandlee, R.C., Clark, J., DeCharron, A.V., De Jong, E.M., Griffifith, D.G., Gunn, J.M., Hensley, S., Johnson, W.T.K., Kirby, C.E., Leung, K.S., Lyons, D.T., Michaels, G.A., Miller, J., Morris, R.B., Piereson, R.G., Scott, J.F., Shaffer, S.J., Slonski, J.P., Stofan, E.R., Thompson, T.W., and Wall, S.D. 1992. *Magellan Mission Summary*. Journal of Geophysical Research **97**, 13067–13090.

Sawford, W.C., Ernst, R.E., Samson, C., Davey, S.C. 2015. *Pit Crater Chains in the Nyx Mons Region, Venus.* Lunar and Planetary Science XXXXVI (2015), Abstract 1283.

Sengör, A.M.C. 2001. *Elevation as Indicator of Mantle-Plume Activity. In*: Ernst, R.E., Buchan, K.L. (Eds.), Mantle Plumes: Their Identification Through Time. Geological Society of America Special Paper **352**, pp. 183-225.

Sengör, A.M.C., Natal'in, B.A. 2001. *Rifts of the World*. *In*: Ernst, R.E., Buchan, K.L. (Eds.), Mantle Plumes: Their Identification Through Time. Geological Society of America Special Paper **352**, pp. 389-482.

Smrekar, S.E., Kiefer, W.S., Stofan, E.R. 1997. *Large Volcanic Rises on Venus*. Lunar and Planetary Exploration Technical Report, NASA/CR-97-205865; NAS 1.26:205865.

Solomatov, V.S., Moresi, L.N. 1996. *Stagnant Lid Convection on Venus*. Journal of Geophysical Research **101**, 4737-4753.

Squyres, S.W., Janes, D.M., Baer, G., Bindschadler, D.L., Schubert, G., Sharpton, V.L., Stofan, E.R. 1992. *The Morphology and Evolution of Coronae and Novae on Venus*. Journal of Geophysical Research **97**, 13611-13634.

Stofan, E.R., Bindschadler, D.L., Head, J.W., Parmentier, E.M. 1991. *Corona Structures on Venus: Models of Origin*. Journal of Geophysical Research **96**, 20933-20946.

Stofan, E.R., Brian, A.W. 2012. *Geologic Map of the Themis Regio Quadrangle (V-53), Venus*. U.S. Geological Survey Scientific Investigations Map 3165, http://pubs.usgs.gov/sim/3165/.

Stofan, E.R., Head, J.W. 1990. *Coronae of Mnemosync Regio: Morphology and Origin*. Icarus **83**, 216-243.

Stofan, E.R., Sharpton, V.L., Schubert, G., Baer, G., Bindschadler, D.L., Janes, D.M., Squyres, S.W. 1992. *Global Distribution and Characteristics of Coronae and Related Features on Venus: Implications for Origin and Relation to Mantle Processes*. Journal of Geophysical Research **97**, 13347-13378.

Stofan, E.R., Smrekar, S.E., Bindschadler, D.L., Senske, D.A. 1995. *Large Topographic Rises on Venus: Implications for Mantle Upwelling*. Journal of Geophysical Research **100**, 23317-23327.

Stofan, E.R., Smrekar, S.E., Martin, P. 2000. *Coronae of Parga Chasma, Venus: Implications for Chasma and Corona Evolution*. Lunar and Planetary Science XXXI (2000), Abstract 1578.

Strom, R.G., Schaber, G.G., Arkani-Hamed, J., Toksoz, M.N. 1992. *Global Resurfacing of Venus*. Lunar and Planetary Science XXIII (1992), Abstract 1379.

Strom, R.G., Schaber, G.G., Dawsow, D.D. 1994. *The Global Resurfacing of Venus*. Journal of Geophysical Research **99**, 10,899-10,926.

Studd, D., Ernst, R.E., Samson, C. 2011. *Radiating Graben-Fissure Systems in the Ulfrun Regio Area, Venus*. Icarus **215**, 279-291.

Studd, D., Ernst, R.E., Samson, C., Grosfils, E.B., Head, J.W., Ivanov, M.A., 2010a. *Radiating Graben-Fissure Systems in Ulfrun Regio: A Contribution to the Venus Global Dyke Swarm Map Project*. Lunar and Planetary Science XXXXI (2010), Abstract 1950.

Studd, D., Ernst, R.E., Samson, C., Grosfils, E.B., Head, J.W., Ivanov, M.A., 2010b. *Mapping in the Ulfrun Regio Area: A Contribution Towards a Global Venus Dyke Swarm Map*. CASI ASTRO Con. **15**, #03.

Studd, D., Ernst, R.E., Samson, C., Grosfils, E.B., Head, J.W., Ivanov, M.A., 2010c. *Interaction Between Radiating Graben-Fissure Systems and Local Geology, Ulfrun Regio, Venus: A Contribution to the Venus Global Dyke Swarm Map Project*. COSPAR Sci. Ass. **38**, B-10-0000-10.

Taylor, F.W. 2014. *The Scientific Exploration of Venus*. Cambridge University Press, 295p.

Turcotte, D.L. 1995. *How Does Venus Lose Heat?*. Journal of Geophysical Research **100**, 16931-16940.

Waerden, B. 1974. *Science Awakening II: The Birth of Astronomy*. Springer, pp. 347

Young, C. 1990. *The Magellan Venus Explorer's Guide*. NASA-JPL, Publication 90-24, Pasadena, Ca.